DISS. ETH NO. 29106

The locus coeruleus noradrenergic system in stress: Shaping the pupillary and transcriptomic stress response

A thesis submitted to attain the degree of
DOCTOR OF SCIENCES
(Dr. sc. ETH Zurich)

presented by

Mattia Giuseppe Privitera

MSc, University of Zurich

born on 12.08.1992

accepted on the recommendation of

Prof. Dr. Johannes Bohacek

Prof. Dr. Denis Burdakov

Prof. Dr. Benno Roozendaal

2023

Abstract

In an ever-changing environment, we are constantly presented with new challenging and stressful situations. Within all organisms, specific molecular, physiological and behavioral adaptations have evolved to perceive, assess and execute appropriate stress responses. A rapid and adequate response not only increases the chance of immediate survival, but also promotes long-term adaptations to improve future outcomes. However, maladaptation to stress has also been associated with the development of various neurological disorders, such as depression, anxiety and post-traumatic stress disorder. A better understanding of the underlying mechanisms is therefore essential to fully grasp how stress responses lead to maladaptation. Various systems across peripheral and central organs have evolved to mediate responses to stress. The central nervous system mainly governs the perception, assessment and execution of stress responses. This includes the complementary actions of various brain areas and neurotransmitter systems; however, the locus coeruleus (LC) noradrenergic system has been proven to play a key role in facilitating responses to stress. Here, I present our research on the LC noradrenergic system and how it shapes pupillary and molecular responses in mice. First, we demonstrate how pupillometry, the measurement of pupil diameter, can be easily applied to rodents and how it can complement electric, chemogenetic and optogenetic manipulations of the locus coeruleus. Thus, pupillometry provides a rapid, non-invasive and translationally relevant tool to facilitate locus coeruleus research. Secondly, long-term adaptations to stress are based on molecular changes in the brain; however, the role of noradrenaline (NA) in this is still barely understood. To this end, we investigated and characterized how stress-dependent activation of the LC-NA system affects transcriptomic responses in the hippocampus, a stress-sensitive projection region of the LC. By combining RNA-sequencing with selective pharmacological, chemogenetic, and optogenetic manipulations of the LC-NA system, we show that NA-release during stress exposure reliably regulates a set of genes in the hippocampus via β-adrenergic receptors. The identity of the gene set suggests LC-mediated mobilization of astrocytic energy and thyroid hormone metabolism as essential mediators of LC function in the hippocampus. I further expand on current models of LC function and propose that these astrocytic pathways underlie LC-mediated facilitation of long-term adaptations to stress and thus offer prominent targets for further research investigating the role of the LC-NA system in health and disease.

Zusammenfassung

In einer sich kontinuierlich verändernden Umwelt werden wir ständig mit neuen herausfordernden Situationen konfrontiert, die wir als Stress wahrnehmen. Unter allen Organismen haben sich dadurch spezifische Anpassungen auf molekularer, physiologischer und Verhaltensebene entwickelt, um auf jeglichen Stress reagieren zu können. Eine schnelle und angemessene körperliche Reaktion auf Stress erhöht nicht nur die unmittelbaren Überlebenschancen, sondern fördert auch langfristige Anpassungen, um zukünftige Stresssituationen besser zu bewältigen. Abnormale Reaktionen auf Stress wurden jedoch auch mit der Entwicklung verschiedener neurologischer Krankheiten wie Depressionen, Angstzuständen und posttraumatischen Belastungsstörungen in Verbindung gebracht. Deshalb ist es unerlässlich, die zugrunde liegenden Mechanismen zu erforschen, um zu verstehen, wie abnormale Reaktionen auf Stress zu diesen Krankheiten beisteuern können. Verschiedene körperliche Systeme in peripheren und zentralen Organen haben sich darauf spezialisiert, auf Stress zu reagieren. Insbesondere Bestandteile des zentralen Nervensystems nehmen Stress wahr, bestimmen eine passende Reaktion und leiten diese ein. Dazu gehören die komplementären Funktionen verschiedener Hirnareale und Neurotransmittersysteme; eine besondere Schlüsselrolle spielt der Locus coeruleus (LC), ein noradrenerger Nucleus im Hirnstamm, welcher Reaktionen auf Stress im Gehirn organisiert und fördert.

Mit dieser Arbeit stelle ich unsere Forschung über den noradrenergen LC vor und wie dieses System in Mäusen die Pupille und Genexpression beeinflusst. Zunächst zeigen wir, wie Messungen der Pupillengrösse (auch Pupillometrie genannt) einfach bei Nagetieren angewendet werden kann und wie sie elektrische, chemogenetische und optogenetische Manipulationen des LC ergänzen. Die Pupillometrie bietet eine schnelle, nicht-invasive Methode, die auf einem breiten Spektrum angewendet werden kann und die tägliche Forschung am LC erleichtert. Zweitens basieren langfristige Anpassungen an Stress auf molekularen Veränderungen im Gehirn, die Rolle von Noradrenalin (NA) in diesem Kontext ist dabei jedoch noch kaum erforscht. Zu diesem Zweck haben wir untersucht, wie die stressabhängige Aktivierung des LC-NA-Systems die Expression von Genen im Hippocampus beeinflusst. Durch die Kombination von RNA-Sequenzierung mit selektiven pharmakologischen, chemogenetischen und optogenetischen Manipulationen des LC-NA-Systems zeigen wir, dass NA im Hippocampus während Stress einen Satz von spezifischen Genen über β-adrenerge Rezeptoren reguliert. Unsere Ergebnisse deuten insbesondere darauf hin, dass der LC die Mobilisierung von Energiesubstraten und Schilddrüsenhormonen in Astrozyten anregt, was eine mögliche Grundlage für weitere Veränderungen im Hippocampus durch den LC bildet.

Zusätzlich bespreche ich aktuelle Hypothesen zur Funktion des noradrenergen LC-Systems und erweitere diese mit der Annahme, dass der LC durch diese astrozytären Signalwege langfristige physiologische Anpassungen vereinfacht und somit prominente Ziele für zukünftige Forschungen am LC-NA-System bilden, um dessen Rolle in neurologischen Krankheiten besser zu verstehen.

Table of contents

Abstract 1

Zusammenfassung 2

Table of contents 3

Glossary 6

Chapter 1. General Introduction 9
1.1 The evolution of the stress response 9
1.2 Stress in health and disease 9
1.3 Mediators of the mammalian stress response 10
1.3.1 Hypothalamic-pituitary-adrenal axis 10
1.4 The central noradrenergic system 12
1.4.1 The Locus Coeruleus (LC) 12
1.4.2 Morphology and afferent inputs 13
1.4.3 Activity patterns 13
1.4.4 Efferent projections 14
1.4.5 Neurotransmitter and co-transmitter release 14
1.4.6 Noradrenaline: Biosynthesis, release and degradation 15
1.4.7 Adrenergic Receptors and Transporters 15
1.4.7.1 Noradrenaline transporter 16
1.4.7.2 α1-Adrenergic Receptors 16
1.4.7.3 α2-Adrenergic Receptors 17
1.4.7.4 β-Adrenergic Receptors 17
1.4.7.5 Adrenergic receptor subtypes and their dynamics 18
1.4.8 Unravelling LC function across the brain 19
1.4.8.1 Effects on peripheral stress systems 20
1.4.8.2 Effects on attention and flexibility: the prefrontal cortex 20
1.4.8.3 Effects on anxiety and memory: the amygdala 21
1.4.8.4 Effects on learning and memory: the hippocampus 22
1.4.9 The LC-NA system in aging and neurological disorders 23
1.4.9.1 Aging and neurodegenerative disorders 23
1.4.9.2 Chronic stress and stress-related disorders 24
1.4.9.3 Major depressive disorder 24
1.4.9.4 Attention deficit and autism spectrum disorders 24
1.5 Current challenges in LC research 25
1.6 Aims of the thesis 25
1.6.1 Facilitating LC research with pupillometry 25
1.6.2 Dissecting the transcriptomic stress response 26

Chapter 2. A complete pupillometry toolbox for real-time monitoring of locus coeruleus activity in rodents **27**
2.1 Abstract 28
2.2 Introduction 28
2.2.1 Development of a miniaturized low-cost pupillometry setup 28
2.2.2 Advantages and limitations of the technique 30

2.2.3 Experimental design 31
2.2.3.1 Animals and experimental parameters 31
2.2.3.2 LC manipulations and pupillometry 31
2.2.3.3 Baseline and power 31
2.3 Methods 32
2.3.1 Biological materials 32
2.3.2 Reagents 32
2.3.3 Equipment 32
2.3.3.1 Software 32
2.3.3.1 Hardware 33
2.4 Procedure 33
2.4.1 Pupillometry equipment setup (Timing 2h) 33
2.4.2 Software setup (Timing 1h) 35
2.4.3 Experiment preparation (Timing 10 min/animal) 35
2.4.4 Pupillometry recording (Timing 5–30 min/animal) 36
2.4.5 Conversion of video files to '.mp4' with FFmpeg (Timing 2–3 min/video) 37
2.4.6 Analysis of video files 38
2.4.6.1 A: Analysis of video files with MATLAB (Timing 2–5 min/video) 38
2.4.6.2 B: Analysis of video files with DLC (Timing 5–10 min/video) 39
2.4.6 Visualization and statistical analysis with the Pupillometry App 39
(Timing 10–20 min) 39
2.4.7 Troubleshooting 40
2.5 Anticipated results 44
2.5.1 Pupillometry as a real-time readout of LC activation 44
2.5.2 Pupillometry as a tool to guide electrical stimulation of the LC 46
2.5.3 Pupillometry reports physiologically relevant modes of LC activation 47
2.5.4 Pupillometry as a tool to guide experimental decisions 47
2.5.5 Pupillometry to explore LC function 50
2.5 Reporting Summary 50
2.6 Data availability 51
2.7 Code availability 51
2.8 Acknowledgements 51
2.9 Author contribution 51
2.10 References 51
2.10 Supplementary Information 53
2.10.1 Pupillometry in darkness (Box 1) 53
2.10.2 Recording the pupillary light reflex (Box 2) 54
2.10.3 Absolute pupil measurements with DLC (Box 3) 55
2.10.4 Supplementary Methods 56
2.10.5 Supplementary Figures 57

Chapter 3. Noradrenaline release from the locus coeruleus shapes stress - induced hippocampal gene expression 59
3.1 Abstract 60
3.2 Introduction 60
3.3 Results 61
3.4 Discussion 71
3.4.1 Dissecting stress with transcriptomics 71

3.4.2 Complex interactions between stress mediators 71
3.4.3 Transcriptomic fingerprinting of NA effects using LC circuit manipulation 72
3.4.4 Differences in the noradrenergic response across the hippocampal axis and sex 73
3.4.5 LC-NA targeted genes 73
3.4.6 Summary 74
3.5 Methods 74
3.5.1 Animals 74
3.5.2 Stereotactic Surgeries 74
3.5.3 Drug injections/infusions 75
3.5.4 Forced swim test 76
3.5.5 Open field test (OFT) 76
3.5.6 Optogenetic stimulation 76
3.5.7 Pupillometry 76
3.5.8 Tissue collection 76
3.5.9 Immunohistochemistry 77
3.5.10 Ultra-high performance liquid chromatography (uHPLC) 77
3.5.11 RNA extraction 78
3.5.12 Bulk RNA sequencing and data analysis 78
3.5.13 Reverse transcription quantitative real-time polymerase chain reaction (RT-qPCR) 79
3.5.14 Statistics 80
3.6 Supplementary Figures 81
3.7 Data availability 86
3.8 Code availability 86
3.9 Acknowledgments 86
3.10 Author Contributions 87
3.11 References 87

Chapter 4. Discussion **90**
4.1 A new era of LC research: Insights from technological advances 90
4.2 Astrocytes: The major target of the LC-NA system 91
4.3 The LC as a major regulator of astrocytic energy metabolism 92
4.4 The LC as a major regulator of brain derived triiodothyronine 92
4.4.1 T3 facilitates neuronal signaling and plasticity 93
4.4.2 The LC-T3 link as a potential disease mechanism 94
4.6 An updated model of the LC-NA system 94

Acknowledgments **95**

Bibliography **96**

Glossary

AAV	Adeno-associated virus
ACTH	Adrenocorticotropic hormone
AD	Alzheimer’s Disease
ADHD	Attention deficit hyperactivity disorder
Apold1	Apolipoprotein L Domain-Containing 1 protein
CA	Cornu Ammonis
cAMP	Cyclic-adenosine monophosphate
ChR2	Channelrhodopsin-2
CNS	Central nervous system
CRF	Corticotropin releasing factor
DBH	Dopamine beta-hydroxylase
dHC	Dorsal hippocampus
Dio2	Type II iodothyronine deiodinase
DNA	Deoxyribonucleic acid
DOPA	3,4-dihydroxyphenylalanine
DREADD	Designer Receptors Exclusively Activated by Designer Drugs
EGFP	Enhanced green fluorescent protein
EW	Edinger-Westphal nucleus
EYFP	Enhanced yellow fluorescent protein
FDR	False discovery rate
fMRI	Functional magnetic resonance imaging
GABA	γ-aminobutyric acid
GPCR	G-protein-coupled receptor
GR	Glucocorticoid receptor
HC	Hippocampus

HPA	Hypothalamic-pituitary-adrenal
HPLC	High-performance liquid chromatography
HPT	Hypothalamic-pituitary-thyroid
iCre	Codon-improved Cre-recombinase
IML	Intermediolateral column
LC	Locus coeruleus
LTD	Long-term depression
LTP	Long-term potentiation
MAPK	Mitogen-activated protein kinase 1
mCh	mCherry
MHPG	3-methoxy-4-hydroxyphenylglycol
mPFC	Medial prefrontal cortex
MR	Mineralocorticoid receptor
mRNA	Messenger RNA
NA	Noradrenaline/Norepinephrine
NAT	Noradrenaline transporter (NET)
Nr4a1	Nuclear Receptor Subfamily 4 Group A Member 1
OFT	Open field test
PBS	Phosphate buffered saline
PD	Parkinson’s Disease
PFA	Paraformaldehyde
PFC	Prefrontal cortex
PNS	Parasympathetic nervous system
Ppp1r3c	Protein phosphatase 1 regulatory subunit 3C
Ppp1r3d	Protein phosphatase 1 regulatory subunit 3D
Ppp1r3g	Protein phosphatase 1 regulatory subunit 3G

PTSD	Post-traumatic stress disorder
PVN	Paraventricular nucleus
RNA	Ribonucleic acid
RT-PCR	Real-Time polymerase chain reaction
SAM	Sympatho-adrenomedullary
SCN	Suprachiasmatic nucleus
SIK1	Salt-inducible kinase 1
SNS	Sympathetic nervous system
T3	Triiodothyronine
T4	Thyroxine
TH	Tyrosine hydroxylase
TRAP	Translating ribosome affinity purification
Tubd1	Tubulin delta 1
uHPLC	Ultra-high-performance liquid chromatography
vHC	Ventral hippocampus

Chapter 1. General Introduction

1.1 The evolution of the stress response

In our ever-changing environment, all organisms - from single cells to humans - are frequently exposed to uncontrollable and threatening stimuli that are perceived as stress. Throughout the evolution of any species, mechanisms from the molecular to the behavioral level - known as the stress response - have evolved to improve how stress is perceived, managed, and ultimately overcome. An efficient stress response is key to the survival and well-being of any organism and a crucial driver of natural selection, as proposed by Charles Darwin in 1859 [1].
The stress response - commonly known as the "fight or flight" response - was first described by Walter Bradford Cannon in 1915 [2]. Based on the concept of Claude Bernard's milieu intérieur, Walter B. Cannon introduced the concept of "homeostasis", referring to a stable physical and chemical internal state maintained by an organism, suggesting that stressful situations can change the internal environment's stability and, for the first time, providing evidence that maintaining homeostasis required central regulation of adrenaline secretion from the adrenal medulla [3].
A century of research has further added to our understanding of the stress response. Many neuroendocrine systems have been identified to play a crucial role in organizing and executing stress-dependent functions of both the central nervous system and peripheral organs [4]. The brain rapidly mounts a stress response by releasing neurotransmitters, hormones, and peptides that orchestrate organism-wide changes in an attempt to meet the challenges encountered in any given situation. Among others, these include glucocorticoids, neuropeptides, and monoamines. Each of these stress mediators shows distinct but overlapping spatial and temporal modes of action in response to stress [5]. Understanding the complexity of the stress response, involving all of these parallel and converging molecular signaling pathways, still presents a major research challenge.

1.2 Stress in health and disease

In humans, stress can have a profound impact on health and is associated with the development of neurological disorders [6]. The stress response has evolved to protect an organism from acute stress and maintain homeostasis [7]. In the central nervous system, this involves inhibiting neuronal pathways that mediate nonadaptive tasks like eating, growth, and reproduction while facilitating neural pathways that enhance acute, time-limited adaptive functions like arousal, vigilance, and focused attention [8]. A healthy stress response will ultimately promote adaptation and future resilience [9], or, as German philosopher Friedrich Nietzsche described it, "What doesn't kill you, makes you stronger." Despite the adaptive value of these evolutionary conserved responses, severe or prolonged (chronic) exposure to stress is also linked to the pathogenesis of many disorders [5,6,8,10]. Physical and neurological disorders are more common in people with a vulnerable genetic and epigenetic background, as well as individuals under constant stress [11]. A wide range of neurological disorders have been associated with stress, including anxiety, depression and post-traumatic stress disorder (PTSD) [12]. In particular, dysfunction of stress mediators like glucocorticoids [13] and NA (see 1.4.9 for details) is associated with many of these

disorders. A better understanding of the stress response - and the systems that regulate it - thus promises the discovery of new therapeutic targets to prevent or treat stress-related disorders.

1.3 Mediators of the mammalian stress response

In mammals, responses to stressful situations are guided by systems across the body. The heterogeneity of potential stressors an organism faces requires flexible molecular and behavioral responses. These responses are executed by the actions of several central and peripheral neurotransmitter and hormonal systems. In particular, combined actions of the prefrontal cortex, amygdala and hippocampus, as well as the glucocorticoid and noradrenergic systems, have been found to be essential mediators of the stress response.

1.3.1 Hypothalamic-pituitary-adrenal axis

Stress-dependent activation of the hypothalamus - especially the paraventricular nucleus (PVN) - further initiates the release of peripheral stress hormones from the adrenal glands, known as the hypothalamic-pituitary-adrenal (HPA) axis. As a major neuroendocrine system, the HPA axis belongs to the perhaps most extensively studied elements of the stress response and regulates homeostasis, immune responses, energy metabolism and CNS function [14].

Peptidergic neurons of the PVN heavily innervate the pituitary gland and release corticotropin-releasing factor (CRF) and vasopressin upon stress-dependent activation. Both peptides stimulate direct pituitary secretion of adrenocorticotropic hormone (ACTH) into the blood from corticotropic cells. ACTH is then transported through the blood to the adrenal glands, where it binds to ACTH receptors in the adrenal cortex and stimulates the production and secretion of corticosteroids, such as glucocorticoids. Among the glucocorticoids, corticosterone (the main glucocorticoid in most vertebrate species) and cortisol (the main glucocorticoid in humans) have emerged as some of the most potent stress hormones. Once released into the bloodstream from the adrenal cortex's zona fasciculata, glucocorticoids exert their effects by binding to mineralocorticoid (MR) and glucocorticoid receptors (GR) in tissues and organs throughout the body [15,16]. Due to differences in their affinity for corticosterone, MRs are already significantly occupied by corticosterone at rest, whereas activation of GRs occurs when corticosteroid levels are high, such as during stress.

Within peripheral organs, glucocorticoids generally lead to the retention of energy substrates - through inhibition of glucose uptake by tissues and gluconeogenesis - and suppress inflammation and immune reactions [17]. Lipophilic glucocorticoids are also able to cross the blood–brain barrier [18,19] and reach MRs and GRs within the central nervous system, where they not only provide negative feedback to the HPA axis but also mediate various stress-dependent effects on the central nervous system (CNS). Both receptors are found widely across both cortical and limbic areas, but their expression is particularly high in stress-sensitive regions [20]. As a result, stress-induced glucocorticoid release also affects the prefrontal cortex, amygdala, and hippocampus [21–23], by altering the function of these stress-circuits through non-genomic and genomic effects mediated through MR and GR binding.

Rapid non-genomic effects of corticosterone are thought to be mediated by the release of protein complexes bound to the MR and GR in the order of seconds to a few minutes upon corticosterone binding. These non-genomic effects have been found to alter the transmission

of various neurotransmitters - including glutamate, catecholamines and acetylcholine - in target areas, such as the prefrontal cortex, hypothalamus and hippocampus [24–30]. At least partially, these changes seem to be mediated through the rapid trafficking of relevant receptors to the cell membrane [31,32]. Thus, corticosterone is able to temporarily alter the excitability of neuronal cells in these stress-relevant circuits.
In addition to these rapid effects, glucocorticoids also induce gene expression changes in target cells. Once bound by its ligand, the MR and GR translocate into the nucleus, where they act as potent transcription factors and alter the transcription of multiple genes containing specific binding sites for the MR or GR [15]. Glucocorticoids are therefore able to regulate transcription across the brain and are thought to mediate many of these changes in response to stress [33].
However, effects mediated through glucocorticoids are rather slow in nature, with brain glucocorticoid levels only peaking after 20 min of stress exposure and its transcriptional effects occurring only within an hour [34,35]. These slower effects further complement or suppress the actions of faster stress responses, such as those mediated by the noradrenergic system [36–38]. Especially within the brain, these antagonistic effects seem to be regulated through bimodal actions of the MR and GR, whereas MR signaling generally amplifies the effects of stress-relevant neurotransmitter systems, while GR signaling is thought to mediate a negative feedback and suppresses neuronal excitation and synaptic plasticity initiated by other systems during stress [4,39,40]. In particular, glucocorticoids seem to be crucial in regulating brain-wide responsiveness to noradrenergic effects [41,42] and interactions of these systems play an important role in consolidation of stress-related memory, through their actions on the prefrontal cortex, amygdala, and hippocampus [43–47].
In conclusion, activity of the HPA axis and slowly increasing levels of circulating glucocorticoids allow for a temporal window within which stress-dependent molecular adaptations can take place [48], and, in particular, regulate the activity of other stress systems, such as the noradrenergic system.

1.3.2 The sympathetic nervous system

In parallel to the HPA axis, descending projections from various areas of the brainstem also recruit the sympathetic nervous system (SNS) [49,50]. Alongside the parasympathetic nervous system (PNS), the SNS is part of the autonomic nervous system, which innervates internal organs, muscles, and glands. Together, these systems regulate bodily functions such as heart rate, muscle contraction, digestion, respiratory rate, pupillary response, urination, and sexual arousal. In contrast to the PNS - which regulates bodily functions at rest - activation of the SNS induces the “fight-or-flight” response as first described by Walter B. Cannon.
The SNS is made up of pre-and postganglionic neurons. Preganglionic cholinergic neurons of the SNS originate in the thoracolumbar division of the spinal cord and receive descending inputs from various regions of the brainstem. Upon activation, these neurons further excite peripheral noradrenergic neurons located in sympathetic ganglions, which directly innervate target tissues and counteract the activity of cholinergic neurons in the PNS. Thus, the "fight-or-flight" response is triggered by immediate peripheral NA release, which regulates various processes via adrenergic receptors [51,52]. Within the lungs, NA increases oxygen uptake through bronchodilation [53,54]. In parallel, in the heart, it increases cardiac output to supply the body with oxygenated blood by increasing heart rate and contraction force [55,56]. NA also increases circulating energy substrates through the breakdown of fat and

glycogen [57–59]. In accordance, energy distribution is also regulated by NA, whereas blood flow is increased in muscles through vasodilation [51]. In addition, the SNS also increases visual perception through sympathetic activation of the pupil. Noradrenergic engagement of the muscles at the iris induces pupil dilation (mydriasis), which allows more light to enter and focus vision [60].
Preganglionic neurons of the SNS also activate the adrenal glands, specifically the adrenal medulla, known as the sympathetic adrenal medullary pathway [61]. Sympathetic activation of chromaffin cells in the adrenal medulla leads to the secretion of catecholamines - mainly adrenaline and NA - into the blood. This further potentiates and prolongs stress-dependent effects mediated by adrenergic receptors in the periphery.
Sympathetic activation also inhibits various functions unrelated to the stress response, including digestion, urination and sexual arousal [62–64]. Taken together, the actions of the SNS promote accumulation and distribution of usable energy substrates and facilitate reactive responses to stress.

1.4 The central noradrenergic system

Peripheral NA, however, is not able to cross the blood-brain barrier and thus has no direct impact on CNS function [65]. Instead, the peripheral response to NA is complemented by the actions of several noradrenergic nuclei within the CNS. Seven noradrenergic nuclei, originally referred to as A1-A7, have been identified in the mammalian brain [66]. However, most noradrenergic neurons of the central nervous system can be found in area A6, located in the pons of the brainstem, known as the locus coeruleus (LC). Thus, the LC is a major gateway for noradrenergic action in the CNS and a century of stress research has found that the LC seems to play a critical role in modulating core behavioral and physiological processes in response to stress [67,68].

1.4.1 The Locus Coeruleus (LC)

The locus coeruleus is found bilaterally in the lateral periventricular gray matter of the fourth ventricle. It was first described in 1786 by Félix Vicq d'Azyr as a pigmented structure in the rostral hindbrain in his treatise "Traité d'Anatomie et de Physiologie" [69]. However, it wasn't until 1964 that the neurons in the LC were found to contain monoamines [70]. The locus coeruleus - which translates to “blue spot” - received its name due to its blue pigmentation caused by neuromelanin granules inside the neurons. Thus, it was originally also termed the nucleus pigmentosus pontis, meaning "heavily pigmented nucleus of the pons". Neuromelanin within the LC is formed by the polymerization of NA and is analogous to neuromelanin formed in other catecholaminergic nuclei such as the substantia nigra.
The LC-NA system seems to have arisen early on in evolution, as it is highly conserved across vertebrate species, including fish, amphibians, birds, and mammals [66,71]. The size of the LC, however, varies between species and correlates with the total number of neurons in the central nervous system, ranging from 3-10 LC neurons in zebrafish, to 3000 neurons in rodents and approximately 50 000 in humans [71–73].

1.4.2 Morphology and afferent inputs

Neurons of the LC can be divided into two major morphological types, small fusiform cells and larger multipolar cells. Both cell types are found across the LC axis; however, fusiform cells seem to be concentrated in the dorsal LC, and the larger multipolar cells are more commonly found in the ventral LC. These two types have further been subclassified into six different groups, including large multipolar cells within the ventral LC, large multipolar cells in the anterior pole of the LC, fusiform cells in the dorsal LC, posterior pole cells, medium-sized multipolar cells (also known as core cells), and small round cells [74,75]. Dendrites of LC neurons have been shown to extend for a few hundred micrometers outside the nucleus core [75–78] and mainly extend into two distinct, focal pericoerulear zones [79]. These peri-LC zones are heavily targeted by non-catecholaminergic afferent synapses and contain a population of local GABAergic interneurons [79–81]. In addition to α2-adrenergic autoreceptors, these afferent inputs from many brain regions integrate and regulate the activity of the LC [82,83]. Only recently, were the brain-wide afferent inputs to the LC definitively determined by extensive trans-synaptic viral tracing [84], revealing that up to 110 brain regions send projections, with varying strengths, to the LC. Hence, suggesting that the LC is strongly integrated into central networks. Individual LC neurons receive a minimum of 9-15 different inputs. These afferent inputs originate primarily from the neocortex, amygdala, hypothalamus, brainstem, cerebellum and spinal cord [82–84].
Among afferent inputs, most prominently the release of CRF, glutamate and endogenous opioids have been found to alter LC activity [85–87]. In particular, increased release of the stress-related neuropeptide CRF leads to strong activation of the LC-NA system and alters LC mediated functions [88,89]. The LC is innervated by various CRF projections from the extended amygdala, bed nucleus of the stria terminalis, PVN, Barrington's nucleus, and the nucleus paragigantocellularis [90–92], suggesting that these areas are important in mediating stress-dependent LC activation.

1.4.3 Activity patterns

The activity of LC neurons is shaped by the integration of these various inhibitory and excitatory inputs to either suppress or engage LC-mediated noradrenaline release throughout the brain. The spontaneous activity of LC neurons, in particular, varies between sleep and wake periods. While almost silent during sleep, LC activity has been shown to strongly promote wakefulness [93,94]. In addition, LC neurons commonly show little activity during other low vigilance behaviors such as feeding and grooming but respond to novel situations and exploration [95].
LC neurons are able to reliably fire action potentials between 1-25 Hz in two distinct firing patterns, tonic and phasic [96]. Although commonly regarded as separate firing modes, they interact and most likely represent extremes of a spectrum of LC activity and mediate different aspects of LC function. Phasic bursts of LC activity (2-4 spikes at 10-25 Hz) are generally seen in response to salient or novel stimuli of every modality (auditory, visual, somatosensory, or olfactory), most likely to re-orient attention and facilitate behavioral responses [97,98]. In contrast, the tonic firing of LC neurons seems to correspond more to general arousal levels. Especially high tonic LC activity (5-8 Hz) is associated with stress and anxiety [97,99]. In conclusion, different LC firing patterns seem to convey different effects and engage target areas differently [100].

1.4.4 Efferent projections

While long thought to be homologous and widely projecting in a non-specific manner across the entire brain, recent findings show that the LC has a topographical organization of neurons depending on their preferred efferent target, forming various noradrenergic subpopulations [68,101–105]. This subdivision also seems to match the morphological classification of LC neurons across its axis, with anterior and central small round and large multipolar cells preferentially targeting regions of the hypothalamus, dorsal fusiform neurons projecting to the cortex and hippocampus, large ventral multipolar cells projecting to the spinal cord and cerebellum, and medium-sized multipolar core cells projecting more broadly across the brain.

Neurons of the locus coeruleus send out unmyelinated axons that project extensively throughout the brain along the dorsal, ventral, and cerebellar noradrenergic bundles [82,83,106–109], reaching areas from the spinal cord to the neocortex. The dorsal noradrenergic bundle - which exclusively contains axons of the locus coeruleus - projects to various areas, including the hippocampus and neocortex. Noradrenergic projections from the dorsal bundle travel mostly in their ipsilateral hemisphere (up to 95%) and are frequently the only source of NA to innervated areas. In contrast, the ventral noradrenergic bundle arises in a number of noradrenergic nuclei of the pons and medulla - including the locus coeruleus - and innervates the hypothalamus, midbrain, and extended amygdala. The LC innervation of these regions is not as lateralized as that of the dorsal bundle and usually offers not the only but a major source of NA [110]. Lastly, the cerebellar pathway exclusively innervates the cerebellum. There are only a few brain areas that show sparse innervation by projections of the LC, these include mainly dopaminergic areas such as the globus pallidus, striatum, nucleus accumbens, and substantia nigra [103].

Distinct topographical modules of LC neurons - according to their projection targets - have also been found to mediate different functions of the LC-NA system (see 1.4.8 for details). For example, LC neurons projecting to the anterior cingulate and amygdala coordinate aversion and/or anxiety, while those innervating the spinal cord promote analgesia [111]. Apart from CNS structures, the LC also innervates brain microvessels, highlighting its role in central vascular function and blood-brain barrier permeability [112,113].

1.4.5 Neurotransmitter and co-transmitter release

Along LC axons, various bead-like enlargements - known as varicosities - can be found. These varicosities act as presynaptic terminals or “boutons”, and have been identified as sites of NA release [114–116]. While some of these sites form classical synapses with adjacent neurons, most presynaptic boutons do not. In contrast to synaptic transmission, most boutons of LC axons - 50-95% depending on the brain region - are located in the interstitial space without any identifiable postsynaptic contact, allowing them to release NA and other co-transmitters into the extracellular space [117–121]. Thus, LC neurons seem to mainly release NA by volume transmission, suggesting that NA may also have a more diffuse hormone-like action in the brain, allowing it to affect various cell types of the CNS [121–123]. This focus on volume transmission has further been shown for other neuromodulatory monoamine systems - such as dopamine and serotonin - and neuropeptide transmitters [124].

Once an action potential propagates through a noradrenergic axon, presynaptic boutons release small granular and large dense core vesicles containing NA and other

co-transmitters. More recently, discrepancies between dopamine concentrations and actual dopaminergic innervations in brain regions - especially in the hippocampus - have led to the suggestion that LC neurons co-release dopamine [125,126]. Indeed, co-release of NA and DA by noradrenergic terminals has been demonstrated in the cortex and hippocampus [127,128]. Apart from NA and DA, LC neurons were also found to co-release various neuropeptides. Identified neuropeptides include vasopressin, somatostatin, neuropeptide Y, enkephalin, neurotensin, CRF, and galanin [103,129]. These neuropeptides also show distinct expression profiles across the LC; while galanin is expressed widely in around 80% of LC neurons, expression of neuropeptide Y seems to be restricted to a few dorsal LC neurons. In contrast to monoamines, neuropeptides are usually kept in large dense core vesicles, which are most likely released only upon strong LC activation. Additionally, there is further evidence that LC neurons also co-transmit adenosine triphosphate (ATP) and glutamate [130–132].
To what extent these co-transmitters of the LC-NA system affect its function or regulate NA release still remains largely unknown. Nonetheless, it is becoming clear that the LC is able to modulate functions of the CNS not only via adrenergic receptors, but potentially also through dopaminergic, neuropeptidergic, purinergic, and glutamatergic signaling.

1.4.6 Noradrenaline: Biosynthesis, release and degradation

NA is a neurotransmitter and hormone belonging to the catecholamine family, which also includes both dopamine and adrenaline. Within the body, NA is produced by several nuclei of the brain, neurons of the sympathetic nervous system, epithelial Merkel cells, and chromaffin cells of the adrenal glands. NA, like all catecholaminergic neurotransmitters, is synthesized from the amino acid tyrosine [133]. The biosynthesis of NA is mediated by three different enzymes: tyrosine hydroxylase, DOPA decarboxylase, and dopamine beta hydroxylase. Among these enzymes, NA synthesis is mainly regulated by the rate-limiting activity of tyrosine hydroxylase. Within the cytosol of noradrenergic cells, tyrosine is first metabolized to L-DOPA by tyrosine hydroxylase and then to dopamine - the direct precursor of NA - by DOPA decarboxylase. Dopamine is then transported into vesicles by the vesicular monoamine transporter and metabolized to NA by dopamine beta hydroxylase. These vesicles store NA in extraordinarily high concentrations of up to 100 mM; in comparison, only a few micromolar remain in the cytosol [134]. After vesicular release into the extracellular space or synapse, NA exerts its function by binding to various adrenergic receptors to mediate different functions (see following subchapters). Unbound NA is further taken up by the NA transporter (NAT) and recycled, or it is directly degraded [135]. Degradation of NA and other catecholamines is performed by the two enzymes catechol-o-methyltransferase and monoamine oxidase, which first metabolize NA to normetanephrine and then to its main metabolite, 3-methoxy-4-hydroxyphenylglycol (MHPG). MHPG is the final degradation product of NA and is further transported into the blood and excreted.

1.4.7 Adrenergic Receptors and Transporters

The actions of NA are mediated through its availability and binding at adrenergic receptors and transporters throughout the body. Among these mediators of noradrenergic function, one transporter and nine different receptors have been identified. All of these receptors belong to the family of G protein-coupled receptors (GPCRs). GPCRs are integral membrane proteins and represent the largest and most functionally diverse family of

cell-surface receptor proteins. Adrenergic receptors can be divided into three distinct subclasses: α1-, α2- and β-adrenergic receptors. These three subclasses engage different intracellular signaling cascades and mediate various functions of the LC-NA system.

1.4.7.1 Noradrenaline transporter

Within the CNS, the activity of NA is further regulated by its availability in the extracellular space. The NA transporter (NAT, also known as NET) belongs to the integral membrane neurotransmitter transporters and is expressed by noradrenergic neurons and glial cells. The NAT is important for maintaining presynaptic and postsynaptic NA homeostasis and regulating the longevity of NA action [136,137]. It is encoded by the solute carrier family 6 member 2 (Slc6a2) gene and - alongside other monoamine transporters - belongs to the family of Na^+/Cl^--dependent transporters. When extracellular NA binds to the NAT, it is transported across the membrane with Na^+ and Cl^- ions back into the cytoplasm, resulting in the termination of noradrenergic signaling [137,138]. NA transport is maintained by the key ion pump Na^+/K^+-ATPase, which maintains a Na^+ concentration gradient across the plasma membrane. Apart from the Na^+ gradient, NAT activity is also regulated through phosphorylation by a number of intracellular signaling molecules [139]. In addition to NA, the NAT has also been demonstrated to mediate dopamine reuptake [140,141].
The NAT is also a popular target for drugs such as used to treat major depression and attention deficit hyperactivity disorder, as well as stimulants like cocaine and amphetamine [141,142].

1.4.7.2 α1-Adrenergic Receptors

α1-Adrenergic receptors have an intermediate affinity (~300 nM) for NA [143] and can further be divided into the three subtypes $\alpha1_A$, $\alpha1_B$ and $\alpha1_D$. Within the central nervous system all three subtypes of α1-adrenergic receptors have been detected. However, expression of $\alpha1_A$, $\alpha1_B$ and $\alpha1_D$ varies across brain regions and cell types. Overall, cortical areas seem to express all three subtypes, while most other brain areas in the CNS seem to predominantly express $\alpha1_A$ or $\alpha1_D$, while only the thalamus shows strong $\alpha1_B$ expression [144,145]. However, detailed expression on the cell-specific level has not been fully resolved within the CNS.
Intracellular effects of all α1-adrenergic receptor subtypes are mainly mediated through their coupling to the $G_{q/11}$ G-protein family [145,146]. Activation of the $G_{q/11}$ is initiated in response to NA binding and leads to a phospholipase C (PLC) mediated increase in the second messengers diacylglycerol (DAG) and inositol trisphosphate (IP_3). IP_3 further diffuses into the cytosol and triggers Ca^{2+} release from intracellular stores within the endoplasmic reticulum. Both intracellular calcium and DAG are strong activators of protein kinase C (PKC), which induces further phosphorylation cascades to activate Ca^{2+} channels, Na^+/H^+ exchangers, and modulation of K^+ channels. Overall, α1-adrenergic receptor activation has an excitatory effect on its target cells. However, these signaling mechanisms can differ slightly among α1-adrenergic receptor subtypes, as will be discussed below in section 1.4.7.5.

1.4.7.3 α2-Adrenergic Receptors

In mammals, the α2-adrenergic receptors can be further classified into three subtypes: $\alpha2_A$, $\alpha2_B$, and $\alpha2_C$. Among adrenergic receptors, α2-receptors possess the highest affinity for NA (~50 nM) [143] and due to their strong expression in noradrenergic neurons, they have long been thought to act as an autoreceptor and mediate a negative feedback loop in response to NA release. However, evidence has shown that these receptors are also expressed outside of the noradrenergic system, where they mediate inhibition of various cell types through the binding of NA [147]. All three subtypes are expressed within the brain but show regional differences [145,148,149]. The $\alpha2_A$ subtype is predominantly expressed within noradrenergic neurons of the LC, while the $\alpha2_B$ - similar to the $\alpha1_B$ - seems to be exclusively expressed in the thalamus. Instead, the $\alpha2_C$-receptor is widely expressed across the cerebral cortex, hippocampus, basal ganglia and olfactory tubercle. In contrast to α1, α2-adrenergic receptors are coupled to the G-protein family G_i /G_o, which upon activation results in the inhibition of adenylyl cyclase mediated cyclic adenosine monophosphate (cAMP) production, activation of K^+-ion channels, and inhibition of voltage-gated Ca^{2+} channels [148,150,151]. Thus, in contrast to the other adrenergic receptor classes, α2-adrenergic receptors mediate the inhibitory effects of NA.

1.4.7.4 β-Adrenergic Receptors

There are 3 subtypes of β-adrenergic receptors: β1, β2 and β3. However, only β1 and β2 are widely expressed within the central nervous system of mammals, while the β3-subtype in comparison is mostly restricted to the periphery [152–156]. Expression of β1 and β2 receptors often overlaps within the brain; however, the β1-receptor subtype was found to be more highly expressed in the rodent cerebral cortex, piriform, amygdala, thalamus, caudate putamen, globus pallidus, substantia nigra, and superior colliculus, while β2-receptor expression was elevated in the parietal, frontal, and piriform cortex, the medial septal nuclei, the olfactory tubercle, and the midbrain.
β-adrenergic receptors are mainly found postsynaptically and - compared to α-adrenergic receptors - display rather low NA affinity (~700-800 nM) [143,157,158]. Once NA is bound, β-adrenergic receptors commonly signal through the G_s protein [146], which - in contrast to α2-adrenergic receptors - activates adenylate cyclase and thus increases the intracellular concentration of cAMP, a potent second messenger. cAMP in turn mediates the activation of various protein kinases, including protein kinase A (PKA), signal-regulated kinases, mitogen-activated protein kinase (MAPK), and mammalian target of rapamycin (mTOR). All β-adrenergic receptors ultimately also lead to the activation of the cAMP response element binding protein (CREB) that mediates protein transcription [159–163]. Moreover, recent findings indicate that β-adrenergic receptors can even induce long-term epigenetic modifications [164].
In addition, cAMP triggers activation of cyclic nucleotide-gated nonspecific cation channels, increasing the intracellular Ca^{2+} concentration [165,166]. Therefore, β-receptors generally increase the excitability of target cells and are able to engage transcription.

1.4.7.5 Adrenergic receptor subtypes and their dynamics

Adrenergic receptors mediate the function of the LC-NA system across the CNS; however, noradrenergic responses are not static but rather dynamic. Through local regulation of NA availability and differences in expression, translocation, affinity, signaling, and desensitization or internalization of adrenergic receptor subtypes, responses to NA can vary between brain areas and cell types. Research into these topics is still very limited and offers the next big challenge in understanding central noradrenergic actions in more detail. In particular, differences between receptor subtypes of the α1-, α2- and β-adrenergic receptor classes - such as the $\alpha1_A$, $\alpha1_B$ and $\alpha1_D$ subtypes- are barely understood in the CNS. Adrenergic receptors are classified based on their affinity for various ligands and their signaling pathways via G-proteins, including $G_{q/11}$ for α1-receptors, G_i/G_o for α2-receptors and G_s for β-receptors. However, there are alterations for some of these aspects among receptor subtypes [145,167]. While the affinities for NA of the three adrenergic receptor classes differ (α2 > α1 > β) [143], differences can also be found between subtypes of the same class. Especially among β-adrenergic receptors, where β1 has a higher affinity for NA than β2 [168].

Furthermore, there is evidence that adrenergic receptor subtypes can also bind distinct members of a G-protein family, leading to differences in the mediated signaling cascades. The class of α1-receptors commonly increases intracellular concentrations of Ca^{2+} through $G_{q/11}$ signaling; however, it was found that $\alpha1_A$-AR-mediated signaling involved Ca^{2+} influx through voltage-gated channels, whereas $\alpha1_B$-AR-mediated Ca^{2+} increase was induced intracellularly through phospholipase C activation [169,170]. Binding to different G-proteins would potentially also explain various other signaling mechanisms attributed to α1-adrenergic receptors, such as activation of phospholipases A2 and D, MAPK, and others [169,171–173]. Similar signaling differences were also discovered among subtypes of α2- and β-adrenergic receptors [151,152,174,175]. Interestingly, evidence suggests that the β2-subtype - in contrast to β1 - can dual signal through G_s and G_i proteins and thus mediate excitation or inhibition of target cells. In addition, activity of β1-receptors was found to be influenced by the membrane potential, while β2 activity was independent from voltage changes across the membrane [176].

Adrenergic receptors only become active once they are incorporated into the cellular membrane. The cell surface was formerly thought to be the GPCRs primary location. However, more recent findings show that many GPCRs are not always expressed on the cell surface membrane, but instead are also found in intracellular compartments [177]. There has been some evidence that cellular trafficking to and from the cellular membrane is regulated differently between adrenergic receptor subtypes. For example, differences in membrane incorporation have been found between $\alpha1_A$, $\alpha1_B$ and $\alpha1_D$ receptors. Whereas $\alpha1_B$ seems to be directly transported to the cell membrane, $\alpha1_A$ receptors are found at the membrane and in intracellular compartments, and $\alpha1_D$ receptors are mainly retained in the cytosol [178,179]. Similarly, $\alpha2_C$ receptors - unlike $\alpha2_A$ and $\alpha2_B$ - were found primarily within intracellular compartments and are rarely located on the plasma membrane [180]. Among β-adrenergic receptors, the β1 and β3 subtypes were shown to be localized intracellularly and on the cell membrane, while the β2-receptor was only found at the membrane of cardiomyocytes [181]. This suggests that NA signaling at certain adrenergic receptors can be modulated on a cellular level. However, the specific processes and signals governing the retention and trafficking of GPCRs within cells are still largely unknown. One such process was suggested

for the $\alpha1_D$ receptor, where truncating of the N-terminus was found to significantly boost receptor expression at the membrane [182].
All GPCRs are further desensitized and internalized after agonist binding and signaling [183]. Adrenergic receptor subtypes also show differences in this aspect. Among α1-adrenergic receptors, the internalization rate of the $\alpha1_A$ subtype was found to be slower than that of the $\alpha1_B$-receptor [178]. It was further demonstrated that the $\alpha2_A$-receptor - in contrast to $\alpha2_B$ and $\alpha2_C$ - does not internalize after agonist exposure [180]. For β-receptors, the β1-subtype was found to be active longer at the membrane compared to the β2-subtype due to a slower internalization rate [184]. Additionally, interactions with other proteins and receptor homo- and heterodimerization further alter adrenergic receptor signaling and trafficking [167,184–186].
Considering expression, dynamics, and cellular localization of adrenergic receptors, it suggests that most noradrenergic effects within the CNS are mediated through signaling at $\alpha1_A$, $\alpha1_D$, $\alpha2_A$, $\alpha2_C$, β1 and β2 adrenergic receptors. Furthermore, it was found that LC-mediated effects follow an inverted-U relationship, resembling the Yerkes-Dodson relationship between arousal and performance [187]. This further suggests that optimal performance is only achieved within a certain range of LC activity, but is suboptimal if LC activity is too low or too high. On the molecular level this translates into regulation of NA concentrations to mediate either effects at α2-adrenergic receptors (low NA levels), α2- and α1-adrenergic receptors (intermediate NA levels) or α2-, α1-, and β-adrenergic receptors (high NA levels). Unbalanced activity of the LC-NA system - especially within stress circuits - is therefore commonly associated with neurological disorders (see 1.4.9). Various compositions of these adrenergic receptors thus allow for a heterogeneous response to NA across the body, which highlights the need for a better understanding of tissue-specific receptor expression.

1.4.8 Unravelling LC function across the brain

Experiencing and processing a stressful situation is a multimodal, complex event that engages various brain regions and neurotransmitter systems [14,21,188,189]. In a matter of seconds, the brain has to perceive a threat, decide on a response, and execute it. Given the nature of the stressor, this can involve a variety of different brain areas; however, a few have emerged as predominantly stress sensitive and mediate important functions of the stress response. Alongside the LC, these include the prefrontal cortex, the amygdala, the hippocampus and areas of the hypothalamus. Together, these areas form a network that regulates important cognitive functions in response to stress. The LC has long been known to respond strongly to alarming, threatening, or noxious stimuli and therefore to a broad array of stressors [190]. In addition, the LC-NA system is ideally built to coordinate and modulate the activity of this stress network, as the LC-NA system is not suited to regulate one specific process but rather - alongside other neuromodulators - integrates and broadcasts information widely to switch brain states [191,192].
Hence, it has most likely evolved to rapidly induce a state that promotes responses to stress. This includes changes in various cognitive processes, such as increased arousal, wakefulness, neuronal protection, attention, learning and memory, emotions, behavioral flexibility and cognitive control [97,99,102,190,193–198], suggesting a role of the LC-NA system in the optimization of behavior to facilitate responses to a challenging environmental situation [97].

1.4.8.1 Effects on peripheral stress systems

The LC directly regulates HPA and SNS function to some degree. Noradrenergic innervation of the PVN has been demonstrated to excite CRF-containing neurons through α1-adrenergic receptors, leading to the activation of the HPA axis [199–201]. However, the majority of NA terminals in the PVN seem to originate within A1 and A2, suggesting that the LC is not the main noradrenergic driver of HPA activation [202–204]. Instead, the LC seems to be important in regulating PVN-mediated growth hormone release, which plays an important role in cytochrome P450 activity within the liver [205,206]. These enzymes are crucial for the metabolism of high-activity endogenous substrates, such as sex- and neurosteroids, arachidonic acid, monoaminergic neurotransmitters, vitamins, and non-endogenous drugs and toxins [207,208].
Alongside some projections from A5 and A7, the LC also provides the major noradrenergic innervation to the spinal cord. LC innervation is seen along all parts of the spinal gray matter, with a particular focus on the dorsal horn [209–211]. These LC projections seem to largely mediate anti-nociceptive functions, coordinate motor performance, alter pupil size, and influence SNS activity [111,212–218].

1.4.8.2 Effects on attention and flexibility: the prefrontal cortex

The prefrontal cortex plays an important role in "top-down", higher-order guidance of thought, attention, behavior and emotion. This includes various cognitive and executive tasks such as working memory, decision making, inhibitory response control, and attentional set-shifting [219,220]. The ventral medial prefrontal cortex (mPFC), in particular, appears to assess behavioral control over a given situation and either inhibit (controllable situations) or activate (uncontrollable situations) stress-responsive brainstem and limbic structures [221]. Thus, making it an important structure for mediating stress resilience.
The PFC is heavily innervated by LC axons through the dorsal noradrenergic bundle [222–224]. Noradrenergic transmission in the PFC seems to be mainly volume based - as only one out of 12 varicosities form synapses with neurons of the PFC [225] - and acts through various adrenergic receptors across prefrontal cortical layers. Most prominently, the $\alpha 2_A$-receptor subtype - and at lower levels, the $\alpha 2_C$-subtype - is expressed not only on LC axons but also on neurons and glia of the PFC [225,226]. These α2-adrenergic receptors are found across the cortical layers of the PFC but seem to be especially densely expressed in layer I of the primate PFC [227]. A similar distribution is found for α1-adrenergic receptors, whereas expression of $\alpha 1_A$ and $\alpha 1_D$ predominates across layers I, IV, and VI [144,227]. However, more recent findings have shown that within the medial prefrontal cortex, α1-adrenergic receptor distribution is segregated [228], demonstrating that $\alpha 1_A$ is predominantly expressed in deeper layer VI and $\alpha 1_D$ is found mostly in intermediate layers II and III. In general, α1-adrenergic receptors have been found widely expressed among pyramidal and GABAergic neurons of the PFC [229], suggesting that they play a major role in regulating neuronal excitability. Furthermore, both the β1- and β2-adrenergic receptors were found to be expressed within the PFC. In contrast to α-receptors, β-adrenergic receptor expression was found to be overall weaker but concentrated in thalamic input layers IIIa and IIIb of the prefrontal cortex [227]. Nevertheless, how the specific segregation of various adrenergic receptors alters the function of each cortical layer of the PFC is still under investigation.

Overall, evidence suggests that the LC-NA system alters higher cognitive function through the PFC. While low to moderate NA levels were found to improve working memory and cognitive performance through $\alpha2_A$-receptors [230–232], elevated NA concentration - through stress-dependent and phasic activation of the LC [233,234] - impaired working memory through α1-adrenergic receptors, but promoted both focused and flexible forms of attention [143,198,235,236]. This attentional control seems to be mediated through the LC's projection to the dorso-medial PFC and orbitofrontal cortex, and increases goal-directed behaviour while decreasing impulsivity [237]. Furthermore, the PFC also plays an important role in conflict-induced behavioural adjustments [238,239], and increased NA release has been shown to improve behavioural flexibility through the PFC [240]. In contrast to α-receptors, β-adrenergic receptors have been shown to be especially important for PFC mediated aversive learning and associated memory formation and retrieval [241–244].

1.4.8.3 Effects on anxiety and memory: the amygdala

While stress - especially through monoaminergic and glucocorticoid inputs - generally impairs normal function of the prefrontal cortex, it strengthens function in more primitive areas of the brainstem and limbic system, such as the amygdala. The amygdala, a set of nuclei located within the temporal lobe, is essential in the regulation of adaptive behavior and the primary entry point for processed sensory information into the limbic system [21,245,246]. Similar to the prefrontal cortex, the amygdala is extensively innervated by monoaminergic axons, which increase amygdalar levels of NA [247,248], serotonin [249,250], and dopamine [251,252] during stress. Stress-dependent activation of the amygdala further facilitates visceral, motor, and memory processes [253]. In particular, amygdala projections from the central, medial, and basolateral subnuclei stimulate hypothalamic regions, resulting in the activation of the HPA axis and consequent glucocorticoid release [254]. Additionally, the amygdala regulates the function of various brainstem nuclei and mediates several autonomic functions and fear responses such as startle and freezing behavior [255–259].
Converging findings from animal and human studies also provide compelling evidence that the amygdala plays a critical role in acquiring and retaining long-term memories of emotional experiences, and is essential in the formation of long-term adaptive responses to stress. In particular, the basolateral nucleus of the amygdala has been found to mediate these effects on stress-dependent memory consolidation [44,246,260–263], through its projections to the nucleus accumbens, hippocampus, entorhinal and insular cortex [44,264–267].
The amygdala receives dense noradrenergic innervation from the LC, especially within the basolateral and central amygdala [268–270]. Noradrenergic modulation of amygdalar function is mainly mediated through signaling at $\alpha1_A$, $\alpha2_A$, $\alpha2_C$, β1 and β2 adrenergic receptors [145]. The basolateral amygdala is of special interest for noradrenergic regulation, as it integrates sensory information from the cortex and thalamus to assess risks and generate appropriate defensive responses to emotionally salient environmental stimuli, especially those perceived as stressful [271–274]. The LC has been found to mediate stress-induced activation of the BLA [247,275]. The projection from the LC to the BLA does not only mediate immediate changes in anxiety-related behaviors [276,277], but also influences the consolidation of emotionally arousing experiences. The influence of NA and other stress mediators on memory formation have been studied in detail within the BLA [278]. NA has been found to facilitate consolidation and strengthen retention of emotionally arousing memories through β-adrenergic receptors [44,275], whereas blocking these

receptors impairs memory consolidation [279,280]. In particular, this enhancing effect of NA seems to be mediated through the activation of cAMP signaling in cells of the BLA [281], suggesting a potential role for NA-mediated changes in transcription in memory consolidation (see Chapter 3 and Discussion). Furthermore, research into BLA-mediated memory consolidation has also offered insights of how NA interacts with other stress mediators to mediate this important aspect of the stress response. Glucocorticoids also promote BLA-mediated memory consolidation through signaling at the GR [282,283]. This effect was further found to be mediated through potentiation of noradrenergic signaling at β-adrenergic receptors, as blocking these receptors abolishes the enhancing effect of glucocorticoids on memory [278,284,285]. Synergistically, this enhancement of noradrenergic activity by glucocorticoids is mimicked by CRF in the BLA [286]. In conclusion, β-adrenergic receptor signaling within the BLA, and its regulation by other stress-mediators, seems to be essential for stress-dependent consolidation of memory [278]. Compared to other CNS areas, expression of α2-adrenergic receptors is especially high in the amygdala [287,288], and together with α1 receptors, seem to negatively regulate effects of β-adrenergic receptors by decreasing BLA activity [287–290]. Moreover, this suggests that LC exerted control over BLA activity is finely regulated to avoid detrimental levels of anxiety and traumatic memory formation.

In contrast to the BLA, LC mediated effects within the extended amygdala are less well understood, as these areas also receive noradrenergic innervations from the A1 and A2 nuclei [270,291]. Within the central amygdala, NA has been found to increase glutamatergic transmission, which leads to altered behavioral responses to stress through α1-adrenergic receptors [292,293]. In addition, areas of the extended amygdala and basolateral amygdala play an important role in motivation and emotional learning, which have been found altered by NA, especially in addiction [294,295]. However, if these effects are mediated directly by the LC is unknown. Instead, the central amygdala seems to be more involved in regulating LC activity [296].

1.4.8.4 Effects on learning and memory: the hippocampus

One of the limbic brain areas particularly well-studied in the context of stress - and its molecular and behavioral consequences - is the hippocampus. It is classically thought of as an essential structure for episodic, declarative, spatial, and contextual learning and memory [297–300] but has also been shown to be involved in the processing of painful stimuli, anxiety, and nociception [301]. These hippocampal functions can be divided along a dorso-ventral axis, which shows differences in function and connectivity [302,303]. Whereas the dorsal hippocampus (dHC) is thought to be involved in spatial navigation, memory, and conceptual information learning, and the ventral hippocampus (vHC) is involved in regulating emotional processing and anxiety [304–307]. The hippocampus is highly interconnected with the mPFC and amygdala, forming a stress-sensitive circuit, and was found early on as a key hub in the central stress response - due to its high levels of GR expression - and plays a major role in inhibitory behavioral feedback during the stress exposure [308–311]. In addition, the hippocampus - in combination with the amygdala - forms detailed memories of stressful experiences through changes in synaptic plasticity [312,313], a crucial process for long-term adaptations in the response to stress. Together, this makes the hippocampus an important site for decision-making in challenging situations by committing and accessing relevant information in the form of memories [314].

Noradrenergic innervation of the hippocampus arises exclusively from neurons located in the dorsomedial LC [84,315]. Moreover, the noradrenergic innervation of the ventral hippocampus was found to be slightly stronger compared to the dorsal hippocampus. Noradrenergic innervation also shows further segregation across hippocampal subregions, among which the subiculum, dentate gyrus, and CA3 are especially densely innervated [315–317]. The hippocampus seems particularly sensitive to NA, as it was estimated to contain 2.1 million noradrenergic varicosities per mm^3 of tissue, which is almost double that of the cerebral cortex [316].
The hippocampus expresses most adrenergic receptor subtypes, with the highest expression of $\alpha1_A$, $\alpha1_D$, $\alpha2_A$, $\alpha2_C$, β1 and β2 [145,318]. More recent advances in single-cell sequencing have further allowed detailed hippocampal assessment of the cellular localization of these receptors. Single-cell evidence suggests that among hippocampal cell types, most adrenergic receptors - $\alpha1_A$, $\alpha2_A$, $\alpha2_C$ and β1 - seem to be present in astrocytes, while excitatory and inhibitory hippocampal neurons instead mainly express $\alpha1_D$, $\alpha2_C$ and β1 receptors. Furthermore, expression of β2-receptors seems to be restricted to microglia and vascular cells [311,319,320].
However, noradrenergic action on hippocampal function has been mainly studied in terms of neuronal activity. The LC-NA system was found to play an important role in the encoding, consolidation, retrieval, and reversal of hippocampal memory [321,322]. These effects are mediated mainly through the manipulation of neuronal activity and synaptic plasticity. LC activity was found to boost the signal-to-noise ratio at hippocampal pyramidal cells by increasing their firing through β-adrenergic receptors [323–326], in contrast, noradrenergic effects on inhibitory neurons seem to be mediated bimodally through α-receptors, where α1 excites and α2 inhibits these neurons [326–328]. Further, NA also mediates long-term changes in synaptic plasticity - such as long-term potentiation (LTP) and long-term depression (LTD) - through β-adrenergic receptor signaling and transcription [329–335]. In addition, evidence suggests that LC dependent effects on memory are also influenced through the co-release of dopamine and its action on D_1/D_5 receptors [128,336,337].
Together, these LC-mediated mechanisms allow for facilitated memory formation of salient, novel, and aversive experiences to promote learning in the context of stress [338–341].

1.4.9 The LC-NA system in aging and neurological disorders

1.4.9.1 Aging and neurodegenerative disorders

The LC-NA system was found to be affected by aging across the lifespan. Significant anatomical alterations in noradrenergic signaling induced by aging, include decreases in LC neuronal numbers, efferent projections, NA uptake, noradrenergic synapses and receptors [342–347]. It was suggested that some of these changes might occur due to the LC's vulnerability to toxin exposure - because of its long, unmyelinated axons and close proximity to blood vessels and the 4th ventricle - and be related to cognitive decline and the emergence of neurodegenerative diseases in later life [348–350]. Neurodegeneration of the LC has been found to be an early occurrence of down syndrome [351], synucleinopathies - such as Parkinson’s disease (PD) [352–354] - and tauopathies like Alzheimer’s disease (AD) [355–358]. There is further evidence that aberrant protein tangles and cognitive dysfunction might spread across the axons of the LC throughout the brain [359–362]. Thus, early detection of LC degeneration could be used as a potent biomarker to identify the onset of neurodegenerative diseases [363]. LC stimulation was further shown to improve some

Alzheimer symptoms in rodents [364]. Regular environmental LC stimulation and the neuroprotective actions of NA are also hypothesized to reduce the risk of developing AD across the lifespan [365,366]. Therefore, a better understanding of the vulnerability of LC neurons might offer new therapeutic targets for preventing neurodegenerative disorders.

1.4.9.2 Chronic stress and stress-related disorders

Exposure to chronic stress is known to alter the function of the LC-NA system, including changes in noradrenergic responsiveness within the brain [367–374]. In particular, chronic stress disinhibits LC activity through blunted glucocorticoid responses and downregulation of autoinhibitory $\alpha 2_A$-receptors within the LC, suggesting that LC neurons become hyperactive in response to consecutive stressors [369,375–377]. Across species, evidence suggests that there is a strong link between LC hyperactivity and the risk of developing stress-related disorders, such as pathological anxiety, panic disorder, and PTSD [378,379]. Hyperactivity of LC neurons will ultimately tip the fine balance between adaptive and maladaptive mechanisms and potentiate stress responses within the PFC, amygdala, and hippocampus, which mediate many underlying disease symptoms [277,380–384].

1.4.9.3 Major depressive disorder

Abnormal levels of NA - and other monoamines - are also prevalent in mood disorders, such as major depressive disorder. However, in contrast to elevated NA levels in stress-related disorders, depressive disorders are marked by chronically low NA levels, despite increases in tyrosine hydroxylase and LC activity [385–387]. Evidence from animal models also shows that genetic knockout of the NAT prevents stress-induced depressive behaviors, while NA depletion increases the probability of depressive relapses in humans. Thus, NA reuptake inhibitors are commonly used to treat depressive symptoms in the clinic. The underlying cause of depressive disorders is still unknown, however it was proposed that it emerges through abnormal regulation of LC firing patterns. In particular, reduced tonic NA release throughout the brain is thought to alter NA sensitivity in affected areas, which leads to exaggerated NA responses and behavioral depression [388–390].

1.4.9.4 Attention deficit and autism spectrum disorders

As a key player in regulating attention, LC function was also found to be affected in attention deficit hyperactivity disorder (ADHD) and autism spectrum disorder (ASD). Similar to depression, unbalanced monoaminergic transmission in the brain has been associated with ADHD. While reduced tonic activity of the LC is found in major depressive disorder, ADHD seems to be associated with exaggerated tonic firing of LC neurons with infrequent phasic activity [391] and might in particular alter PFC control over attention [237,392]. This mechanism might be shared in individuals with ASD, who show similar atypical activity of the LC-NA system and attentional deficits [393]. In human patients, pupillometry has proven a valuable noninvasive tool to study these altered LC activity patterns and potentially offers a simple way to detect ADHD and ASD in humans early on [394–396]. Both ADHD and ASD might emerge through developmental alterations in LC function, affecting neuronal activity and postsynaptic receptor expression [397,398]. However, the molecular causes of ADHD and ASD still remain elusive.

1.5 Current challenges in LC research

While the role of the LC-NA system in behavior has been unraveled to a large extent over the last 60 years, little is known about how this system mediates its effects on a molecular level. The involvement of the LC-NA system in various clinical conditions further highlights the need for a better understanding of circuit and molecular mechanisms engaged by the LC in health and disease. A few key questions have emerged as crucial in resolving LC function, including: 1) How does the LC-NA system differ between sexes? 2) Which LC modules/circuits are recruited by different stressors?; 3) How do alterations in local NA concentrations - through tonic and phasic firing patterns - engage different functions across the brain?; 4) How does co-transmitter release contribute to LC function?; 5) Which mechanisms regulate local adrenergic receptor composition and trafficking?; 6) Which cells and molecular pathways mediate long-term alterations induced by NA?; 7) How are these mechanisms altered by detrimental stress exposure?

1.6 Aims of the thesis

1.6.1 Facilitating LC research with pupillometry

The rise of novel optogenetic and pharmacogenetic techniques in the field of neuroscience finally allows us to tackle some of these questions. However, due to the size and location of the LC, successful manipulation by these methods can be challenging and require adequate validation. Commonly used validation methods - such as electrophysiological and immunohistochemical assessments of neuronal activity - are not only done *postmortem* but are also time-consuming, expensive, and not always reliable. While there are often no better alternatives available, the widespread projections of the LC allow one to exploit physiological functions to determine successful manipulation. Changes in pupil size are an important autonomic reflex mechanism of the stress response that improves visual perception [399,400] and have been shown to correlate with LC activity [401].
Through its projections to the Edinger Westphal nucleus (EW) and the intermediolateral nucleus (IML), the LC is able to inhibit parasympathetic control over the pupil and induce pupil dilation [60,83,214,402]. Investigation into noradrenergic regulation of pupil size also has considerable translational potential, as it offers a tangible biomarker in disorders related to abnormal noradrenergic function [365,403,404]. In chapter 2, I included my work on pupillometry, where we demonstrate how pupillometry can be easily accessed in rodents and how it provides a much faster and better validation method in response to various LC manipulations.

1.6.2 Dissecting the transcriptomic stress response

A well-studied consequence of stress exposure is a structural remodeling of neural architecture, especially across the PFC, amygdala and hippocampus [308,405]. This includes an elaborate transcriptomic response across the brain [406,407], which is needed for homeostasis and long-term adaptations in response to stress, such as memory formation [408,409]. Stress-induced transcriptional changes in the brain were long thought to be exclusively regulated by excitatory amino acids and glucocorticoids [310,410,411]. However, the contribution of other stress mediators - especially the LC-NA system - has been largely neglected. Transcriptomic alterations were found across various stress-related diseases [412–414], and especially in the hippocampus, which plays an important role in stress susceptibility [415–417]. In chapter 3, I showcase our extensive work on the characterization of LC-NA-mediated transcriptomic changes in the hippocampus and the identification of potential relevant molecular noradrenergic pathways to modulate hippocampal function during stress.

Chapter 2. A complete pupillometry toolbox for real-time monitoring of locus coeruleus activity in rodents

Mattia Privitera[*1,6], Kim David Ferrari[*2,6], Lukas M. von Ziegler [1,6], Oliver Sturman [1,6], Sian N. Duss[1,6], Amalia Floriou-Servou[1,6], Pierre-Luc Germain [1,6], Yannick Vermeiren [3,4], Matthias T. Wyss [2,6], Peter P. De Deyn [3,4,5], Bruno Weber[#2,6], Johannes Bohacek[#1,6]

[1] Laboratory of Molecular and Behavioral Neuroscience, Institute for Neuroscience, Department of Health Sciences and Technology, ETH Zurich, Switzerland

[2] Experimental Imaging and Neuroenergetics, Institute of Pharmacology and Toxicology, University of Zurich, Switzerland

[3] Department of Biomedical Sciences, Laboratory of Neurochemistry and Behavior, Institute Born-Bunge, University of Antwerp, Wilrijk (Antwerp), Belgium

[4] Department of Neurology and Alzheimer Center, University of Groningen and University Medical Center Groningen (UMCG), Groningen, Netherlands

[5] Department of Neurology, Memory Clinic of Hospital Network Antwerp (ZNA) Middelheim and Hoge Beuken, Antwerp, Belgium

[6] Neuroscience Center Zurich, ETH Zurich and University of Zurich, Switzerland

* = equal contribution

= corresponding authors:

Johannes Bohacek: Johannes.bohacek@hest.ethz.ch

Bruno Weber: bweber@pharma.uzh.ch

Published: 06 July 2020, Nature Protocols volume 15, pages 2301–2320 (2020)
DOI: https://doi.org/10.1038/s41596-020-0324-6

2.1 Abstract

The locus coeruleus (LC) is a region in the brainstem that produces noradrenaline and is involved in both normal and pathological brain function. Pupillometry, the measurement of pupil diameter, provides a powerful readout of LC activity in rodents, primates and humans. The protocol detailed here describes a miniaturized setup that can screen LC activity in rodents in real-time and can be established within 1–2 d. Using low-cost Raspberry Pi computers and cameras, the complete custom-built system costs only ~300 euros, is compatible with stereotaxic surgery frames and seamlessly integrates into complex experimental setups. Tools for pupil tracking and a user-friendly Pupillometry App allow quantification, analysis and visualization of pupil size. Pupillometry can discriminate between different, physiologically relevant firing patterns of the LC and can accurately report LC activation as measured by noradrenaline turnover. Pupillometry provides a rapid, non-invasive readout that can be used to verify accurate placement of electrodes/fibers in vivo, thus allowing decisions about the inclusion/exclusion of individual animals before experiments begin.

2.2 Introduction

The locus coeruleus (LC)–noradrenaline (LC-NA) system supports a vast number of fundamental brain functions. It modulates attention, arousal, synaptic plasticity and memory formation, it mediates the stress response, regulates sleep/wake states and is involved in cerebral blood flow regulation [1-3]. Dysfunction of the LC-NA system underlies numerous psychiatric pathologies including depression, anxiety disorders, stress susceptibility, PTSD and Down syndrome [4-7], and the loss of LC neurons is the earliest pronounced feature of both Parkinson's and Alzheimer's disease [8-12]. Despite its importance, the location of the LC deep in the brainstem, as well as its small size (~1,500 neurons in each hemisphere in mice and ~20,000 in humans) [13,14] make systematic investigations of this nucleus technically challenging in both rodents and humans. Recent advances in optogenetics and pharmacogenetics enable precise labeling and manipulation of LC cells in rats and mice, yet proper placement of electrodes or optic fibers is still very challenging due to the size and location of the LC. Typically, researchers assess efficient targeting of the LC by post mortem histology/immunohistochemistry, leading to post-hoc exclusion of individual animals. While pupillometry (i.e., the measurement of changes in pupil diameter) is routinely applied for assessing LC function in humans and primates [15-20], its use in rodent models is not yet commonplace. Nonetheless, recent work shows that pupillometry provides an in vivo assessment of LC activity in awake or anesthetized rats and mice [21-25]. In this protocol, we describe how to set up and use a pupillometry system, which we developed and previously used to assess modulation of the LC-NA system in awake and anesthetized mice [24,25].

2.2.1 Development of a miniaturized low-cost pupillometry setup

Commercially available setups (https://neuroptics.com/) to measure pupil diameter are not only costly but also bulky, preventing pupil measurements when space is limited, such as during stereotaxic surgery in rodents or in head-restrained two-photon calcium imaging setups. We established a custom-built pupillometry setup using ultra low-cost Raspberry Pi computers and cameras [24,25]. This customizable system requires minimal space and

seamlessly integrates even into narrow experimental setups (Fig. 1a–c). We use MATLAB-based data analysis to facilitate a fast and simple measurement of pupil radius over time. In our experience, this is sufficient to validate accurate stimulation of the LC. However, reliable and high-quality pupil tracking requires successful handling of various experimental constraints, including poor contrast under low-light conditions, spontaneous pupil movement and interference from reflections. Therefore, as an alternative to the MATLAB-based analysis, we have also used the recently described motion-tracking software DeepLabCut (DLC) [26,27] for precise, robust and versatile pupil tracking. We developed a user-friendly, web-based Pupillometry App to facilitate data visualization and analysis. Here, we provide a detailed workflow that describes every step from building the setup to data collection, data processing and data analysis (Fig. 1d). All of the required software is freely available online, allowing the tracking, analysis and quantification of pupil size to be performed using any laboratory computer. We also provide protocols describing how to perform pupillometry recordings in darkness (Box 1), to measure pupil changes in response to light stimuli (Box 2) and to quantify relative as well as absolute pupil size (Box 3). In ‘Anticipated results’, we demonstrate that pupillometry is sensitive enough to discriminate between different physiologically relevant firing patterns of the LC, and that it can accurately report LC activation as measured by noradrenaline turnover. Pupillometry is thus a rapid, non-invasive tool to verify accurate placement of electrodes/fibers in vivo, allowing decisions about the inclusion/exclusion of individual animals at an early stage of ongoing experiments.

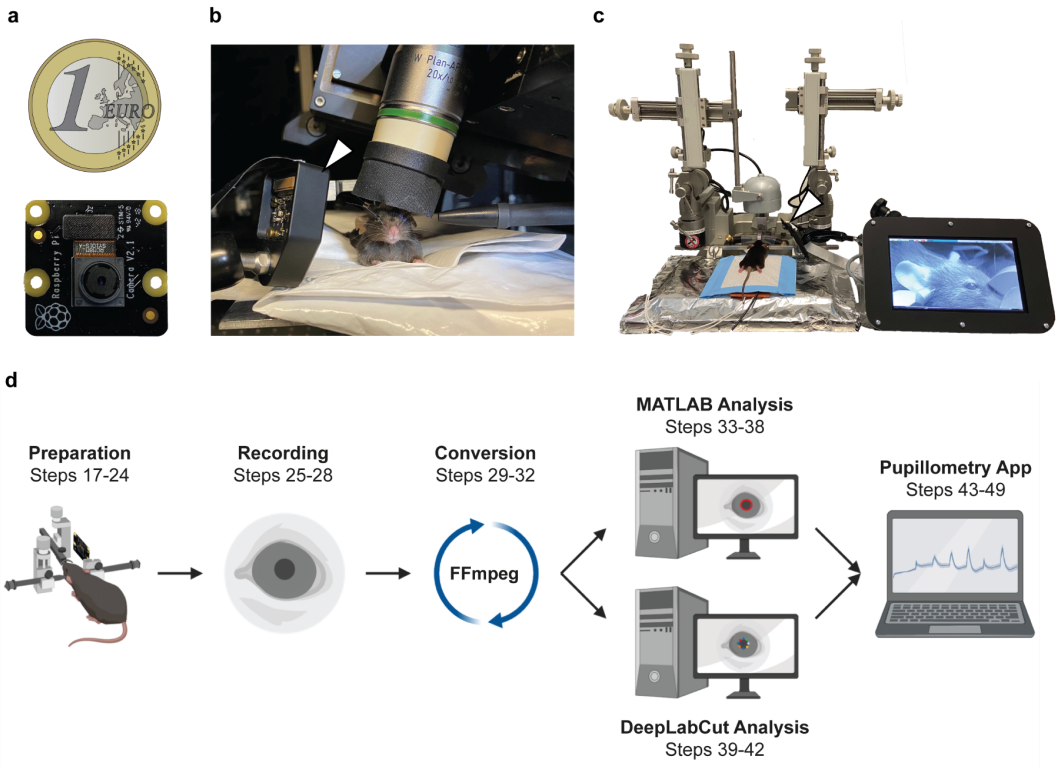

Figure 1. Pupillometry using a small and lightweight camera. (a) The Raspberry Pi NoIR Camera V2 Module is approximately the same size as a 1-Euro coin. (b) The camera module (inside custom housing and indicated with a white arrow tip) in a two-photon microscopy setup. (c) Camera module (indicated with a white arrow tip) in a stereotaxic surgery setup connected to a Raspberry Pi with touchscreen. An additional IR flood light illuminates the mouse from above. (d) Workflow overview for pupillometry recordings and data analysis. Steps from the written protocol are indicated for each section. Created with Biorender.com.

2.2.2 Advantages and limitations of the technique

Apart from pupillometry, no currently available technique provides a non-invasive real-time quantification of LC activity in vivo. However one limitation of the current technique is that pupil diameter changes are part of the response of the visual system. There is no correlation between luminance-mediated changes in pupil diameter and LC-mediated changes; thus, it is necessary to correct for changes in luminance when performing experiments (Box 2). In addition, the LC has a modular organization, where certain ensembles of cells project to specific brain regions [28,29]. As a consequence, only those LC neurons that project to the Edinger-Westphal nucleus and/or the superior cervical ganglion can elicit a pupil response via parasympathetic and sympathetic pathways [30]. While stimulation of the entire LC triggers a robust pupil response, retrograde labeling techniques can be used to manipulate specific ensembles of LC neurons. Using this technique in preliminary experiments, we have observed that selective stimulation of LC neurons that project to the hippocampus do not result in pupil dilation (unpublished observation). Therefore, pupillometry may not always be a suitable readout of projection-specific LC activity.

The only alternative real-time readouts of LC and noradrenergic activity use invasive recording or imaging techniques, the latter involving novel, genetically encoded noradrenaline sensors [31-33]. These techniques require extensive technical and experimental expertise and may not be available to the majority of laboratories conducting research on the LC-NA system. While pupillometry has long been a widely used clinical measure, the advent of functional magnetic resonance imaging (fMRI)-compatible eye-tracking systems has popularized its use in human neuro-imaging research [15,34]. While pupil dilation during brain imaging has often been considered a nuisance variable that needed to be controlled for statistically [35,36], it has recently emerged as a relevant biological variable in the context of arousal and noradrenergic activation and is now a widely used measure in human cognitive neuroscience [20,34-36]. Popularizing pupillometry in rodent models - where the LC-NA system can be systematically manipulated - will help elucidate the neuronal processes and brain states that drive the pupil response, and reveal how they relate to behavior in health and disease [20,21,24,37]. Pupillometry can thus provide an important translational link for comparative studies using both preclinical and clinical data.

The miniaturized low-cost setup in combination with DLC-based tracking is versatile and can be used for any tracking task, such as tracking the movement of whole animals or body parts (e.g., limbs, fingers and whiskers). Therefore, our protocol describes a low-cost, miniaturized video tracking device compatible with any task that requires video recording and tracking over time. A very promising recent approach was the development of a head-mounted light-weight camera device, allowing pupil tracking in freely moving rodents [37]. Our setup uses the same camera system, and our analysis pipeline is compatible with the head-mounted system, although this approach is not described here.

2.2.3 Experimental design

2.2.3.1 Animals and experimental parameters

This protocol has been optimized for validating LC activation in C57Bl6/J mice, but in principle it can be used to measure changes in pupil size in various setups and species, as long as the pupil is clearly visible with sufficient contrast between pupil and iris. Due to these constraints, pupil tracking may be challenging in albino strains or in animals that suffer from pathological eye conditions (e.g., cataracts). Using light stimuli to trigger changes in pupil diameter is an efficient positive control procedure to ensure successful recording of changes in pupil size (Box 1). We have not detected any sex-dependent differences in the pupil response when manipulating LC function in mice. For experiments in our laboratory, we use young adult mice (aged 2–4 months); however, we expect pupillometry to work equally well in younger or older animals. While pupillometry provides an easy and fast readout of LC activation when performed in anesthetized animals [24], we have previously shown that our setup can also be used to record from awake animals [25]. However, this requires experimental animals to be head-restrained and trained accordingly, which is technically more difficult and time consuming.

2.2.3.2 LC manipulations and pupillometry

Using pupillometry recordings to evaluate manipulation of the LC requires stereotaxic surgeries. Surgical procedures must be performed according to the regulations and guidelines of the local authorities, and animals must be allowed enough time for recovery. When viral vectors are delivered, proper virus expression is necessary, and pupillometry can be used to assess whether virus expression is sufficient to allow LC activation in a given animal. For electrical and optogenetic stimulation of the LC, many laboratories use unilateral activation, in which case pupillometry recordings should be performed on the ipsilateral eye, where LC activation elicits a larger pupil response [30]. Because the pupil is sensitive to light, special precautions should be taken when using optogenetic LC activation during pupillometry recordings. Excessive light spreading from the optic fiber should be avoided (e.g., use dark nail polish to paint dental cement). That being said, we have controlled for this possibility by including a ‘laser-only’ control group, and we have not detected changes in pupil size due to the 473-nm laser light itself. However, this might be different for other stimulation parameters and laser wavelengths; thus, the inclusion of proper control groups is important.

2.2.3.3 Baseline and power

While we show that a broad range of LC stimulation protocols can be used to manipulate pupil size, it is critical to include an appropriate baseline recording before LC stimulation. A stable baseline recording avoids artifacts from unspecific fluctuations in pupil size and enables proper statistical analyses. Importantly, our protocol is intended to test the efficacy of LC stimulation within a single animal; thus, analysis of pupil size over time can directly reveal the effect of LC stimulation, as shown by recordings for individual mice in Supplementary Fig. 2. In some cases, changes in pupil size need to be compared between experimental groups, for example, to test the effect of different LC stimulation paradigms.

We performed a statistical power analysis based on data from optogenetic LC activation (5 Hz/10 mW for 10 s (see ‘Anticipated results’); n = 9/10), which revealed that three mice per group are necessary to find a significant effect of optogenetic stimulation between ChR2-EYFP animals compared to EYFP controls in 95% of experiments (alpha < 0.05, and beta < 0.05).

2.3 Methods

2.3.1 Biological materials

- For all experiments shown, we have used adult mice from either C57BL/6J or C57BL/6-Tg(Dbh-icre)1Gsc (DBH-iCre) [38] mouse strains. To manipulate LC activity, prior surgical interventions are necessary to (i) implant stimulation electrodes, (ii) inject viral constructs (chemogenetics and optogenetics) and/or (iii) implant optic fibers (optogenetics). The procedures we have used are described in Supplementary Methods. All experiments must be done in accordance with the guidelines and regulations of the relevant authorities. These procedures were approved under licenses ZH161/17 and ZH169/17 by the local veterinary authorities, conforming to the guidelines of the Swiss Animal Protection Law, Veterinary Office, Canton Zurich (Act of Animal Protection 16 December 2005 and Animal Protection Ordinance 23 April 2008). In principle, this pupillometry protocol should be compatible with tracking the pupil in most vertebrate species that have normal eye pigmentation. The setup has been optimized for C57Bl/6 mice, where tracking is rather challenging due to poor contrast between iris (brown) and pupil (black). However, detecting and tracking the pupil in albino animals is difficult and might require special adjustments to achieve the necessary contrast between pupil and iris.

2.3.2 Reagents

- Isoflurane. We do not recommend the use of injectable anesthesia, as many commonly used drugs (e.g., medetomidine and xylazine) impact noradrenergic activity.

2.3.3 Equipment

2.3.3.1 Software

- Raspbian operating system (https://www.raspberrypi.org/downloads/)
- balenaEtcher (https://www.balena.io/etcher/)
- Raspberry Pi Code (https://github.com/ein-lab/pupillometry-raspi)
- FFmpeg (https://ffmpeg.org/)
- MATLAB (https://www.mathworks.com)
- MATLAB Code (https://github.com/ein-lab/pupillometry-matlab)
- DLC (http://www.mousemotorlab.org/deeplabcut; https://github.com/AlexEMG/DeepLabCut); See Nath et al. [27]
- Pupillometry App (https://bohaceklab.hest.ethz.ch/pupillometry/ (web version) or https://github.com/ETHZ-INS/pupillometry (source code))

2.3.3.1 Hardware

- Computer. Special computer specifications are required for the use of DLC. See Nath et al. [27] for more details.
- Micro SD Card and adapter (https://www.transcend-info.com/Embedded/Products/No-423)
- Raspberry Pi 3 B/B+ (or newer) (https://www.raspberrypi.org/products/)
- Raspberry Pi Touchscreen Display (https://www.raspberrypi.org/products/raspberry-pi-touch-display/)
- Raspberry Pi NoIR Camera V2 (https://www.raspberrypi.org/products/pi-noir-camera-v2/)
- Camera serial interface (CSI) flexible cable (1 m) (https://www.adafruit.com/product/2143)
- 2x power supply cables for Raspberry Pi and touchscreen (https://www.raspberrypi.org/products/raspberry-pi-universal-power-supply/)
- IR light source. The size of the IR light source should be chosen to fit the given setup. (https://www.amazon.com/Infrared-Illuminator-Power-Vision-Camera/dp/B01D73XM24/)
- Mass storage device (USB flash drive or hard disk)
- Wireless keyboard and mouse
- Screwdriver
- Suitable holding mechanisms/arms for camera and IR light source (For example: https://www.amazon.com/Toolour-Soldering-Rotatable-Alligator-Electronics/dp/B07JVF88TV/). Holding mechanisms/arms should be chosen to fit the setup, ideally allowing for flexibility while providing stability for the camera and IR light.
- Luxmeter
- Stereotaxic frame and anesthesia setup

2.4 Procedure

2.4.1 Pupillometry equipment setup (Timing 2h)

Further information on how to build this pupillometry setup can be found at https://ein-lab.github.io/pupillometry-raspi/.

1. Download the Raspbian operating system and write it to an SD card using balenaEtcher. Raspbian is available in three different bundles. Download ‘Raspbian with desktop and recommended Software’. For a detailed description of how to install the Raspbian OS, visit: https://www.raspberrypi.org/documentation/installation/installing-images/.

2. Before assembly, make sure that all hardware and tools are ready and that software preparation is completed.

3. Place the Raspberry on the brass spacers of the touchscreen board. Make sure that the micro-USB connectors on both boards are aligned and fasten the Raspberry in place with the four Phillips screws provided.

4. Install the SD card prepared in Step 1. The pins must face the Raspberry's printed circuit board. Care must be taken to avoid damage to the SD card slot.

5. Connect the screen printed circuit board and the Raspberry Pi using the short ribbon cable that came with the touchscreen. Make sure the metal contacts on the ribbon cable are facing toward the contacts inside the socket and away from the black bracket. Ignore the four colored cables provided with the touchscreen. These are needed only if you use an older Raspberry Pi and/or if you plan to power the Raspberry from the screen directly. This option is not recommended, as screen, camera and light need more power than a single average power supply can provide.

6. Connect the long CSI cable for the camera to the remaining socket on the Raspberry Pi. Lift the black bracket and push the cable in; then, lock it in place by replacing the bracket. Make sure that the metal contacts on the ribbon cable are facing toward the contacts in the socket and away from the black bracket. Please be aware that this part of the assembly will likely not be accessible anymore once it is inside the housing.

7. Install the housing and secure it with the provided screws. Ensure correct orientation of the assembly.

8. Connect the Raspberry NoIR V2 camera to the far end of the long ribbon cable. Make sure the metal contacts on the ribbon cable are facing toward the contacts in the socket and away from the black bracket.

9. (Optional) Connect the mouse and keyboard to the Raspberry Pi's USB ports. Although a computer mouse is not necessary when using a touchscreen, it simplifies handling of the system.

10. Power the system by connecting the first micro-USB power supply with the socket on the touchscreen board (the one closer to the screen) and then the second power supply to the second micro-USB socket. Always power the touch screen first; otherwise, the Raspberry Pi will start without display output. Depending on your display stand or case, you might find that the screen is upside down. This setting can be changed. Please refer to Troubleshooting.

11. Wait for the Desktop screen to appear and open a terminal window from the menu bar.

12. Test if the camera is detected by running the following command and press 'Enter'. The output should state supported=1 detected=1.

    vcgencmd get_camera

PAUSE POINT
The protocol can be paused after Step 12 and continued at a later time point.

2.4.2 Software setup (Timing 1h)

13. Raspberry Pi. Connect the Raspberry Pi to the internet, either via wireless internet (WiFi) or ethernet.

14. Open a terminal window from the menu bar.

15. Enter the following command and press ‘Enter’.

    curl -sSL https://git.io/JeKP0 | bash

    This will run a series of commands to install necessary software and enable the relevant Raspberry Pi settings. The Raspberry Pi will reboot after completion.

16. Computer. Download and install either FFmpeg with MATLAB and our MATLAB analysis files (https://github.com/ein-lab/pupillometry-matlab) or FFmpeg with DLC (https://github.com/AlexEMG/DeepLabCut). Help with DLC installation and setup can also be found at http://www.mousemotorlab.org/deeplabcut.

    PAUSE POINT
    Steps 13–16 have to be carried out only once. After the hardware and software have been set up, the protocol can be paused and continued at any later time point.

2.4.3 Experiment preparation (Timing 10 min/animal)

17. Before starting the experiment, ensure that equipment, tools and reagents are ready.

18. Set your experimental room illumination.Illumination intensity can be adapted to match experimental settings but must remain constant for any given experiment, as lighting intensity will affect pupil size. For all experiments shown in ‘Anticipated results’, room illumination was measured within the stereotaxic frame and set to 25–35 lux. Recordings in darkness require some adjustments, which are described in Box 1.

19. Connect the memory device (USB flash drive or external hard disk), wireless USB keyboard and mouse to the USB ports of the Raspberry Pi. Turn on the Raspberry Pi and display by connecting them both to a power supply. Always power the display before powering the Raspberry Pi. Otherwise, the screen will remain black.

20. Once the Raspberry Pi has launched, open the terminal and enter the following command to set a save location on your memory device. Confirm by pressing ‘Enter’.

    cd /media/pi/your_memory_device/experiment_folder

The Raspberry Pi itself possesses only limited memory capacity; therefore, the use of an external memory storage device is highly recommended.

21. Start a grayscale video stream by using the raspivid command in the terminal as in the following example and press ‘Enter’. A live video stream from the camera will appear on the screen.

    raspivid -t 0 -rot 180 -sat -100

    The -rot n command rotates the video output by ‘n’ degrees. Depending on your setup, the rotation command may not be required.

22. Induce anesthesia by exposing the mouse to 4% (vol/vol) isoflurane. Once the animal is fully asleep, place the animal into the stereotaxic frame under 2% (vol/vol) isoflurane (constant flow). Keep animals in the stereotaxic frame on a heating pad (at body temperature) to guarantee the well-being of experimental animals, especially during long recording sessions.

23. Prepare the animal for LC stimulation. Depending on the chosen LC manipulation strategy, attach the optic fiber patch cord, implant and/or connect the electrode or set an intraperitoneal catheter for drug administration. In addition, lightly fix the earbars so that the animal is stable in the stereotaxic frame. Noxious stimuli elicit pupillary responses; handling the animals in the stereotaxic frame should be done carefully to avoid unnecessary pupil dilation. Light head fixation reduces movement artifacts that may cause problems during pupil tracking.

24. Position the IR light source and the camera around the animal so that the pupil is clearly visible, illuminated and in focus. Avoid reflections that overlap with the pupil if possible. In case the pupil is fluctuating in size and/or moving, wait until the pupil has stabilized and settled in the visible part of the eye before starting to record. The quality of recorded videos determines how well the pupil tracking will work. Aim for the best contrast and avoid IR reflections within the pupil and animals with already widely dilated pupils. The MATLAB algorithm is very sensitive to artifacts. Reflections on the pupil (especially on the pupil border) may lead to tracking problems.

2.4.4 Pupillometry recording (Timing 5–30 min/animal)

This protocol has been optimized for short (<20 min) pupil recordings. To ensure the well-being of experimental animals, we advise to keep recordings as short as possible (<20 min) or use artificial tears (Systane Hydration; 1 drop every 30 min) to avoid damage to the eye. The use of artificial tears might affect pupil tracking.

25. End the video live stream with the key combination ‘Ctrl + C’ on the Raspberry Pi.

26. Start recording a video with the Raspberry Pi camera, by using the raspivid command in the terminal with slightly modified parameters, as seen in the following example code, and press ‘Enter’. This will immediately start recording a video, according to the set video parameters in the command, and save it under the

selected name. This command has to be adjusted to match the individual experimental settings. The example here starts a grayscale video (Videoname.h264) for 10 min at 5 frames/s with the contrast set to 40.

raspivid -o Videoname.h264 -sa -100 -vs -rot 180 -fps 5 -t 6000000 -co 40

We advise testing and choosing video parameters for a given experimental setup before starting experiments. For a more detailed description of the raspivid command and how to personalize video recording parameters, see https://www.raspberrypi.org/documentation/raspbian/applications/camera.md.
Coordinate this step with the chosen LC manipulation. It is advised to include a baseline recording of ≥1–2 min before starting the stimulation. The analysis speed in later steps (using MATLAB or DLC analysis) depends on the length of the video and the number of frames.

27. The recording will stop automatically if the timeout parameter -t was used in Step 26. The recording can also be terminated manually by using the key combination ‘Ctrl + C’. The video file will be saved to the specified location as an ‘.h264’ file.

28. Once the recording is finished, remove the animal from the stereotaxic frame and let it recover from anesthesia. To continue with pupillometry recordings, repeat Steps 21–27 or turn off the Raspberry Pi by issuing the command sudo halt in the terminal and press ‘Enter’. After executing the command sudo halt, the display goes black immediately, even though the Raspberry Pi is still shutting down. Allow ≥30 s before unplugging the device from the power supply. Use unique names for each recording. Otherwise, previously recorded videos will be overwritten.

PAUSE POINT
All downstream steps can be carried out at a later time point.

2.4.5 Conversion of video files to ‘.mp4’ with FFmpeg (Timing 2–3 min/video)

29. Connect your memory device to the computer where FFmpeg and MATLAB or DLC was installed.

30. Open the 'Command Prompt’ terminal on the computer and use the cd command to set the working directory as the location of the ‘.h264’ video files and press ‘Enter’.

cd path_of_the_video_folder

31. With FFmpeg, convert each ‘.h264’ video file to ‘.mp4’ format. Simultaneously, videos can be cropped to show only the eye, which will facilitate further video analysis. For example:

ffmpeg -framerate 5 -i Videoname.h264 -filter:v "crop=1000:1000:1000:1000" Videoname.mp4

It is important to specify the same frame rate that was used in Step 26 when recording the video. Cropping videos down to the size of the eye is recommended to facilitate efficient video analysis. The size and location of the cropping window may have to be adapted between videos. For a more detailed description of how to use FFmpeg and add other features, please visit https://ffmpeg.org/.

PAUSE POINT
All downstream steps can be carried out at a later time point.

2.4.6 Analysis of video files

32. Proceed with analyzing the MP4 video files using option A for pupil tracking with MATLAB or option B for pupil tracking with DLC.

2.4.6.1 A: Analysis of video files with MATLAB (Timing 2–5 min/video)

(i) Open MATLAB, and in the file browser, navigate to the pupillometry-matlab folder (see Step 16).

(ii) Right-click the folder and select ‘Add to path’ → ‘Selected Folders and Subfolders’.

(iii) In the command window, type pup01 = pupilMeasurement() and press ‘Enter’. This runs pupilMeasurement() without any additional parameters. Optional parameters can be adjusted and are given as name-value pairs, for example, pupilMeasurement('doPlot', true, 'frameInterval', 5) to display a plot and analyze only every fifth frame. For a list of all available optional parameters, please refer to the MATLAB sample script from the GitHub repository, or type help pupilMeasurement.

(iv) From the dialog box, choose one or several MP4 video files and click ‘Open’. Then, select a directory to save the output.

(v) MATLAB now presents you with the first frame of the first video file. Indicate the diameter across the pupil by left-clicking the left edge of the pupil and right-clicking the right edge of the pupil. Try to draw the longest diameter across the pupil to provide as many seed points as possible. Right-clicking confirms the selection, and the window closes immediately. The experimenter should be blinded for group assignment to avoid any labeling bias.

(vi) Wait for the progress bar to reach 100% and repeat Step iv for all videos. Results will now be saved as ‘.mat’ files in the results folder indicated in Step iv.

PAUSE POINT
The results can be analyzed in the Pupillometry App (Step 33) at a later time point.

2.4.6.2 B: Analysis of video files with DLC (Timing 5–10 min/video)

Pupil tracking with DLC requires a network that has been trained on a set of videos to recognize the pupil. The DLC network that was used for pupil tracking in this protocol is freely accessible on https://zenodo.org/deposit/3631569. Although we provide our own DLC network, we strongly recommend training a new network tailored to each individual setup. New DLC networks can be based on our pre-trained network to facilitate the training process. A detailed description for training DLC networks has recently been provided by Nath et al. [27].

(i) Open Anaconda and start an IPython session within your DLC environment and import the package with the following command and press ‘Enter’:

import deeplabcut

(ii) Set the config path according to your config file location and press ‘Enter’.

config_path = 'path_of_the_config_file'

(iii) To analyze videos, use the following command and indicate the path to the MP4 video files. To start the analysis, press ‘Enter’. Analysis data will be saved in the MP4 video file folder as ‘.csv’ files.

deeplabcut.analyze_videos(config_path,['path_of_video_to_be_analyzed'],save_as_csv=True)

(iv) Once all videos have been analyzed, labeled videos can be created for a visual assessment of performance using the following command and pressing ‘Enter’. This will generate the labeled videos and save them into the folder of the original MP4 videos.

deeplabcut.create_labeled_video(config_path,['path_of_previously_analyzed_video'])

It is good practice to check each labeled video to confirm that pupil tracking was successful.

PAUSE POINT
The results can be analyzed in the Pupillometry App (Step 33) at a later time point.

2.4.6 Visualization and statistical analysis with the Pupillometry App (Timing 10–20 min)

33. Access the Pupillometry App from your internet browser via https://bohaceklab.hest.ethz.ch/pupillometry/ or install the package locally from the source at https://github.com/ETHZ-INS/pupillometry. The Pupillometry App provides a detailed user manual (Supplementary Manual) and an example dataset to guide new users through the app.

34. Navigate to the ‘Files & samples’ tab and directly upload your ‘.mat’ data files (MATLAB analysis), or for the DeepLabCut pathway, upload the ‘.csv’ data files into in the ‘Upload and transform DLC files’, which will automatically read and transform them. In addition, upload a ‘.csv’ metadata file with the necessary experimental parameters (Animal ID, Group, etc.). The “Upload and transform DLC files” tab also allows you to download a metadata file template that already contains the filenames of the uploaded files. This can also be used with ‘.mat’ files. If videos have varying frame numbers, use the ‘Align files’ button to equalize the number of frames.

35. Go to the ‘Bins’ tab, indicate the used frame rate and set baseline and stimulation bins according to the experimental settings.

36. Check each animal trace and, if necessary, remove tracking artifacts from your data in the ‘Clean up’ tab.

37. Customize pupillometry plots in the ‘Settings’ tab, if required. Grouping variables have to be set in the ‘.csv’ metadata file.

38. Go to the ‘Plot’ tab to view and export pupillometry plots.

39. If needed, statistical analysis of pupillometry experiments can be performed in the ‘Statistical tests’ tab, or raw data can be exported via the ‘Export’ tab for external analysis.

2.4.7 Troubleshooting

Table 1: Troubleshooting

Step	Problem	Possible reason	Solution
1	MicroSD card not writable	SD card adapter’s write protection switch is in wrong position	Move the slider on the SD card adapter
10	Screen remains black	Components powered in wrong order	Power the screen first and the Raspberry Pi second
		Cables not properly seated	With the Raspberry Pi turned off and power disconnected, reseat all ribbon cables and carefully check for correct orientation

10	Display upside down	Screen setting needs to be adjusted	Edit the file /boot/config.txt on the microSD card and add a new line `lcd_rotate=2` to the bottom of the file
12/21/26	Camera not detected	Cable not properly connected	With the Raspberry Pi turned off and power disconnected, remove camera ribbon cable, check the orientation of the pins towards the pins in the socket and reconnect
19	Raspberry Pi hangs on boot	An unexpected power cut might have corrupted data on the microSD card	Remove the microSD card and repeat steps 3-5 and 9
19	Screen shows yellow lightning symbol	Raspberry Pi's power supply is undersized	Use a USB power supply that supplies at least 2.5 A
20	External hard disk not recognized	The Raspberry Pi may not supply enough power to the drive	Try using a powered USB hub to connect the drive or use a hard drive with external power
24	Video is too dark and the pupil is barely visible	Infrared light is turned off or too far away from the animal, which leads to a bad contrast	Check the infrared light and move it closer to the eye
24	The pupil is visible but is obscured by reflections	Angle of the infrared light to the pupil is not optimal	Move the infrared light around to find a good spot where the eye is well illuminated and the reflections are on the outskirts of the eye, where they are unlikely to interfere with pupil tracking

24	Pupil of the animal is extremely dilated from the start	This can either be related to lighting conditions (darkness), pain, or it can occur without any obvious reason	Check the animal for possible pain sources like too tight ear bars and relieve the pressure. If there are no obvious noxious stimuli, wait a few minutes to see if the pupil constricts by itself. In case this does not help, short light exposure (1-2 s) induces a strong pupil constriction. Over the next few seconds, the pupil slowly adapts to the ambient lighting conditions, and the recording can begin once the pupil size has stabilized. If this does not solve the problem either, continue with the next animal and try again later.
24	Pupil of the animal is moving around and/or moving outside the visible part of the eye	This usually happens within the first few minutes of the animal being in the setup	Wait until the pupil has settled by itself in the visible part of the eye before starting to record
24	A milky white spot covers the eye of the animal which is not related to light reflection	The animal suffers from retinal damage and cataract formation	Try recording from the other eye. If both eyes are affected the animal has to be excluded
31	Converted videos are the wrong length	The frame rate of the recording and the conversion do not match	Make sure you specify the same frame rate both when starting a recording and when converting the videos
31	Cropped video does not include the whole eye	Cropping parameters were wrong for the given video	Change the cropping parameters and convert again
32A iii	MATLAB Error: Undefined function or variable ‘pupilMeasurement’	Toolbox folder not on MATLAB path	Right-click the folder containing contents from pupillometry-matlab repository and select "Add to path" and "Selected folders and subfolders"
32A vi	MATLAB Error: No circular structure for radius r in this frame	MATLAB is unable to identify pupil	Re-run and carefully select line at a different angle

			Re-run with `'enhanceContrast'` flag enabled and/or set `'startFrame'` to a different value
			Inspect the video for resolution, pupil contrast and artifacts during the whole recording
32B iv	DeepLabCut did not track the pupil properly	This could be a video or network issue	If the video is too dark, try to change its brightness/contrast and analyze again. If it is not video related, train a new DeepLabCut network based on diverse videos to improve the flexibility of the network.
34	“Files & samples” tab shows “error” after uploading data and metadata files	There is a mismatch between data files and metadata information	Check the metadata file and correct wrong file names/spelling mistakes. Do not use any special characters in filenames or variables (+*#&;’%? etc.).
34	Missing files after DLC import	Computation of the pupil diameter was not possible for some files due to bad tracking quality	Optimize DLC tracking or reduce likelihood cutoff and/or completeness cutoff to ensure that the center point and at least one pupil edge point are retained
37	“Plot” tab shows no graph after setting plot parameters	There is a problem either with other settings within the app or with the grouping variables in the metadata file	Check all settings. For example a normalized graph requires a baseline bin and will not work unless a baseline bin is set.
37	Ribbon plots are broken up / show artefacts	There is a problem with missing data in plotting intervals	Increase the interval size in the “Settings tab”

39	No statistical results are shown	There is a problem with either the bins or any variable	Ensure proper bins are defined in the “Bins” tab. In the “Statistical tests” tab, ensure the testing variable and animal variable are correctly set. If you use your custom model ensure a proper null model is provided. Ensure variables allow for the selected test (e.g. a variable with only one group cannot be used to test group differences).

2.5 Anticipated results

2.5.1 Pupillometry as a real-time readout of LC activation

The relationship between LC activity and pupil diameter is well established [23,30,39]. Here, we take advantage of this tight relationship to demonstrate that pupillometry provides a sensitive real-time readout of in vivo LC manipulation. To strongly and selectively activate the LC, we first used Designer Receptors Selectively Activated by Designer Drugs (DREADDs, hM3Dq), which can stimulate LC firing [40], trigger noradrenaline (NA) release throughout the brain and elicit a strong and long-lasting pupil dilation [24,41]. Transgenic mice that include codon-improved Cre recombinase under the dopamine-beta-hydroxylase promoter (DBH-iCre mice) received stereotaxic injections of a virus expressing either excitatory DREADDs (AAV5-hSyn-DIOhM3Dq-mCherry; hM3Dq-mCherry) or mCherry alone (AAV5-hSynDIO-mCherry; mCherry) bilaterally into the LC (coordinates from bregma: +5.4 mm AP; ±1.0 mm ML; −3.8 mm DV) (Fig. 2a). Pupil recordings were performed unilaterally. Baseline pupil size was recorded for 2 min before administration of an ultra-low dose of the potent DREADDs agonist clozapine (0.03 mg/kg i.p.) [24,41]. Within a minute of clozapine injection, we observed a slow but steady pupil dilation in the hM3Dq-mCh group, which led to a strong and long-lasting increase in pupil dilation throughout the recording period (Fig. 2b). In contrast, the pupil size of control mice (mCherry) did not change in response to clozapine injection and remained stable throughout the 10-min recording session. This shows that a short pupillometry recording reliably reports chemogenetic LC activation in real time. All tracking in this report was performed with DeepLabCut, and all analyses use linear mixed effects models [42], an analysis comparable to repeated one- or two-way ANOVAs. This allows us to correct for changes in pupil radius that are dependent on interindividual differences between animals and on baseline drifts over time. All effect sizes/standard errors are reported in pixels. For detailed description and examples, please refer to the Pupillometry App user manual (Supplementary Manual).

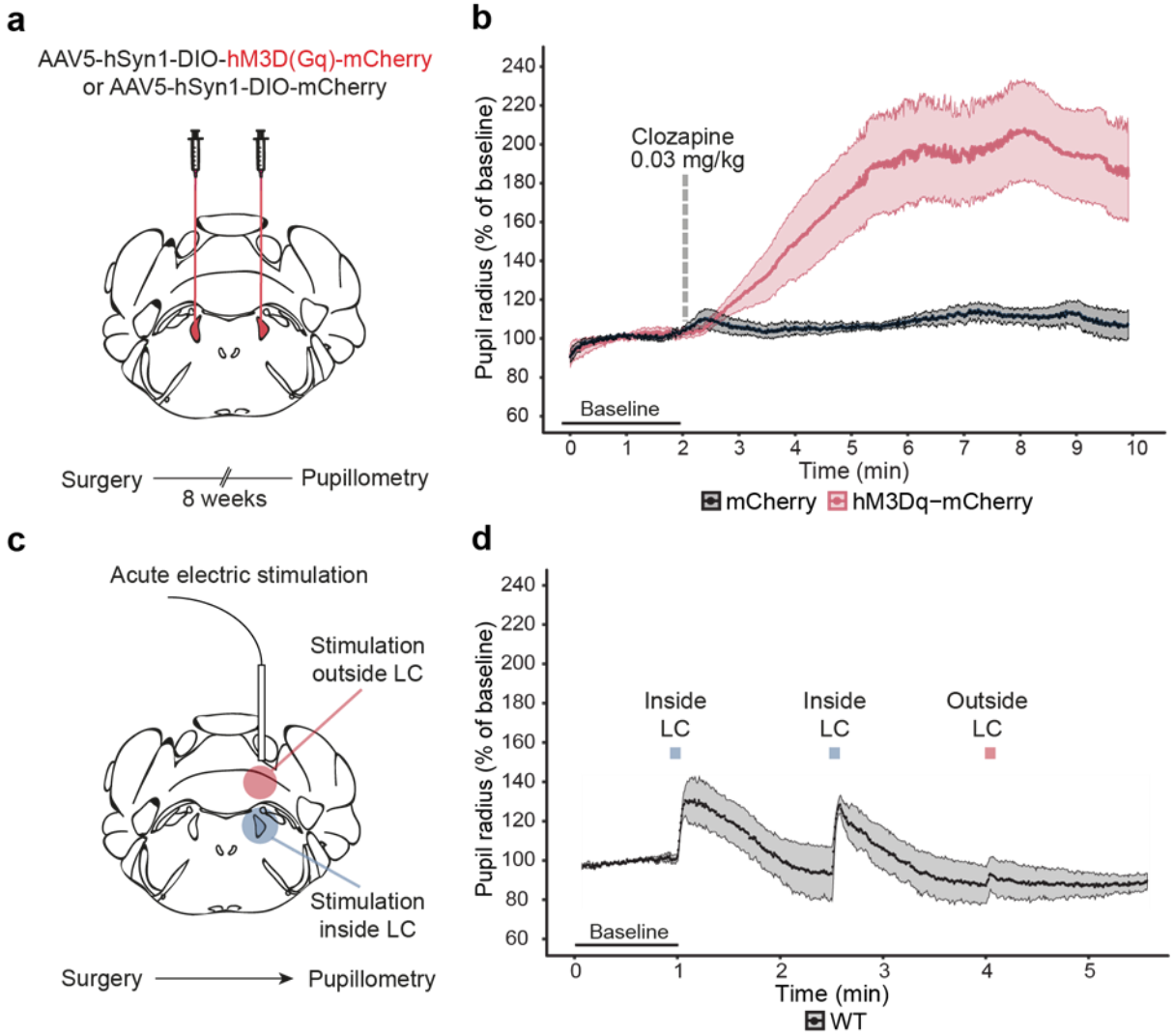

Figure 2. Pupillometry as a real-time readout for LC activation. (a) Experimental design for bilateral chemogenetic LC activation. (b) Pupillometry traces from the right eye during chemogenetic LC activation. To determine whether chemogenetic LC activation induced pupil dilation in hM3Dq-mCherry (n = 7) or mCherry (n = 7) mice, we tested our raw data on a linear mixed effects model (Formula: Radius ~ Stimulation * Virus + (1|Animal)). We found a virus-specific increase in pupil radius after chemogenetic LC activation (β = 12.23, s.e.m. = 3.930, t(28) = 3.112, P = 0.009). Post-hoc analysis showed that clozapine (0.03 mg/kg) injection reliably increased pupil size only in hM3Dq-mCherry (β = 14.21, s.e.m. = 2.78, t(12) = 5.113, P = 0.0013) but not mCherry (β = 1.98, s.e.m. = 2.78, t(12) = 0.712, P = 0.90) mice. (c) Experimental design for acute unilateral electric LC activation during stereotaxic surgery. (d) Pupil traces of wild-type (WT) animals (n = 3) receiving electrical stimulation inside the LC and outside the LC during stereotaxic electrode implantation. To determine whether electric stimulation induced pupil dilation in WT mice (n = 3), we used a linear mixed effects model (Formula: Radius ~ Stimulation * Location + (1|Animal/Time)). We found a significant interaction between stimulation and location (β = 4.6, s.e.m. = 1.53, t(7) = 3.006, P = 0.019). Acute electric stimulation inside the LC elicited small yet reproducible pupil dilations (β = 5.4, s.e.m. = 0.88, t(7) = 6.12, P = 0.0021), but had no effect on pupil size when the stimulation was given 2 mm above the LC (β = 0.81, s.e.m. = 1.25, t(7) = 0.65, P = 0.91). All data represent means ± s.e.m. Procedures were approved under licenses ZH161/17 and ZH169/17 by the local veterinary authorities, conforming to the guidelines of the Swiss Animal Protection Law, Veterinary Office, Canton Zurich (Act of Animal Protection 16 December 2005 and Animal Protection Ordinance 23 April 2008).

2.5.2 Pupillometry as a tool to guide electrical stimulation of the LC

Successful targeting of the LC for electrical stimulation depends on proper placement of the electrode during stereotaxic surgery. Due to its small size, consistent targeting of the LC can be challenging, and incorrect placement of electrodes is common. Pupillometry readings during stereotaxic surgery can be used to immediately determine the accuracy of the placement of the implanted electrode. Acute electric stimulation during stereotaxic surgery elicited a pupil dilation when the electrode was placed in the LC (coordinates from bregma: +5.4 mm AP; +0.9 mm ML; −3.8 mm DV) but had no effect when placed 2 mm above the LC (coordinates from bregma: +5.4 mm AP; +0.9 mm ML; −1.8 mm DV, Fig. 2c,d). Thus, pupillometry allows the validation of correct electrode placement during surgery. Importantly, this approach might also prove useful when targeting recording electrodes to the LC, particularly when using systems that allow stimulation and recording. In addition, we performed pupillometry recordings in a two-photon setup (Fig. 1b) on headfixed animals with chronically implanted electrodes. Electrical LC stimulation (monophasic constant current pulse of 50 Hz, 2 ms, 200 µA for 2 s) induced pupil dilation in this setting (Box 1), demonstrating that the miniaturized setup can be integrated into complex experimental setups with little space.

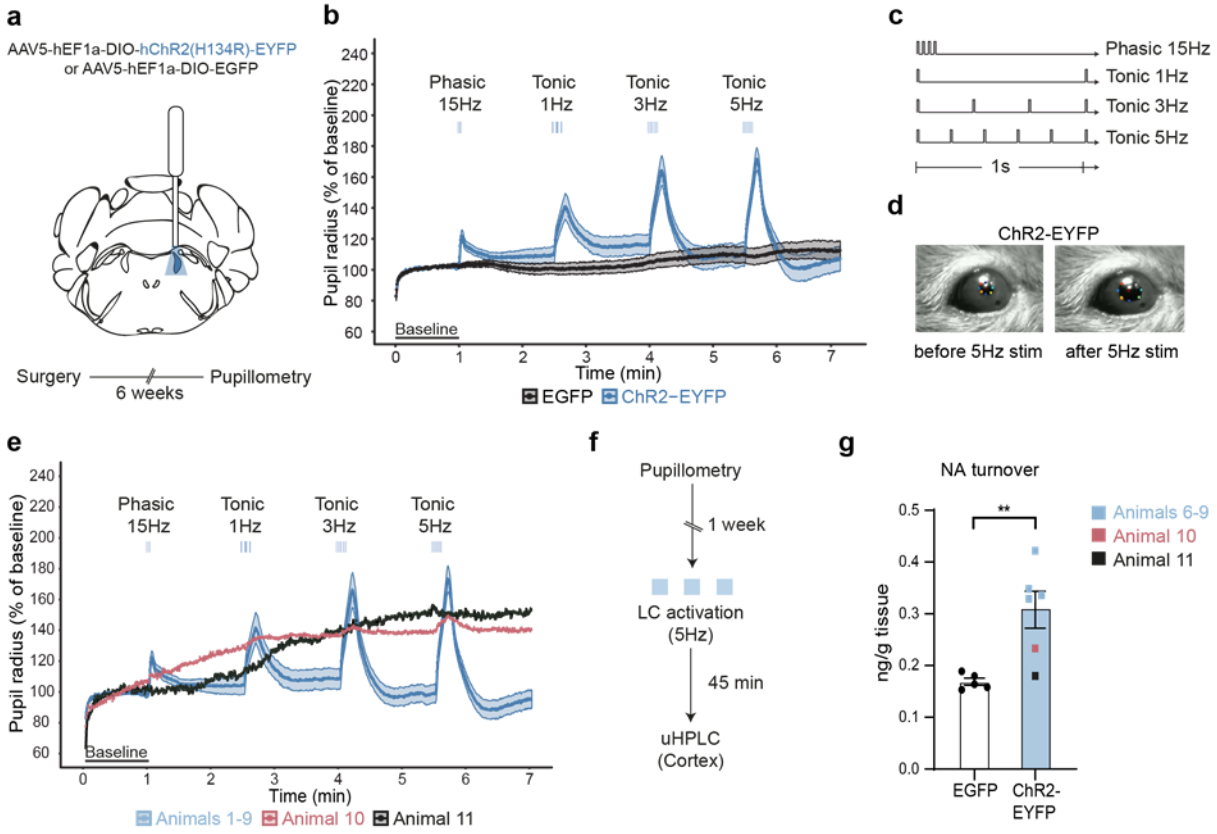

Figure 3. Pupillometry is a sensitive readout of physiologically relevant modes of LC activity. (a) Experimental design for unilateral optogenetic LC activation. (b) Pupillometry traces from the ipsilateral eye. To see if optogenetic LC activation induced pupil dilation in ChR2-EYFP (n = 11) or EGFP (n = 10) mice, we tested our raw data on a linear mixed effects model (Formula: Radius ~ Stimulation * Virus + (1|Animal/Time)). We found a virus-specific increase in pupil radius after optogenetic LC activation (β = 5.43, s.e.m. = 0.626, t(168) = 8.678, P < 0.0001). Post-hoc analysis showed that phasic (15 Hz, four pulses, 10 ms each pulse) and tonic (1 Hz/3 Hz/5 Hz for 10 s, 10 ms each pulse) firing patterns reliably increased pupil size only in ChR2-EYFP (β = 5.47, s.e.m. =

0.432, t(82) = 12.678, P < 0.0001) but not EGFP (β = 0.04, s.e.m. = 0.453, t(82) = 0.099, P = 0.99) mice. (c) Optogenetic stimulation paradigms for phasic and tonic LC activation. (d) Images showing the pupil size before and after optogenetic LC activation with 5 Hz, while being tracked by our DLC network. (e) Pupil traces of ChR2-EYFP animals separated according to their response to LC activation. Optogenetic LC activation induced strong pupil dilations in 9 out of 11 animals (Animals 1–9), but in 2 animals, it elicited only a very weak (Animal 10) or no response (Animal 11). (f) Experimental design to evaluate the levels of NA and its main metabolite 3-methoxy-4-hydroxyphenylglycol (MHPG) in the brain. One week after pupillometry recordings, NA turnover (as calculated by the MHPG/NA ratio) was assessed 45 min after LC stimulation (5 Hz/10-ms pulses, alternating 3 min bins off/on for 18 min4) in the cortex of EGFP (n = 5) and ChR2-EYFP (n = 6) animals. (g) LC activation increased cortical NA turnover in ChR2-EYFP mice (unpaired t test; t(9) = 3.50, P = 0.0067). In accordance with pupillometry results, Animal 10 showed only a weak increase, and Animal 11 showed no change in cortical NA turnover. All data represent means ± s.e.m. Procedures were approved under licenses ZH161/17 and ZH169/17 by the local veterinary authorities, conforming to the guidelines of the Swiss Animal Protection Law, Veterinary Office, Canton Zurich (Act of Animal Protection 16 December 2005 and Animal Protection Ordinance 23 April 2008).

2.5.3 Pupillometry reports physiologically relevant modes of LC activation

The LC displays a range of firing patterns depending on the animal's behavioral state. While minimally active during sleep, LC neurons fire tonically during wakefulness at a rate that ranges from 1 Hz (drowsy/tired) up to 8 Hz under highly stressful conditions [2,4,43,44]. In response to salient stimuli, the LC fires short high-frequency bursts (3–5 action potentials at 10–20 Hz) [43,45,46]. To demonstrate that pupillometry can discriminate between different, physiologically relevant stimulation paradigms, we combined optogenetic LC stimulations and pupil recordings in DBH-iCre mice that unilaterally expressed either channelrhodopsin (AAV5-hEF1a-DIO-hChR2(H134R)-EYFP; ChR2-EYFP) or a control virus (AAV5-hEF1a-DIO-EYFP; EGFP) in noradrenergic LC neurons (Fig. 3a). A short burst of optogenetic LC stimulation (15 Hz, four pulses, 10 ms each pulse) reliably triggers a transient pupil response, and increasing frequencies of tonic LC stimulation reveal a graded pupil response, which is absent in control mice (Fig. 3b). It is important to note that the higher response of tonic versus phasic stimulation is presumably due to the higher number of stimulation pulses that were delivered over the 10-s period in the tonic paradigm, whereas the phasic stimulation was a single burst of only four pulses (Fig. 3c). Despite the fact that the pupil is light sensitive, exposure to flashing 473-nm laser light had no effect on pupil size (EGFP control group), even under dim lighting (30 lux). Importantly, noxious stimuli can trigger LC activation under anesthesia [47,48]; thus, we delivered electrical shocks to the tail (biphasic constant current pulse of 30 Hz, 2 ms, 200 μA for 5 s) while recording pupil size. We observed that tailshock reliably induced pupil dilations (Supplementary Fig. 1). This demonstrates that physiological LC responses can also be measured using pupillometry.

2.5.4 Pupillometry as a tool to guide experimental decisions

Similar to electrical LC stimulation, optic fiber placement is crucial for successful optogenetic experiments. Compared to classic post-mortem validation techniques, pupillometry enables easy and reliable assessment of LC activation in each individual animal, before the start of an experiment. When performing optogenetic experiments (Fig. 3a–c), we noticed that two mice showed very weak (Animal 10) or no (Animal 11) pupil dilation in response to stimulation (Fig. 3e and Supplementary Fig. 2). To determine whether LC activation was indeed unsuccessful in these animals, we stimulated all mice optogenetically (5 Hz/10 mW) 45 min before sacrifice4 and measured cortical NA turnover applying reversed-phase

ultra-high-performance liquid chromatography (uHPLC, Figure 3f). We have shown previously that our uHPLC method39 is a highly sensitive and reliable readout of LC activation and alteration, as previously measured both in rodent and human brain tissue and biofluids [24,49-51]. In accordance with our pupillometry data, all mice responded with a strong increase in NA turnover, except for the two mice for which the pupil response was weak or absent (Fig. 3g). This confirms that pupillometry is a highly sensitive readout for successful LC stimulation and, indeed, allows decisions about the inclusion/exclusion of animals to be made before further experimental procedures. This will further refine the use of animals in research.

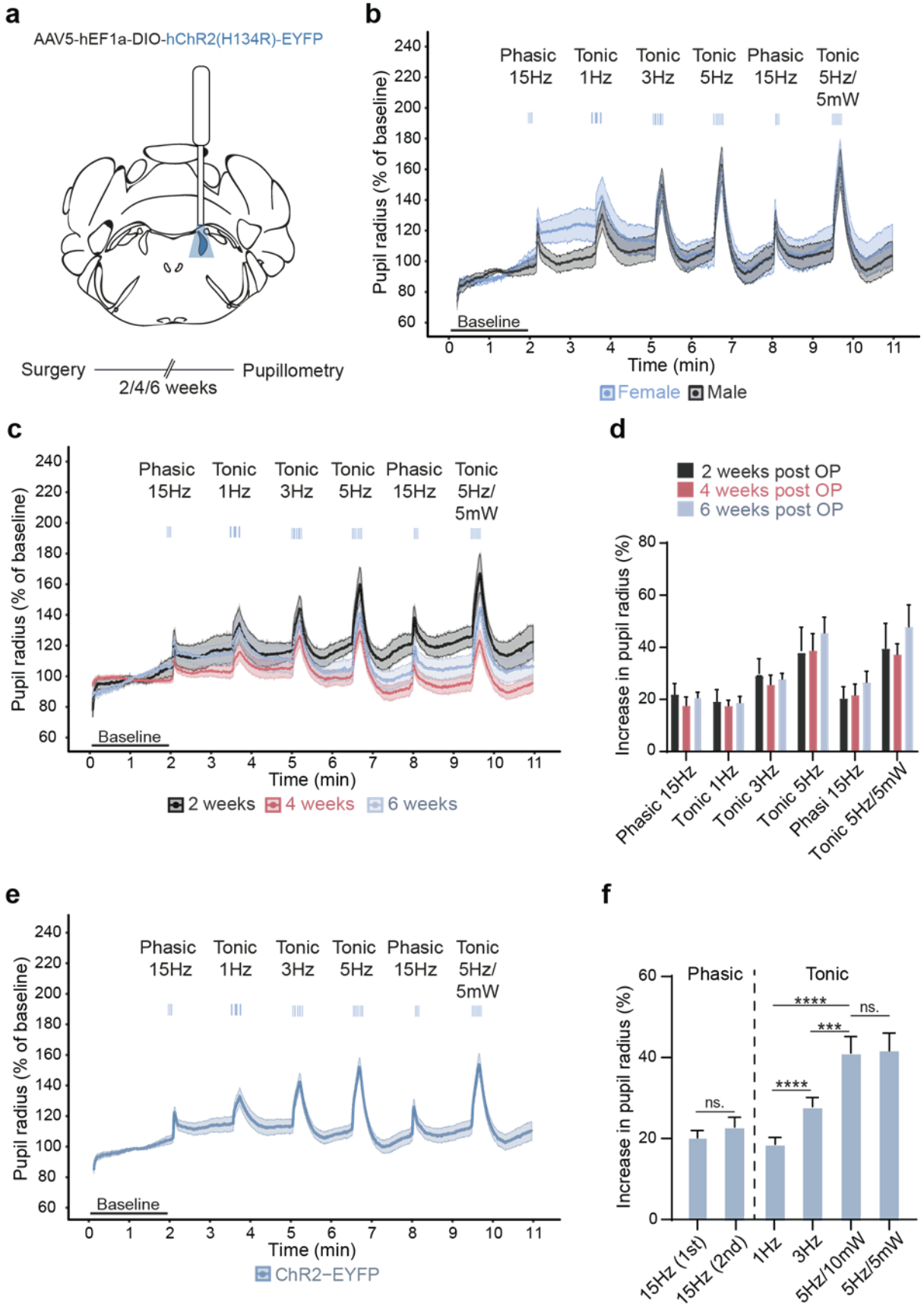

Figure 4. Repeated pupillometry recordings with various stimulation parameters in females and males. (a) Experimental design to assess the impact of unilateral optogenetic LC activation at different time points after surgical operation (post-OP), with different stimulation frequencies (as described in Fig. 3c), and different laser

power (5 Hz/5 mW versus 5 Hz/10 mW) on the pupil radius in male and female mice. (b) Pupillometry traces (2, 4 and 6 weeks combined) of female (n = 5) and male (n = 6) ChR2-EYFP mice. To see if there is a sex-dependent difference in pupil response upon LC stimulation, we used a linear mixed effects model (Formula: Radius ~ Stimulation * Sex + (1|Animal/Week post OP/Time)). We saw an increase in pupil size in response to optogenetic LC activation (β = 3.45, s.e.m. = 0.237, t(196) = 14.573, P < 0.0001) but did not detect any sex-related differences in pupil response (β = 0.46, s.e.m. = 0.320, t(396) = 1.429, P = 0.155). (c) Pupillometry traces (female and male mice combined, n = 11) at 2, 4 or 6 weeks after surgery. We used a linear mixed effects model (Formula: Radius ~ Stimulation * Week post-OP + (1|Animal/Time)) to assess if there is a difference between optogenetic LC stimulation and time after surgery. We saw an increase in pupil size in response to optogenetic LC activation (β = 3.75, s.e.m. = 0.960, t(396) = 3.906, P = 0.0001) but did not detect any time-related differences in pupil response to stimulation (Week 4: β = 0.04, s.e.m. = 1.357, t(380) = 0.028, P = 0.978; Week 6: β = 0.11, s.e.m. = 1.357, t(380) = 0.083, P = 0.934). (d) For each stimulation frequency, we detected no time-dependent differences in pupil size increase (repeated-measures two-way ANOVA; F(10, 150) = 0.5073, P = 0.88). Instead, the strength of the pupil response was mediated by the stimulation frequency (repeated-measures two-way ANOVA; F(1.959, 19.59) = 23.03, P < 0.0001). (e and f) Visualization of the stimulation dependency of LC-mediated pupil responses, averaged across sexes and time points (n = 11). (f) Repeated-measures one-way ANOVA reveals that different LC stimulation paradigms differentially impact pupil dilation (F(2.128, 68.10) = 26.00, P < 0.0001). Tukey post-hoc tests show no difference between a 15-Hz pulse at the beginning (1st) and toward the end (2nd) of the recording. However, increasing frequencies of tonic stimulation paradigms led to a graded increase in pupil dilation. We detect no difference in pupil response between tonic stimulation with 5 and 10 mW. ***P < 0.001; ****P < 0.0001. All data represent means ± s.e.m. Procedures were approved under licenses ZH161/17 and ZH169/17 by the local veterinary authorities, conforming to the guidelines of the Swiss Animal Protection Law, Veterinary Office, Canton Zurich (Act of Animal Protection 16 December 2005 and Animal Protection Ordinance 23 April 2008).

2.5.5 Pupillometry to explore LC function

Pupillometry also opens the possibility to address fundamental biological questions about the LC. We measured the pupil response after repeated optogenetic stimulation at different time points after surgery (2, 4 or 6 weeks) in male and female mice to determine (i) if sex affects the pupil response, (ii) if pupillometry recordings are stable over the course of several weeks and (iii) if pupillometry can be used to select an appropriate laser power for LC activation. First, the pupil response to optogenetic LC stimulation showed no differences between males and females (Fig. 4b). Second, the overall pupil response to optogenetic LC activation did not change over the studied time period (Fig. 4c,d). Third, after averaging across time and sex, we again observed that different LC stimulation patterns led to different pupillary responses (Fig. 4e,f). Within a recording session, repeated presentation of a phasic burst stimulus triggers a reliable increase in pupil radius. Interestingly, 5-Hz stimulation with different laser intensities (5 mW versus 10 mW) led to the same pupil response (Fig. 4e,f). Therefore, we also tested whether we could trigger a reliable pupil response with only 1-mW stimulation intensity. Indeed, tonic stimulation (5 Hz for 10 s, 10 ms each pulse) at 1 mW also elicited a clear pupil response, which we also quantified in absolute values (millimeters) (see Box 3 for absolute quantification of pupil size). Because exposure to strong laser light can adversely affect neuronal function [52,53], pupillometry can be used to verify optimal stimulation paradigms and lower stimulation intensities.

2.5 Reporting Summary

Further information on research design is available in the Nature Research Reporting Summary linked to this article.

2.6 Data availability

The datasets generated during the current study (‘Anticipated results’) are available from the corresponding authors upon request.

2.7 Code availability

All software and code described in this protocol are freely available online:

- Raspberry Pi Code (https://github.com/ein-lab/pupillometry-raspi)
- MATLAB Code (https://github.com/ein-lab/pupillometry-matlab)
- Pupillometry App (https://bohaceklab.hest.ethz.ch/pupillometry/ (web version)/ https://github.com/ETHZ-INS/pupillometry (source code))

2.8 Acknowledgements

B.W. acknowledges support by the University of Zurich and the Swiss National Science Foundation (grant 310030_182703). J.B. acknowledges support by the ETH Zurich, ETH Project Grant ETH-20 19-1, and the Swiss National Science Foundation (grant 310030_172889/1). The authors acknowledge Rongrong Xiang and Matthew J. P. Barrett for their initial work on the MATLAB analysis, Marc Zuend for extensive testing of prototypes, Christa Schläppi for testing the pupillometry guidelines and Alexandra von Faber-Castell for testing the assembly guide.

2.9 Author contribution

Conceptualization, M.P., K.D.F., B.W. and J.B.; methodology, M.P., K.D.F. and O.S.; investigation, M.P., K.D.F, A.F.-S., S.N.D., Y.V. and M.T.W.; software, K.D.F., L.M.v.Z., P.-L.G. and O.S.; writing—original draft, M.P., K.D.F, L.M.v.Z., O.S., S.N.D. and J.B.; figures, M.P. and K.D.F.; writing—review and editing, M.P., K.D.F., L.M.v.Z., O.S., A.F.-S., P.-L.G., Y.V., S.N.D., M.T.W., P.P.D.D., B.W. and J.B.; funding acquisition, B.W., P.P.D.D. and J.B.; resources, B.W. and J.B.

2.10 References

1. Sara, S. J. The locus coeruleus and noradrenergic modulation of cognition. Nat. Rev. Neurosci. 10, 211–223 (2009).
2. Berridge, C. W. & Waterhouse, B. D. The locus coeruleus–noradrenergic system: modulation of behavioral state and state-dependent cognitive processes. Brain Res. Rev. 42, 33–84 (2003).
3. Chandler, D. J. et al. Redefining Noradrenergic Neuromodulation of Behavior: Impacts of a Modular Locus Coeruleus Architecture. J. Neurosci. 39, 8239–8249 (2019).
4. McCall, J. G. et al. CRH Engagement of the Locus Coeruleus Noradrenergic System Mediates Stress-Induced Anxiety. Neuron 87, 605–620 (2015).
5. Naegeli, C. et al. Locus Coeruleus Activity Mediates Hyperresponsiveness in Posttraumatic Stress Disorder. Biol. Psychiatry 83, 254–262 (2018).
6. Isingrini, E. et al. Resilience to chronic stress is mediated by noradrenergic regulation of dopamine neurons. Nat. Neurosci. 19, 560–563 (2016).
7. Fortress, A. M. et al. Designer receptors enhance memory in a mouse model of Down syndrome. J. Neurosci. 35, 1343–1353 (2015).

8. Vermeiren, Y. & De Deyn, P. P. Targeting the norepinephrinergic system in Parkinson's disease and related disorders: The locus coeruleus story. Neurochem. Int. 102, 22–32 (2017).
9. Delaville, C., Deurwaerdère, P. D. & Benazzouz, A. Noradrenaline and Parkinson's Disease. Front. Syst. Neurosci. 5, 1–12 (2011).
10. Mather, M. & Harley, C. W. The Locus Coeruleus: Essential for Maintaining Cognitive Function and the Aging Brain. Trends Cogn. Sci. 20, 214–226 (2016).
11. Peterson, A. C. & Li, C. S. R. Noradrenergic dysfunction in Alzheimer's and Parkinson's Diseases-An overview of imaging studies. Front. Aging Neurosci. 10, 1–16 (2018).
12. Weinshenker, D. Long Road to Ruin: Noradrenergic Dysfunction in Neurodegenerative Disease. Trends Neurosci. 41, 211–223 (2018).
13. Sara, S. J. & Bouret, S. Orienting and Reorienting: The Locus Coeruleus Mediates Cognition through Arousal. Neuron 76, 130–141 (2012).
14. Manaye, K. F., McIntire, D. D., Mann, D. M. A. & German, D. C. Locus coeruleus cell loss in the aging human brain: A non‐random process. J. Comp. Neurol. 358, 79–87 (1995).
15. Murphy, P. R., O'Connell, R. G., O'Sullivan, M., Robertson, I. H. & Balsters, J. H. Pupil diameter covaries with BOLD activity in human locus coeruleus. Hum. Brain Mapp. 35, 4140–4154 (2014).
16. Joshi, S., Li, Y., Kalwani, R. M. & Gold, J. I. Relationships between Pupil Diameter and Neuronal Activity in the Locus Coeruleus, Colliculi, and Cingulate Cortex. Neuron 89, 221–234 (2016).
17. Wang, C.-A., Blohm, G., Huang, J., Boehnke, S. E. & Munoz, D. P. Multisensory integration in orienting behavior: Pupil size, microsaccades, and saccades. Biol. Psychol. 129, 36–44 (2017).
18. Lehmann, S. J. & Corneil, B. D. Transient Pupil Dilation after Subsaccadic Microstimulation of Primate Frontal Eye Fields. J. Neurosci. 36, 3765–3776 (2016).
19. Varazzani, C., San-Galli, A., Gilardeau, S. & Bouret, S. Noradrenaline and dopamine neurons in the reward/effort trade-off: a direct electrophysiological comparison in behaving monkeys. J. Neurosci. 35, 7866–7877 (2015).
20. Schwalm, M. & Jubal, E. R. Back to Pupillometry: How Cortical Network State Fluctuations Tracked by Pupil Dynamics Could Explain Neural Signal Variability in Human Cognitive Neuroscience. eneuro vol. 4 ENEURO.0293–16.2017 (2017).
21. Reimer, J. et al. Pupil Fluctuations Track Fast Switching of Cortical States during Quiet Wakefulness. Neuron 84, 355–362 (2014).
22. Reimer, J. et al. Pupil fluctuations track rapid changes in adrenergic and cholinergic activity in cortex. Nat. Commun. 7, 13289 (2016).
23. Breton-Provencher, V. & Sur, M. Active control of arousal by a locus coeruleus GABAergic circuit. Nat. Neurosci. In Press (2019).
24. Zerbi, V. et al. Rapid Reconfiguration of the Functional Connectome after Chemogenetic Locus Coeruleus Activation. Neuron 103, 702–718.e5 (2019).
25. Zuend, M. et al. Arousal-induced cortical activity triggers lactate release from astrocytes. Nature Metabolism (2020) doi:10.1038/s42255-020-0170-4 .
26. Mathis, A. et al. DeepLabCut: markerless pose estimation of user-defined body parts with deep learning. Nat. Neurosci. (2018) doi:10.1038/s41593-018-0209-y.
27. Nath, T. et al. Using DeepLabCut for 3D markerless pose estimation across species and behaviors. Nat. Protoc. 14, 2152–2176 (2019).
28. Uematsu, A. et al. Modular organization of the brainstem noradrenaline system coordinates opposing learning states. Nature Neuroscience vol. 20 1602–1611 (2017).
29. Schwarz, L. A. & Luo, L. Organization of the locus coeruleus-norepinephrine system. Curr. Biol. 25, R1051–R1056 (2015).
30. Liu, Y., Rodenkirch, C., Moskowitz, N., Schriver, B. & Wang, Q. Dynamic Lateralization of Pupil Dilation Evoked by Locus Coeruleus Activation Results from Sympathetic, Not Parasympathetic, Contributions. Cell Reports vol. 20 3099–3112 (2017).
31. Patriarchi, T. et al. Ultrafast neuronal imaging of dopamine dynamics with designed genetically encoded sensors. Science 4422, eaat4422 (2018).
32. Feng, J. et al. A Genetically Encoded Fluorescent Sensor for Rapid and Specific In Vivo Detection of Norepinephrine. Neuron 102, 745–761.e8 (2019).
33. Patriarchi, T. et al. Imaging neuromodulators with high spatiotemporal resolution using genetically encoded indicators. Nat. Protoc. (2019) doi:10.1038/s41596-019-0239-2.
34. Gee, J. W. de et al. Dynamic modulation of decision biases by brainstem arousal systems. eLife vol. 6 (2017).
35. Grueschow, M., Polania, R., Hare, T. A. & Ruff, C. C. Arousal Optimizes Neural Evidence Representation for Human Decision-Making. SSRN Electronic Journal doi:10.2139/ssrn.3155606.
36. Hellrung, L. et al. Flexible adaptive paradigms for fMRI using a novel software package 'Brain Analysis in Real-Time' (BART). PLoS One 10, e0118890 (2015).
37. Meyer, A. F., Poort, J., O'Keefe, J., Sahani, M. & Linden, J. F. A Head-Mounted Camera System Integrates Detailed Behavioral Monitoring with Multichannel Electrophysiology in Freely Moving Mice. Neuron 100, 46–60.e7 (2018).
38. Parlato, R., Otto, C., Begus, Y., Stotz, S. & Schutz, G. Specific ablation of the transcription factor CREB in sympathetic neurons surprisingly protects against developmentally regulated apoptosis. Development vol. 134 1663–1670 (2007).
39. Gilzenrat, M. S., Nieuwenhuis, S., Jepma, M. & Cohen, J. D. Pupil diameter tracks changes in control state predicted by the adaptive gain theory of locus coeruleus function. Cogn. Affect. Behav. Neurosci. 10, 252–269 (2010).

40. Vazey, E. M. & Aston-Jones, G. Designer receptor manipulations reveal a role of the locus coeruleus noradrenergic system in isoflurane general anesthesia. Proc. Natl. Acad. Sci. U. S. A. 111, 3859–3864 (2014).
41. Gomez, J. L. et al. Chemogenetics revealed: DREADD occupancy and activation via converted clozapine. Science 357, 503–507 (2017).
42. Bates, D., Mächler, M., Bolker, B. & Walker, S. Fitting Linear Mixed-Effects Models Usinglme4. Journal of Statistical Software vol. 67 (2015).
43. Aston-Jones, G. & Bloom, F. E. Norepinephrine-containing locus coeruleus neurons in behaving rats exhibit pronounced responses to non-noxious environmental stimuli. J. Neurosci. 1, 887–900 (1981).
44. Foote, S. L., Aston-Jones, G. & Bloom, F. E. Impulse activity of locus coeruleus neurons in awake rats and monkeys is a function of sensory stimulation and arousal. Proc. Natl. Acad. Sci. U. S. A. 77, 3033–3037 (1980).
45. Clayton, E. C., Rajkowski, J., Cohen, J. D. & Aston-Jones, G. Phasic activation of monkey locus ceruleus neurons by simple decisions in a forced-choice task. J. Neurosci. 24, 9914–9920 (2004).
46. Aston-Jones, G. & Cohen, J. D. An integrative theory of locus coeruleus-norepinephrine function: adaptive gain and optimal performance. Annu. Rev. Neurosci. 28, 403–450 (2005).
47. Aston-Jones, G., Foote, S. L. & Bloom, F. E. Low doses of ethanol disrupt sensory responses of brain noradrenergic neurones. Nature 296, 857–860 (1982).
48. Chen, F.-J. & Sara, S. J. Locus coeruleus activation by foot shock or electrical stimulation inhibits amygdala neurons. Neuroscience 144, 472–481 (2007).
49. Van Dam, D., Vermeiren, Y., Aerts, T. & De Deyn, P. P. Novel and sensitive reversed-phase high-pressure liquid chromatography method with electrochemical detection for the simultaneous and fast determination of eight biogenic amines and metabolites in human brain tissue. J. Chromatogr. A 1353, 28–39 (2014).
50. Vermeiren, Y. et al. The monoaminergic footprint of depression and psychosis in dementia with Lewy bodies compared to Alzheimer's disease. Alzheimers. Res. Ther. 7, 7 (2015).
51. Janssens, J. et al. Cerebrospinal fluid and serum MHPG improve Alzheimer's disease versus dementia with Lewy bodies differential diagnosis. Alzheimers. Dement. 10, 172–181 (2018).
52. Vogt, N. Optogenetics turns up the heat. Nature methods vol. 16 681 (2019).
53. Owen, S. F., Liu, M. H. & Kreitzer, A. C. Thermal constraints on in vivo optogenetic manipulations. Nat. Neurosci. 22, 1061–1065 (2019).
54. 18 - The pupil. in Physiology of the Eye (Fourth Edition) (ed. Davson, H.) 468–477 (Academic Press, 1980).

2.10 Supplementary Information

2.10.1 Pupillometry in darkness (Box 1)

Certain experimental procedures, e.g. two-photon imaging, require the pupil to be recorded in absence of (visible) light. When performing pupillometry in darkness, the pupil may already be fully dilated. To pre-constrict the pupil, a small non-dispersing light source can be pointed at the contralateral eye (not the one recorded from), to avoid additional reflections. Both pupils will then equally constrict, owing to the consensual pupillary light reflex (see Box 2). The image below shows a mouse in a two-photon imaging setup. The right eye is recorded with a Raspberry Pi NoIR V2 camera while the left eye is illuminated with UV light (375nm) to pre-constrict the pupil otherwise dilated in absolute darkness. The graph on the right shows the pupil response to electrical LC stimulation (monophasic constant current pulse of 50 Hz, 1 ms, 200 uA for 2 s) after 1 min of baseline (n=2).

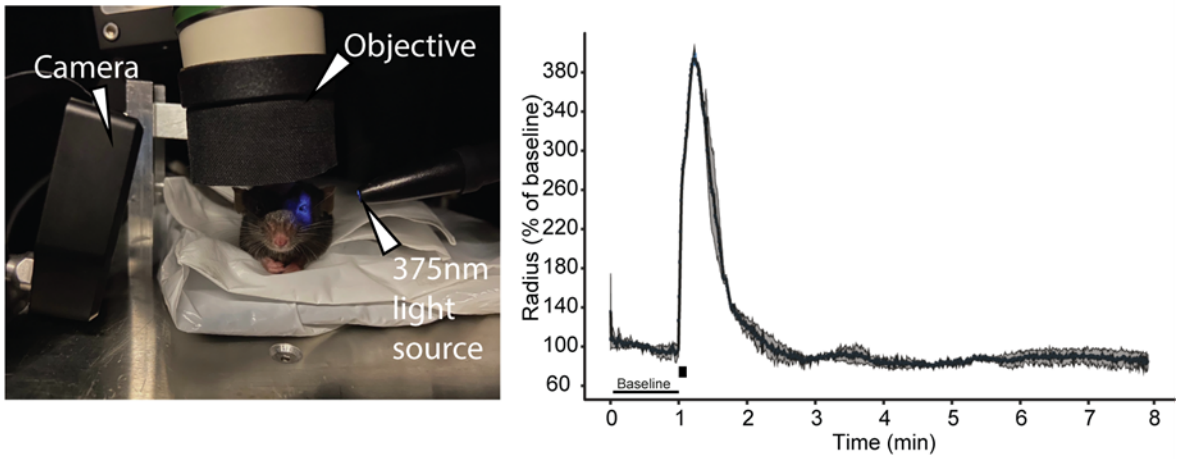

A. Hardware & Equipment

- 375nm 5mm UV-LED (e.g. NSPU510CS)
- 68 ohm resistor (depends on the forward voltage of the LED and the source voltage)
- (Optional) 10k potentiometer to control LED brightness
- 2 Wires with female dupont connector on one end
- Small tube with 5mm inner diameter and a small opening on one side (e.g. from an old ball-point pen)
- Soldering equipment
- Superglue
- 5V DC source (e.g. pins 4 (+5V) and 6 (GND) on Raspberry Pi)

B. Procedure for mounting the LED-lightsource

1. Solder resistor to LED cathode.

2. Solder one wire to the other end of the resistor and the other one to the LED anode. If using a potentiometer, solder one wire to one of the outer pins of the potentiometer and the other end of the resistor to the middle pin of the potentiometer.

3. Glue LED into the bigger end of the tube, pointing to the inside and wait until glue is cured.

4. Ensure correct polarity and connect the wires to 5V power.

5. Point the light at the eye contralateral to the recording

6. (Optional) Adjust light intensity by turning the potentiometer knob.

2.10.2 Recording the pupillary light reflex (Box 2)

The protocol presented here can be adapted with minor modifications to measure light-induced pupil diameter changes, i.e. the pupillary light reflex . The pupillary light reflex affects both eyes equally, no matter if one or both eyes are illuminated[418]. Therefore, the

pupillometry recording can be performed on one eye, while the light stimuli are directed only to the contralateral eye, thus avoiding light-interference with the video recordings. We recommend using a controllable LED light source for Raspberry Pi, for example via I2C bus. By using the aforementioned light source, intensity and timing of the light stimulus may be controlled via a python script executed on the Raspberry Pi. The figure shows recording of the pupil's response to a 30s stimulus (blue box) of UV (375nm; purple line) or white light (black line). The light-sources were built as described in Box 1. Traces each depict a single recording normalized to the 1 min baseline indicated at the bottom left.

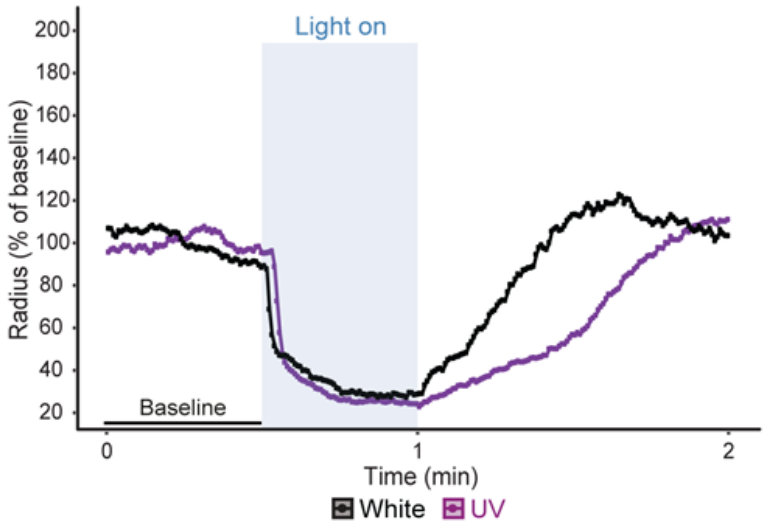

2.10.3 Absolute pupil measurements with DLC (Box 3)

The protocol presented here can be adapted to gain absolute pupil measurements. This requires a calibration object. First, the calibration object of known dimensions has to be installed in a fixed position close to the eye. It has to be oriented orthogonally to the camera and be approximately the same distance away from the camera as the eye. A new DeepLabCut network has to be trained that tracks two additional points (pc1 and pc2), one on each side of the calibration object (as shown in the figure below, panel on the left). To transform the DLC data into a metric representation, the distance between the two tracked calibration points in pixels has to first be calculated using the formula:

$$d_{px} = \sqrt{(pc1_{x\,(px)} - pc2_{x\,(px)})^2 + (pc1_{y\,(px)} - pc2_{y\,(px)})^2}$$

where pc1 is point 1 and pc2 point 2 of the calibration object and x(px)/y(px) the x/y-coordinates in pixels. We advise to use median values for pc1 and pc2 coordinates. Then, the absolute dimension of the calibration object in mm (dmm) has to be divided by this value to obtain the pixel to mm conversion ratio.

$$ratio_{mm\,/\,px} = d_{mm} \,/\, d_{px}$$

Now, x and y coordinates of all tracked points at each frame can be multiplied by the conversion ratio resulting in a metric description of the tracked points.

$$p_{x\,(mm)} = p_{x\,(px)} * ratio_{mm\,/\,px}$$
$$p_{y\,(mm)} = p_{y\,(px)} * ratio_{mm\,/\,px}$$

This has to be done for each DLC ".csv" file independently and can be done with any software with relative ease (Excel, R or MATLAB). The web app is fully compatible with the transformed data, however plots will still indicate pixels in the axis description. We therefore advise using the exportable plot, which allows for custom axis descriptions. The figure shows the same pupil trace in response to optogenetic LC activation (5 Hz / 1 mW / 10 s, 10 ms pulse duration, n=4) once analyzed in absolute (millimeters, middle panel) and once in relative (% of baseline, right panel) measurements. Note that the baseline pupil size varies between mice, which leads to larger standard variation if absolute values are reported, compared to normalized measurements.

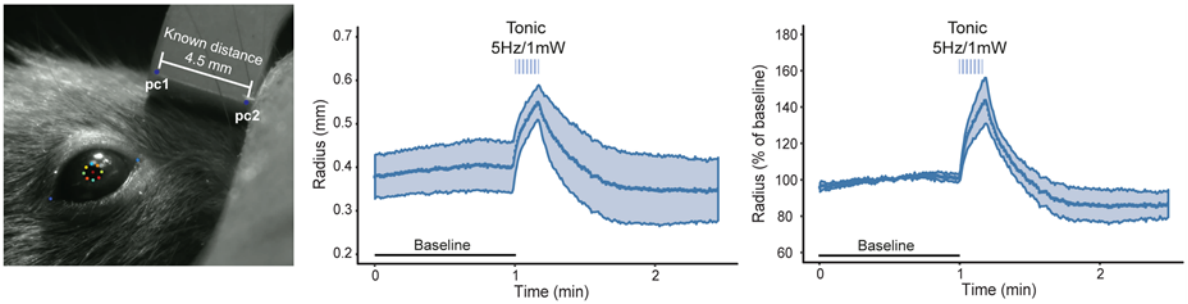

2.10.4 Supplementary Methods

Stereotaxic Surgeries. Surgeries for chemo- and optogenetic experiments were performed at least 2 weeks prior to pupillometry recordings, while surgeries for electrical locus coeruleus stimulation were performed immediately before pupillometry recordings. 2 to 3-month-old mice were subjected to stereotactic surgery. The mice were anesthetized with isoflurane and placed in a stereotaxic frame. For analgesia, animals received a subcutaneous injection of 2 mg/kg Meloxicam and a local anesthetic (Emla cream; 5% lidocaine, 5% prilocaine) before and after surgery. The health of the animals was evaluated by post-operative checks over the course of 3 consecutive days.

Electrical stimulation. For the electrical stimulation experiment, an electrode (200 µm diameter) was unilaterally placed within the locus coeruleus (coordinates from bregma: anterior/posterior -5.4 mm, medial/lateral 0.9 mm, dorsal/ventral -3.8 mm) or outside the locus coeruleus (coordinates from bregma: anterior/posterior -5.4 mm, medial/lateral 0.9 mm, dorsal/ventral -1.8 mm).

Chemogenetics. For the chemogenetic experiment 1 µL of virus (either ssAAV-5/2-hSyn1-dlox-hM3D(Gq)_mCherry(rev)-dlox-WPRE-hGHp(A) or ssAAV-5/2-hSyn1-dlox-mCherry(rev)-dlox-WPRE-hGHp(A)) were injected bilaterally into the locus coeruleus. Coordinates from bregma: anterior/posterior -5.4 mm, medial/lateral +/-1.0 mm, dorsal/ventral -3.8 mm.

Optogenetics. For optogenetic experiments 1 µL of ssAAV-5/2-hEF1α-dlox-hChR2(H134R)_EYFP(rev)-dlox-WPRE-hGHp(A) or ssAAV-5/2-hEF1a-dlox-EGFP(rev)-dlox-WPRE-bGHp(A) was delivered unilaterally to the locus coeruleus. Coordinates from bregma: anterior/posterior -5.3mm (female mice), or -5.4 mm (male mice); medial/lateral 1.0 mm, dorsal/ventral -3.8 mm). Optic fibers (200 µm diameter, 0.22 NA) were implanted unilaterally above the locus coeruleus (from bregma: anterior/posterior -5.4 mm, medial/lateral 0.9 mm, dorsal/ventral -3.5 mm).

2.10.5 Supplementary Figures

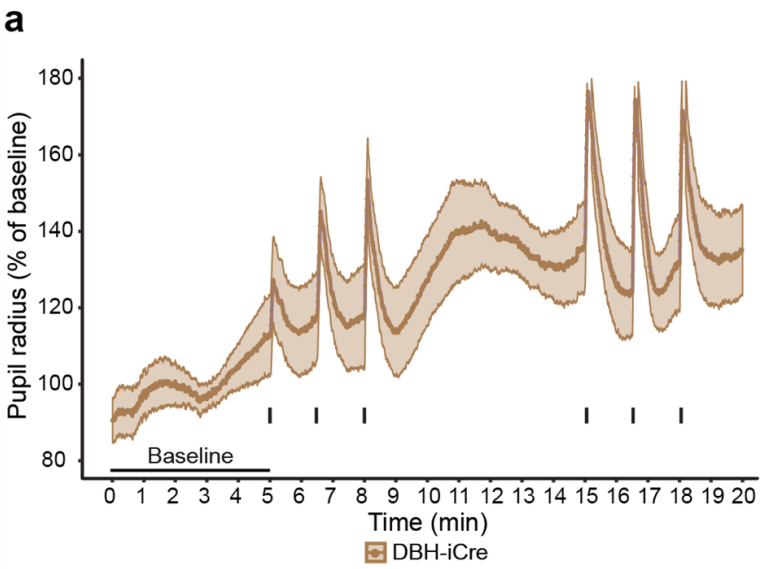

Supplementary Fig. 1: Tailshock reliably induces pupil dilations. (a) Pupillometry trace of DBH-iCre animals (n=10) that received multiple tailshocks (vertical black lines below the pupillometry trace) over a period of 20 min. Tailshocks (biphasic constant current pulse of 30 Hz, 2 ms, 1 A for 5 s) reliably led to pupil dilation (Formula: *Radius ~ Stimulation + (1|Animal);* β=4.26, SE=0.705, t(104)=6.050, p<0.0001). Data represent mean +/- SEM. Procedures were approved under licenses ZH161/17 and ZH169/17 by the local veterinary authorities, conforming to the guidelines of the Swiss Animal Protection Law, Veterinary Office, Canton Zurich (Act of Animal Protection 16 December 2005, and Animal Protection Ordinance 23 April 2008).

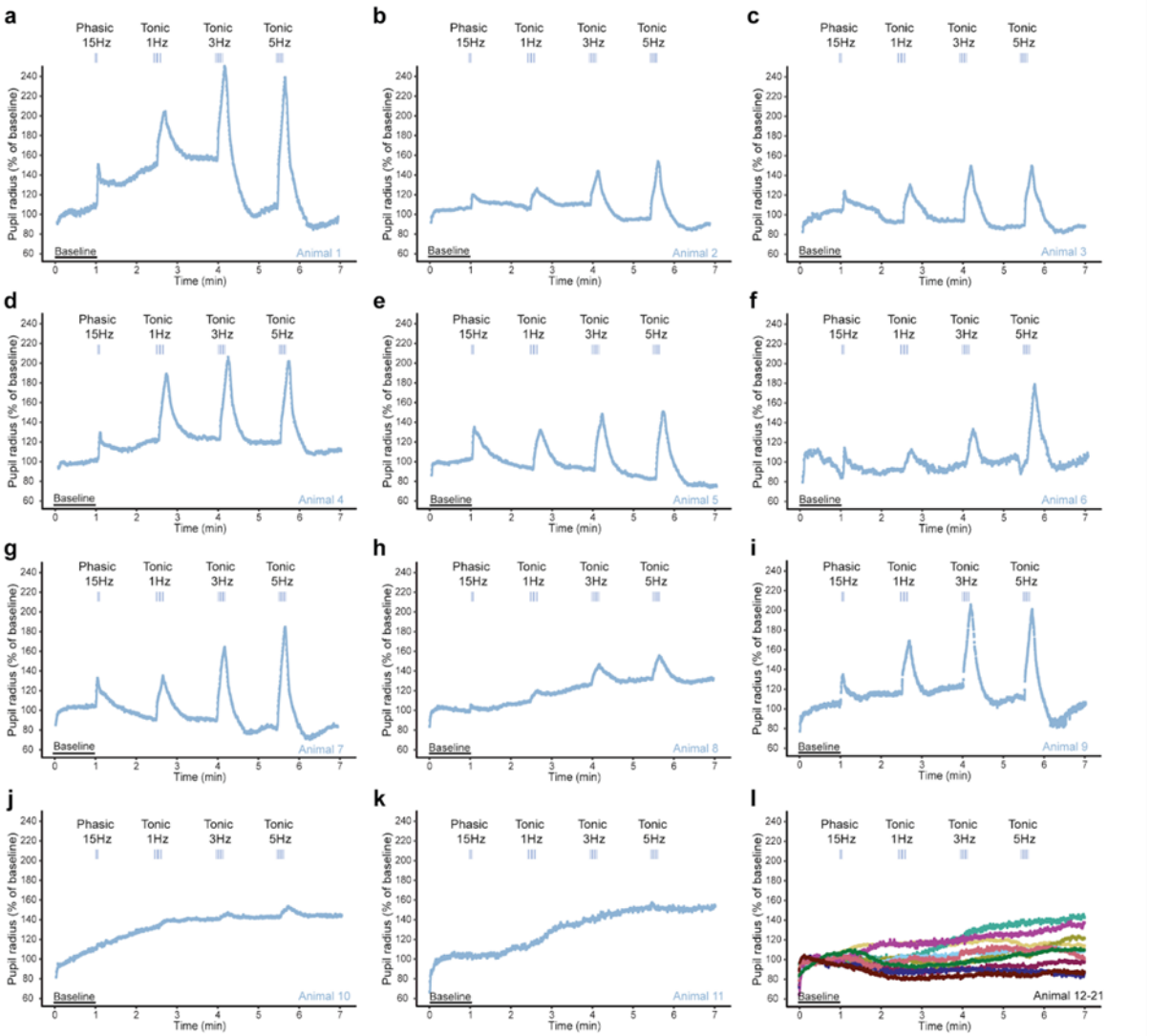

Supplementary Fig. 2: Individual pupillometry traces of ChR2-EYFP and EGFP mice, associated with Figure 3. (a-k) Individual pupillometry traces of ChR2-EYFP animals (1-11) that underwent unilateral optogenetic LC activation (Figure 3b shows the average of these traces). **(l)** Individual pupillometry traces of EYFP animals (12-21) that are shown in Figure 3b. Procedures were approved under licenses ZH161/17 and ZH169/17 by the local veterinary authorities, conforming to the guidelines of the Swiss Animal Protection Law, Veterinary Office, Canton Zurich (Act of Animal Protection 16 December 2005, and Animal Protection Ordinance 23 April 2008).

Chapter 3. Noradrenaline release from the locus coeruleus shapes stress - induced hippocampal gene expression

Mattia Privitera[1,2], Lukas M. von Ziegler[1,2], Amalia Floriou-Servou[1,2], Sian N. Duss[1,2], Runzhong Zhang[1], Sebastian Leimbacher[1], Oliver Sturman[1,2], Rebecca Waag[1,2], Fabienne K. Roessler[1], Annelies Heylen[3,5], Yannick Vermeiren[3,4], Debby Van Dam[3,5], Peter P. De Deyn[3,5,6] & Johannes Bohacek[1,2#]

[1] Laboratory of Molecular and Behavioral Neuroscience, Institute for Neuroscience, Department of Health Sciences and Technology, ETH Zurich, Switzerland

[2] Neuroscience Center Zurich, ETH Zurich and University of Zurich, Switzerland

[3] Laboratory of Neurochemistry and Behavior, Experimental Neurobiology Unit, Department of Biomedical Sciences, University of Antwerp, Wilrijk (Antwerp), Belgium

[4] Division of Human Nutrition and Health, Chair Group of Nutritional Biology, Wageningen University & Research (WUR), Wageningen, Netherlands.

[5] Department of Neurology and Alzheimer Center, University of Groningen and University Medical Center Groningen (UMCG), Groningen, Netherlands

[6] Department of Neurology, Memory Clinic of Hospital Network Antwerp (ZNA) Middelheim and Hoge Beuken, Antwerp, Belgium

Corresponding Author: Johannes Bohacek, johannes.bohacek@hest.ethz.ch

Preprint Published: 02 February 2023, BioRxiv
DOI: https://doi.org/10.1101/2023.02.02.526661

3.1 Abstract

Exposure to an acute stressor triggers a complex cascade of neurochemical events in the brain. However, deciphering their individual impact on stress-induced molecular changes remains a major challenge. Here we combine RNA-sequencing with selective pharmacological, chemogenetic and optogenetic manipulations to isolate the contribution of the locus coeruleus - noradrenaline (LN-NA) system to the acute stress response. We reveal that NA-release during stress exposure regulates a large and reproducible set of genes in the dorsal and ventral hippocampus via β-adrenergic receptors. For a smaller subset of these genes, we show that NA release triggered by LC stimulation is sufficient to mimic the stress-induced transcriptional response. We observe these effects in both sexes, independent of the pattern and frequency of LC activation. Using a retrograde optogenetic approach, we demonstrate that hippocampus-projecting LC neurons directly regulate hippocampal gene expression. Overall, a highly selective set of astrocyte-enriched genes emerges as key targets of LC-NA activation, most prominently several subunits of protein phosphatase 1 (Ppp1r3c, Ppp1r3d, Ppp1r3g) and type II iodothyronine deiodinase (Dio2). These results highlight the importance of astrocytic energy metabolism and thyroid hormone signaling in LC mediated hippocampal function, and offer new molecular targets for understanding LC function in health and disease.

3.2 Introduction

When an organism faces an acutely stressful situation, a set of evolutionarily conserved mechanisms are triggered to re-route all available resources to body functions that enhance performance and increase the chance of survival [1,2]. In the brain, stress exposure immediately activates the locus coeruleus-noradrenaline (LC-NA) system. Although the LC is a heterogeneous structure with modular organization, it appears that in strongly stressful situations broad activation of the LC - and subsequent widespread NA release throughout the brain - serves as a broadcast signal to orchestrate re-routing of computational resources to meet situational demands [3,4]. On the network level, for example, NA release from the LC is sufficient to trigger a rapid reconfiguration of large-scale networks that shift processing capacity towards salience processing [5,6]. On a circuit level, forebrain regions seem to be particularly important targets of the LC-NA system to influence cognitive processes and ultimately behavior. This involves the engagement of anxiety and memory circuits including the amygdala, hippocampus and prefrontal cortex, which leads to an increase in avoidance behavior [5,7–9] and supports memory formation of salient events [10–13].
While the insights into network and circuit dynamics of the LC have been galvanized by recent advances in circuit neuroscience tools, our understanding of the molecular impact of NA release has remained largely unexplored. However, we know that the stress response triggers multifaceted molecular cascades that profoundly change brain function and behavior in response to stressful events [1,2]. These molecular changes are mediated by a large number of neurotransmitters, neuropeptides and hormones, which operate on different time scales, to allow rapid activation, sustained activity and successful termination of the stress response. Many of the rapid molecular changes induced by stress exposure seem to be driven by NA. For example, several of the genes that are induced by an acute stress challenge can be blocked by β-adrenergic receptor antagonists [14]. However, a similar analysis on the genome-wide level has not been conducted. Further, it remains unknown whether NA release alone is sufficient to trigger transcriptomic changes in the first place.

Here, we profile the molecular fingerprint of stress-induced NA release by combining pharmacologic, chemogenetic and optogenetic manipulation of the LC-NA system with genome-wide transcriptomic analyses. We focus on the hippocampus, as it receives its sole NA supply from the LC [15–17], and because the molecular response to acute stress has been characterized in great detail in this region [18–20]. As the dorsal hippocampus (dHC) and ventral hippocampus (vHC) are involved in different circuits [21] and are transcriptionally very distinct [20,22], we analyze these regions separately.

3.3 Results

A recent multi-omic characterization of the acute stress response in the mouse hippocampus revealed that stress-induced transcriptional changes peak between 45-90 min after stress exposure, before gradually returning to baseline [18]. To determine how NA might contribute to these effects, we first measured the dynamics of NA turnover in response to a cold swim stress exposure in the brain. Using ultra-high performance liquid chromatography (uHPLC), we determined concentrations of NA and its main metabolite 3-Methoxy-4-hydroxyphenylglycol (MHPG) at various time points over 3 hours after swim stress exposure in the cortex (Fig. 1a). NA turnover (as measured by the MHPG/NA ratio) peaked at 45 min and returned to baseline within 90 min after stress onset (Fig. 1b). Therefore, we chose the 45 min time point to assess the contribution of NA signaling to stress-induced transcriptomic changes. To this end, we blocked adrenergic receptors using either the α1-adrenergic receptor antagonist prazosin, or the β-adrenergic receptor antagonist propranolol prior to stress exposure (Fig. 1c). In line with our previous work [14,18,20], acute swim stress induced a robust transcriptional response 45 min after stress exposure in both dorsal hippocampus (dHC) and ventral hippocampus (vHC) (see Veh-C vs Veh-S in Fig. 1d, Supplementary Fig. 1a). Prazosin only mildly impacted stress-dependent transcriptional changes in the dHC and vHC (see Veh-S vs Pra-S in Fig. 1d, Supplementary Fig. 1a). Surprisingly, prazosin seemed to slightly amplify - rather than prevent - some stress effects (Supplementary Fig. 1b). In contrast, propranolol had a profound impact, preventing many of the stress-induced changes in the dHC and vHC (see Veh-S vs Pro-S in Fig. 1d, Supplementary Fig. 1a). Indeed, a direct comparison between the stress group and the stress + propranolol group found many genes that were significantly altered by propranolol administration (Fig. 1e, Supplementary Fig. 1c). This response to propranolol was very similar in the dHC and vHC (Fig. 1f).

While blocking β-adrenergic receptors was able to block stress-induced gene expression, we did not test whether propranolol might decrease gene expression already at baseline, independent of stress. Additionally, all tests had thus far been conducted in male mice, raising the question about potential sex differences in NA-mediated transcriptomic responses. To address these two issues, we repeated the experiment in both sexes and included a group that received a propranolol injection but was not exposed to stress (Fig. 1g). As we did not detect major differences between noradrenergic responses in the dHC and vHC, we restricted our analysis to the vHC for this experiment. Using an appropriate multiplicative statistical model (stress * injection) we found again that many stress-responsive genes also had a significant stress:propranolol interaction (Fig. 1h). We also found no significant differences in propranolol-mediated effects between male and female mice (Fig. 1h). Furthermore, we could show that the stress-induced genes that were sensitive to propranolol treatment in the initial experiment were again activated by stress and blocked by propranolol (Supplementary Fig. 1d); at the same time, we confirmed that

propranolol did not change the expression level of these genes in the absence of stress (Fig. 1h). We then expanded our analysis across all vHC samples of both experiments. We employed a method that corrects for inter-experimental baseline effects prior to the statistical analysis of the combined dataset [23]. The results corroborate the initial findings, providing a *bona fide* list of stress-responsive genes that are blocked by propranolol (Supplementary Fig. 1e). To differently visualize this, we manually selected a few genes whose stress-induced induction was blocked by propranolol pre-treatment either partially (*Apold1*), or completely (*Dio2*, *Sik1* and *Ppp1r3c*) (Supplementary Fig. 1f). We then used these genes to test whether direct activation of hippocampal β-adrenergic receptors is sufficient to induce these changes. To this end, we infused animals with the β-adrenergic receptor agonist isoproterenol into the dHC and assessed the expression of these genes by targeted qRT-PCR assays in the dHC (Supplementary Fig. 1g). Isoproterenol directly increased hippocampal expression of *Apold1*, *Dio2* and *Sik1* (Supplementary Fig. 1h). Taken together, this shows that for a large number of genes, NA signaling via β-adrenergic receptors is required to regulate the stress-induced transcriptional response, or to determine the magnitude of stress-induced changes.

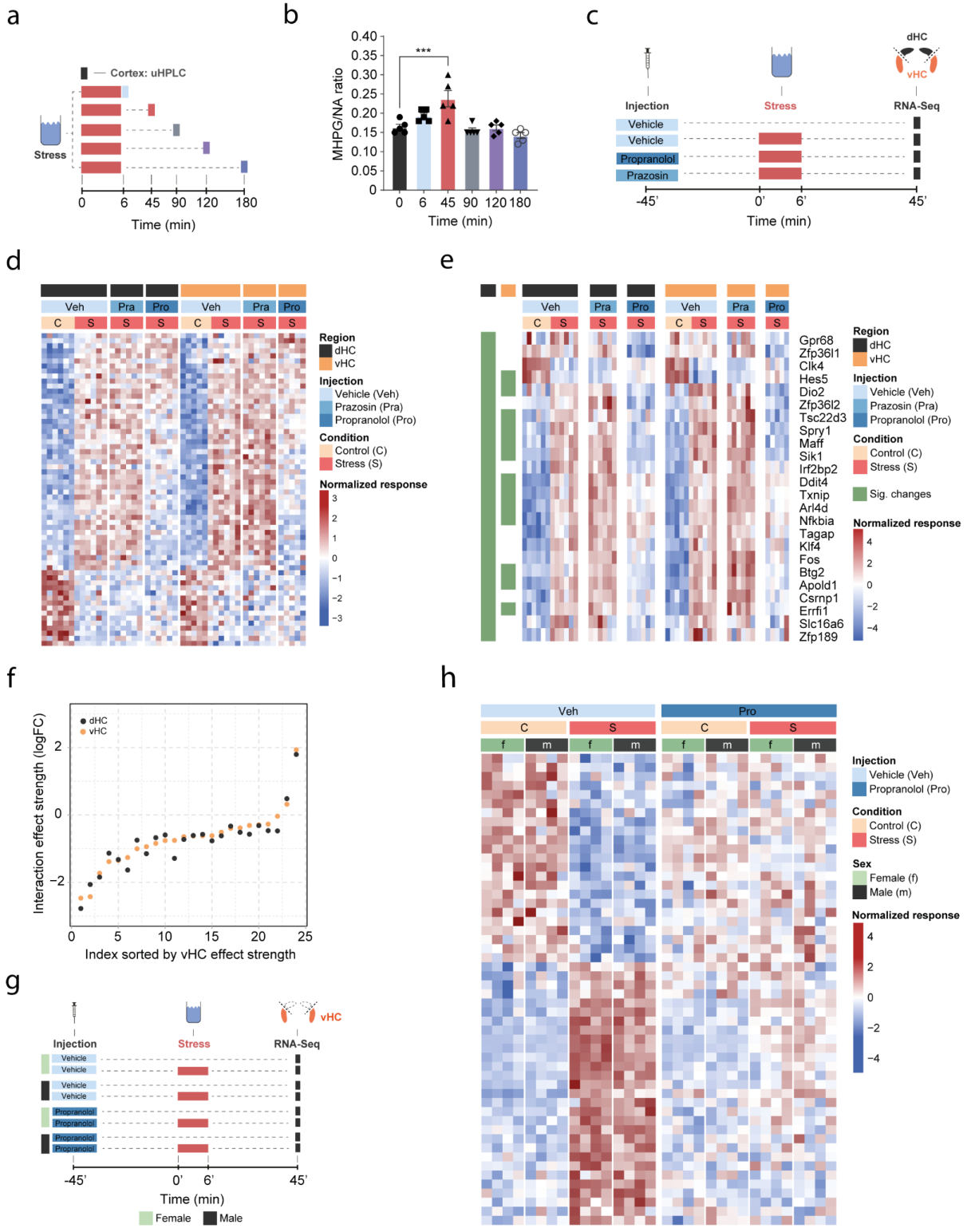

Fig. 1: β-adrenergic receptors mediate stress-induced transcriptomic changes in the hippocampus and are independent of subregion and sex. a, Experimental design for assessing stress-induced cortical noradrenaline (NA) turnover at various time points following stress exposure. **b**, Stress-dependent changes in cortical NA turnover, as measured by the ratio of 3-Methoxy-4-hydroxyphenylglycol (MHPG) and NA levels. NA turnover significantly increased within 45 min and returned to baseline within 90 min of stress onset (one-way ANOVA with Tukey's post hoc tests; $F(5, 24) = 10.55$, $p < 0.0001$). **c**, Experimental design for assessing the effect of prazosin (Pra, 1 mg/kg, i.p.) and propranolol (Pro, 10 mg/kg, i.p.) on stress-dependent transcriptomic changes in the dorsal (dHC) and ventral (vHC) hippocampus 45 min after stress exposure. **d**, Heatmap showing the expression of all differentially expressed genes across dHC and vHC and pharmacological treatments 45 min

after acute swim stress exposure. $n = 6$ per group. **e**, Heatmap selectively showing those stress-responsive genes that are affected by the β-adrenergic receptor antagonist propranolol 45 min after acute swim stress exposure in the dHC and vHC (FDR-adjusted $p < 0.05$). **f**, Strength of the propranolol effect on the transcriptomic stress response in the dHC and vHC for genes with a significant propranolol effect in either region (same genes as in panel **e**). Data are sorted by interaction strength in the vHC (orange) and the corresponding interaction strength in the dHC are shown in black for the same gene. **g**, Experimental design for assessing propranolol-dependent changes in the vHC of female and male mice. **h**, Heatmap showing expression of all stress-dependent genes that are affected by propranolol treatment between male and female mice in the vHC 45 min after acute swim stress exposure (FDR-adjusted $p < 0.05$). $n = 4$ per group. Individual data points are shown with bars representing mean ± s.e.m. $n = 5$ per group. ***$p < 0.001$.

An acute stress exposure triggers the release of a plentitude of stress mediators - neurotransmitters, peptides and hormones - that interact to regulate molecular changes [2]. As it is unclear how NA interacts with other stress mediators, we asked whether we could isolate the molecular changes for which NA release is not only required, but sufficient, by triggering NA release in the hippocampus. Because hippocampal NA supply is provided exclusively by long-range projections from the LC [15–17], we first pharmacologically activated NA release using the α2-adrenergic receptor antagonist yohimbine, which strongly disinhibits noradrenergic neurons (Fig. 2a). As expected, systemic administration of yohimbine (3 mg/kg, i.p.) led to a strong increase in cFos expression within the LC (Fig. 2b) and increased NA turnover in the cortex (Supplementary Fig. 2a). Because NA mediates the stress-induced increase in anxiety [5,7], we also evaluated behavioral changes in the open field test. We had shown previously that acute stress increases anxiety in the open field test [18,24] (Supplementary Fig. 3a), and very similarly yohimbine also suppressed locomotion and exploratory behaviors (Supplementary Fig. 3b). To directly compare the impact of stress and yohimbine injection on the transcriptomic response in the hippocampus, we then exposed mice to acute swim stress, or to yohimbine injection without stress exposure (Fig. 2c). Yohimbine induced a clear and consistent transcriptional response in the dHC and vHC. Direct comparison between stress and yohimbine disclosed no significant differences (Fig. 2d-e, Supplementary Fig. 2b), suggesting that yohimbine administration alone can mimic a large fraction of the stress-induced transcriptional response. To more specifically probe whether selective activation of the LC-NA system alone is sufficient to trigger the observed changes in gene expression, we turned to direct activation of the LC. First, we used the chemogenetic actuator hM3Dq [25] to trigger a strong and prolonged activation of the LC (Fig. 2f). In support of previous work [5,26], injection of an ultra-low dose of the potent hM3Dq-actuator clozapine (0.03 mg/kg) led to a strong cFos increase in tyrosine hydroxylase (TH) positive LC neurons in hM3Dq+, but not in hM3Dq- animals (Fig. 2g). Chemogenetic LC activation, similar to yohimbine, also induced an anxiety-like phenotype in the open field test (Supplementary Fig. 3c). Transcriptomic analysis revealed that chemogenetic LC activation induced significant transcriptomic changes that were similar in the dHC and vHC (Fig. 2h). Overall, these transcriptional changes affected fewer genes than those observed after systemic noradrenergic activation by yohimbine administration.

Despite its specificity, chemogenetic LC activation does not provide the temporal control to restrict LC activation to shorter periods of time. Thus, we repeated the experiment using optogenetic LC activation (Fig. 2i). To mimic stress-induced LC activity, LC neurons were unilaterally stimulated with 5 Hz in a 3 min off/on paradigm for 21 min, which has previously been shown to phenocopy stress-induced effects on behavior in mice [7,8]. Again, tissue was collected 45 min after the start of stimulation, and in a separate cohort also 90 min afterwards, to study how LC-mediated responses evolve over time. Optogenetic LC

activation led to a significant cFos increase only in the stimulated LC hemisphere of ChR2+ animals, and these changes were significant at both time points (Fig. 2j). Stimulated ChR2+ animals also showed a significant increase in the MHPG/NA ratio 45 and 90 min after stimulation onset compared to controls (Fig. 2k). Additionally, we found that tonic 5 Hz activation of the LC led to immediate pupil dilation in ChR2+, but not in ChR2- animals (Fig. 2l), as previously described [26]. Unilateral 5 Hz stimulation also reduced exploratory rearing behaviors in ChR2+ animals in the open field test (Supplementary Fig. 3d). Similar to the effects of acute stress and chemogenetic LC activation, unilateral 5 Hz stimulation of the LC induced significant transcriptomic changes at the 45 min time point in the ipsilateral vHC of ChR2+ mice compared to controls (Fig. 2m). Notably, most of these changes disappeared again 90 min after stimulation onset, indicating that the LC-NA system mainly induces an early wave of transcriptomic changes in the hippocampus, which are not maintained over longer periods of time.

Next, we leveraged the extensive transcriptional data presented thus far to test which genes were consistently responsive to the various manipulations of the noradrenergic system across experiments. First, we compared gene expression changes induced by yohimbine, chemogenetic and optogenetic LC activation in the vHC. This allowed us to identify a small set of genes that are very consistently regulated across all modes of LC activation (Fig. 2n). Second, we ranked genes across all the transcriptomic experiments according to their responsiveness to NA manipulations (based on p-value). This analysis includes acute stress exposure with pharmacological inhibition of NA receptors, as well as yohimbine treatment, chemogenetic and optogenetic LC activation. We then calculated the cumulative rank for each gene across all experiments to find genes with the most consistent response to NA manipulations (Supplementary table 1). This analysis reproduced most of the genes identified in Figure 2n, and additionally revealed more genes with particularly robust changes in response to LC-NA manipulations across experiments (Fig. 2o, Supplementary Fig. 4). The top 10 genes were *Dio2*, *Ppp1r3c*, *Ppp1r3g*, *Sik1*, *Tsc22d3*, *Ppp1r3d*, *F3*, *Sertad1*, *Nr4a1* and *Timp3*. For visualization, the top 4 of these genes are shown across all LC-NA manipulations in Supplementary Fig. 4. Going forward, we use this as a *bona fide* list of LC-NA-responsive genes.

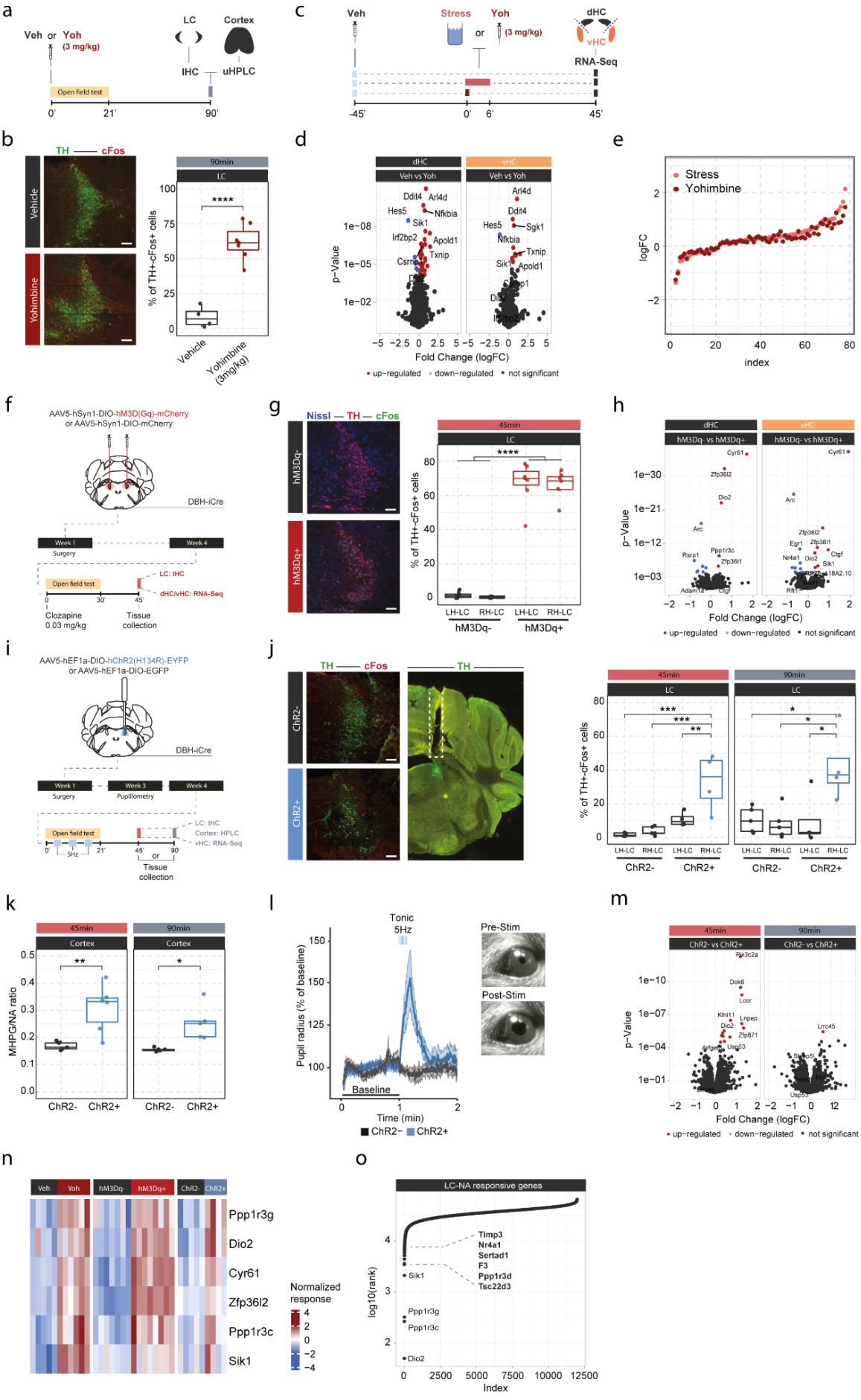
a
Veh or Yoh (3 mg/kg)
LC
Cortex
IHC
uHPLC
Open field test
0'
21'
90'
b
TH — cFos
Vehicle
Yohimbine
90min
LC
% of TH+cFos+ cells
****
Vehicle
Yohimbine (3mg/kg)
c
Veh
Stress
Yoh
or
(3 mg/kg)
dHC
vHC
RNA-Seq
-45'
0'
6'
45'
d
dHC
vHC
Veh vs Yoh
p-Value
Fold Change (logFC)
up-regulated
down-regulated
not significant
e
Stress
Yohimbine
logFC
index
f
AAV5-hSyn1-DIO-hM3D(Gq)-mCherry
or AAV5-hSyn1-DIO-mCherry
DBH-iCre
Week 1
Surgery
Week 4
Open field test
LC: IHC
dHC/vHC: RNA-Seq
Clozapine
0.03 mg/kg
Tissue
collection
g
Nissl — TH — cFos
hM3Dq-
hM3Dq+
45min
LC
% of TH+cFos+ cells
****
LH-LC
RH-LC
h
dHC
vHC
hM3Dq- vs hM3Dq+
p-Value
Fold Change (logFC)
up-regulated
down-regulated
not significant
i
AAV5-hEF1a-DIO-hChR2(H134R)-EYFP
or AAV5-hEF1a-DIO-EGFP
DBH-iCre
Week 1
Surgery
Week 3
Pupillometry
Week 4
Open field test
LC: IHC
Cortex: HPLC
vHC: RNA-Seq
5Hz
21'
45'
90'
or
Tissue
collection
j
TH — cFos
TH
ChR2-
ChR2+
45min
90min
LC
% of TH+cFos+ cells
***
**
*
LH-LC
RH-LC
ChR2-
ChR2+
k
45min
90min
Cortex
MHPG/NA ratio
**
*
ChR2-
ChR2+
l
Tonic
5Hz
Pre-Stim
Post-Stim
Pupil radius (% of baseline)
Baseline
Time (min)
ChR2−
ChR2+
m
45min
90min
ChR2- vs ChR2+
p-Value
Fold Change (logFC)
up-regulated
down-regulated
not significant
n
Veh
Yoh
hM3Dq-
hM3Dq+
ChR2-
ChR2+
Ppp1r3g
Dio2
Cyr61
Zfp36l2
Ppp1r3c
Sik1
Normalized
response
o
LC-NA responsive genes
log10(rank)
Timp3
Nr4a1
Sertad1
F3
Ppp1r3d
Tsc22d3
Sik1
Ppp1r3g
Ppp1r3c
Dio2
Index

Fig. 2: Locus Coeruleus-mediated transcriptomic changes in the hippocampus. a, Experimental design for assessing LC activation and cortical NA release induced by injection of yohimbine (3 mg/kg, i.p.). **b**, Representative images and quantification of LC activation in mice 90 min after injection of vehicle or yohimbine as measured by cFos (red) and tyrosine hydroxylase (TH, green) coexpression within LC neurons. Yohimbine injection increased cFos expression within LC neurons compared to vehicle-injected animals (unpaired t test; t(8.9) = -8.814, p = 1.083e-05). Vehicle, n = 4; Yohimbine n = 7. Scale bar: 100µm. **c**, Experimental design for comparing molecular changes in the hippocampus after acute swim stress exposure or yohimbine administration. **d**, Volcano plots showing differentially expressed RNA transcripts in the dorsal (dHC) and ventral (vHC) hippocampus between control (Veh) and yohimbine (Yoh) injected animals 45 min after injection. Red and blue values represent changes with FDR-adjusted p<0.05 (Veh n = 6, Yoh n = 6). **e**, Strength of the yohimbine effect in comparison to the transcriptomic stress response. Data are sorted by interaction strength in the stress group (orange) and the corresponding interaction strength of the yohimbine group are shown in dark red for the same gene. **f**, Experimental design for assessing LC activation and hippocampal transcriptomic changes induced by chemogenetic LC activation. **g**, Representative images and quantification of LC activation in mice 45 min after injection of clozapine (0.03 mg/kg) in hM3Dq- and hM3Dq+ animals as measured by cFos (green) and tyrosine hydroxylase (TH, red) coexpression within LC neurons. Neurons are stained with Nissl (blue). Clozapine injection increased cFos expression within LC neurons in hM3Dq+ animals compared to hM3Dq- animals (one way anova; F(3, 23) = 135.4, p = 9.34e-15). hM3Dq- n = 6, hM3Dq+ n = 7. Scale bar: 100µm. **h**, Volcano plots showing differentially expressed RNA transcripts between hM3Dq- and hM3Dq+ animals 45 min after injection of clozapine (0.03 mg/kg) in the dHC and vHC. Red and blue values represent changes withwith FDR-adjusted p<0.05 (hM3Dq- n = 6, hM3Dq+ n = 7). **i**, Experimental design for assessing LC activation, cortical NA release, pupillometry and hippocampal transcriptomic changes induced by optogenetic 5 Hz LC activation. **j**, Representative images and quantification of LC activation in mice after 5 Hz optogenetic LC activation as measured by cFos (red) and tyrosine hydroxylase (TH, green) coexpression within LC neurons in stimulated and non-stimulated LC hemispheres of ChR2- and ChR2+ animals. 5 Hz stimulation increased cFos expression within LC neurons in stimulated LC hemispheres of ChR2+, but not in ChR2- animals 45 min (one-way ANOVA with Tukey's post hoc tests; F(3, 14) = 12.91, p = 0.000256) and 90 min after stimulation onset (one way ANOVA with Tukey's post hoc tests; F(3, 14) = 5.866, p = 0.00824). ChR2- (45 min), n = 5; ChR2- (90 min), n = 5; ChR2+ (45 min), n = 4; ChR2+ (90 min), n = 4. Scale bar: 100µm. **k**, Quantification of cortical MHPG/NA ratio, as measured by uHPLC, after 5 Hz optogenetic LC activation in ChR2- and ChR2+ animals. 5 Hz stimulation increased cortical NA turnover in ChR2+ animals (unpaired t test; 45 min: t(3.6) = 8.444, p = 0.001681; 90 min: t(4.0854) =3.4127, p = 0.02608). ChR2- 45min, n = 5; ChR2- 90min, n = 5; ChR2+ 45min, n = 6; ChR2+ 90min, n = 5. **l**, Average pupil size changes in response to 5 Hz optogenetic LC activation in ChR2- and ChR2+ animals. 5 Hz stimulation increased pupil size in ChR2+, but not ChR2- animals. **m**, Volcano plots showing differentially-expressed RNA transcripts between ChR2- and ChR2+ animals 45 and 90 min after 5 Hz optogenetic LC activation in the ventral (vHC) hippocampus. Red and blue values represent changes with FDR-adjusted p<0.05 (ChR2- n = 10, ChR2+ n = 11). **n**, Heatmap showing genes that are commonly differentially expressed by yohimbine, chemogenetic and optogenetic induced LC activation. **o**, Logarithmic cumulative rank of genes across all experiments from figure 1 and 2 in terms of their NA responsiveness. A lower cumulative rank indicates that a gene is among the more significant hits across all analyses (for full list of included analyses see methods). Labels indicate the 10 genes identified to be most responsive to LC-NA stimulation. *p < 0.05, **p < 0.01, ***p < 0.001, ****p < 0.0001.

Our optogenetic data have demonstrated that LC neurons engage transcriptomic responses when firing at 5 Hz. Recent work has suggested that the effects of LC stimulation on brain processes, from behavior to brain network activity, depend on the firing pattern and frequency of the LC [27–29]. To investigate if the molecular responses would differ between these stimulation conditions, we optogenetically activated the LC using two tonic paradigms (3 and 5 Hz), and one phasic paradigm (15 Hz, see schematic in Fig. 3a). Stimulation was again conducted unilaterally in a 3 min off/on paradigm for 21 minutes for each of the stimulation groups, and tissue was collected for RNAseq 45 min after stimulation onset (Fig. 3a). To increase statistical power in the face of higher variability due to the relatively small sample sizes (n=5-6 mice per group), we restricted our analysis to the ten most LC-NA-responsive genes identified earlier. Surprisingly, we found that expression of these genes was mostly indiscriminately affected by tonic 3 Hz, 5 Hz and phasic 15 Hz LC

stimulation (Fig 3b). These findings suggest that in contrast to circuit-wide changes, the molecular consequences to NA release seem to be rather robust and not sensitive to different firing intensities of the LC. While these transcriptomic changes seem to depend on LC-NA activity, our approach so far was not able to resolve whether NA mediates gene expression via direct effects within the hippocampus. Specifically, due to the widespread projections of the LC, it is possible that activation of other brain regions or other neurotransmitter systems might have led to indirect regulation of gene expression in the hippocampus. Thus, we selectively targeted only a subpopulation of LC neurons projecting to the hippocampus (LC_{HC}) using a unilateral, retrograde optogenetic approach (Fig. 3c). Retrograde virus expression was restricted to dorsomedially located LC neurons ipsilateral to the injection site (Fig. 3d), as previously described [16]. To confirm successful LC_{HC} stimulation, we directly assessed NA turnover in the cortex and dHC. Indeed, 5Hz stimulation of LC_{HC} neurons led to an increased MHPG/NA ratio 45 min after stimulation onset in the ipsilateral dHC but not in the cortex (Fig. 3e). In addition, 5 Hz stimulation of LC_{HC} neurons did not impact pupil size, emphasizing the modular organization of the LC (Fig. 3f). Within the vHC of the same animals we then assessed the transcriptional impact of targeted LC_{HC} 5 Hz activation on the top ten NA-sensitive genes in the vHC at the 45 min time point. Indeed, activation of hippocampus-projecting LC neurons affected most target genes, including *Dio2*, *Ppp1r3c* and *Ppp1r3g* (Fig. 3g-h).

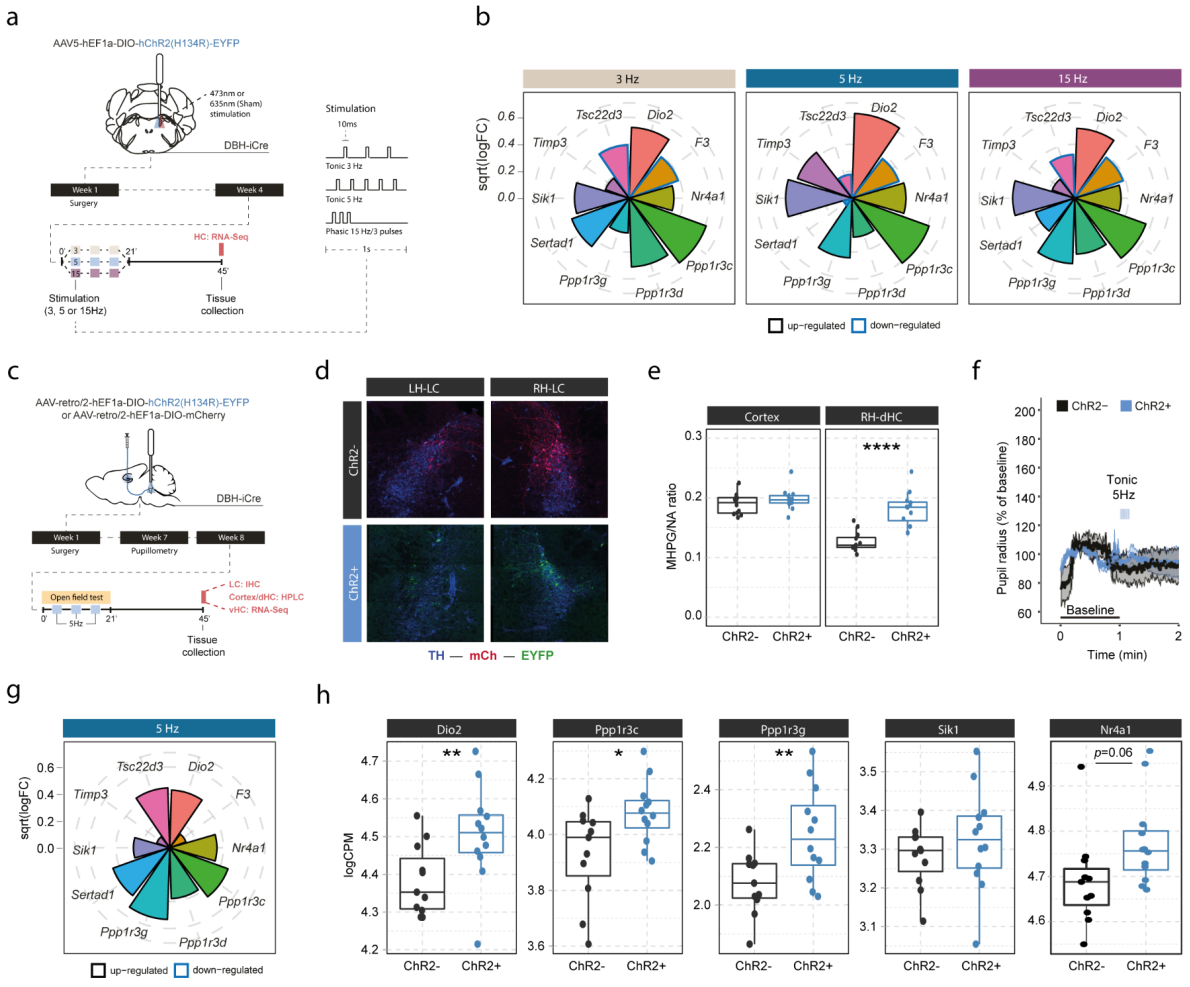

Fig. 3: LC-NA mediated molecular responses in the hippocampus are independent of LC firing pattern and frequency and are directly stimulated via hippocampus-projecting LC neurons. a, Experimental design for assessing molecular changes in the hippocampus induced by optogenetic LC activation with tonic (3 Hz and 5 Hz) and phasic (15 Hz) firing patterns. **b**, Radial plots showing expression changes (based on the logFC) of the most LC-NA-responsive genes after optogenetic LC activation in ChR2+ animals compared to controls (Sham $n = 6$, 3 Hz $n = 6$, 5 Hz $n = 7$, 15 Hz $n = 6$). Black borders indicate that the gene is upregulated, blue border downregulated. **c**, Experimental design for assessing molecular changes in the hippocampus induced by retrograde optogenetic 5 Hz activation of hippocampus projecting LC neurons (LC_{HC}). **d**, Representative images of retrograde mCherry (mCh, red) and ChR2-EYFP (EYFP, green) expression in tyrosine hydroxylase (TH, blue) positive LC neurons across hemispheres. **e**, Cortical and right dorsal hippocampal (RH-dHC) NA turnover as measured by ultra-high performance liquid chromatography 45 min after 5 Hz optogenetic activation of LC_{HC} neurons in ChR2- and ChR2+ animals. 5 Hz stimulation of LC_{HC} neurons increased dorsal hippocampal but not cortical NA turnover in ChR2+ animals (unpaired t test; t(17.43) = -5.5997, p = 2.911e-05). ChR2-, n = 12; ChR2+, n = 12. ****$p < 0.0001$. **f**, Average pupil size changes in response to 5 Hz optogenetic activation of LC_{HC} projecting neurons in ChR2- and ChR2+ animals. **g**, Radial plots showing expression changes (based on the logFC) of the top ten LC-NA responsive genes in response to optogenetic LC_{HC} activation with tonic 5 Hz stimulation in ChR2+ animals compared to ChR2- 45 min after stimulation onset (ChR2- $n = 12$, ChR2+ $n = 12$). **h**, Selective boxplots of NA-responsive genes *Dio2*, *Ppp1r3c*, *Ppp1r3g*, *Sik1* and *Nr4a1* in response to 5 Hz optogenetic activation of LC_{HC} projecting neurons in ChR2- and ChR2+ animals 45 min after stimulation onset. (ChR2- $n = 12$, ChR2+ $n = 12$). 5 Hz optogenetic activation of LC_{HC} projecting neurons increased hippocampal expression of *Dio2*, *Ppp1r3c*, *Ppp1r3g* and *Nr4a1*. *$p < 0.05$, **$p < 0.01$, ***$p < 0.001$, , ****$p < 0.0001$.

To understand in more detail how these genes are affected by stress we compared their expression across various publicly available datasets. First, we investigated whether the expression of *Dio2, Ppp1r3c, Ppp1r3g, Sik1* and *Nr4a1* is specific to acute swim stress exposure or independent of the stress context. Therefore, we compared their expression in a dataset comparing the effect of multiple stressors on the hippocampal transcriptome [20]. We found that these genes are not only upregulated by swim stress, but also by novelty stress, restraint and footshock stress (Fig. 4b). This suggests that expression of these genes is robustly induced by a wide range of stressors.

We then interrogated a recently published stress resource, which tracks stress-induced transcriptional changes over time in the hippocampus [18]. Across 4 hours following acute swim stress exposure, we found two distinctive expression patterns among these genes. While *Sik1* and *Nr4a1* show the characteristics of an immediate early gene with a sharp rise and fall in expression within 90 min of stress onset, upregulation of *Dio2, Ppp1r3c* and *Ppp1r3g* is maintained for at least 2-4 hours following stress exposure (Fig. 4d), suggesting that mechanisms are in place to prolong expression beyond the initial rise in NA. Reanalysis of a hippocampal single-nucleus RNA-sequencing dataset after a swim stress challenge [18] revealed that stress-induced upregulation of *Dio2, Ppp1r3c* and *Ppp1r3g* seems predominantly restricted to astrocytes, while *Sik1* and *Nr4a1* show a broader expression among glia, neuronal and vascular cells.

Finally, to determine if these transcripts are also actively translated in astrocytes after stress exposure, we re-analysed a dataset using translating ribosome affinity purification followed by RNA sequencing (TRAPseq) - in astrocytes of the somatosensory cortex after a similar acute swim stress paradigm as described here [30]. We found that *Dio2*, *Ppp1r3c, Ppp1r3g* and *Nr4a1* are significantly upregulated after stress exposure. Altogether, these results highlight that the NA-dependent gene expression changes that occur in response to stress exposures are most prominent in astrocytes.

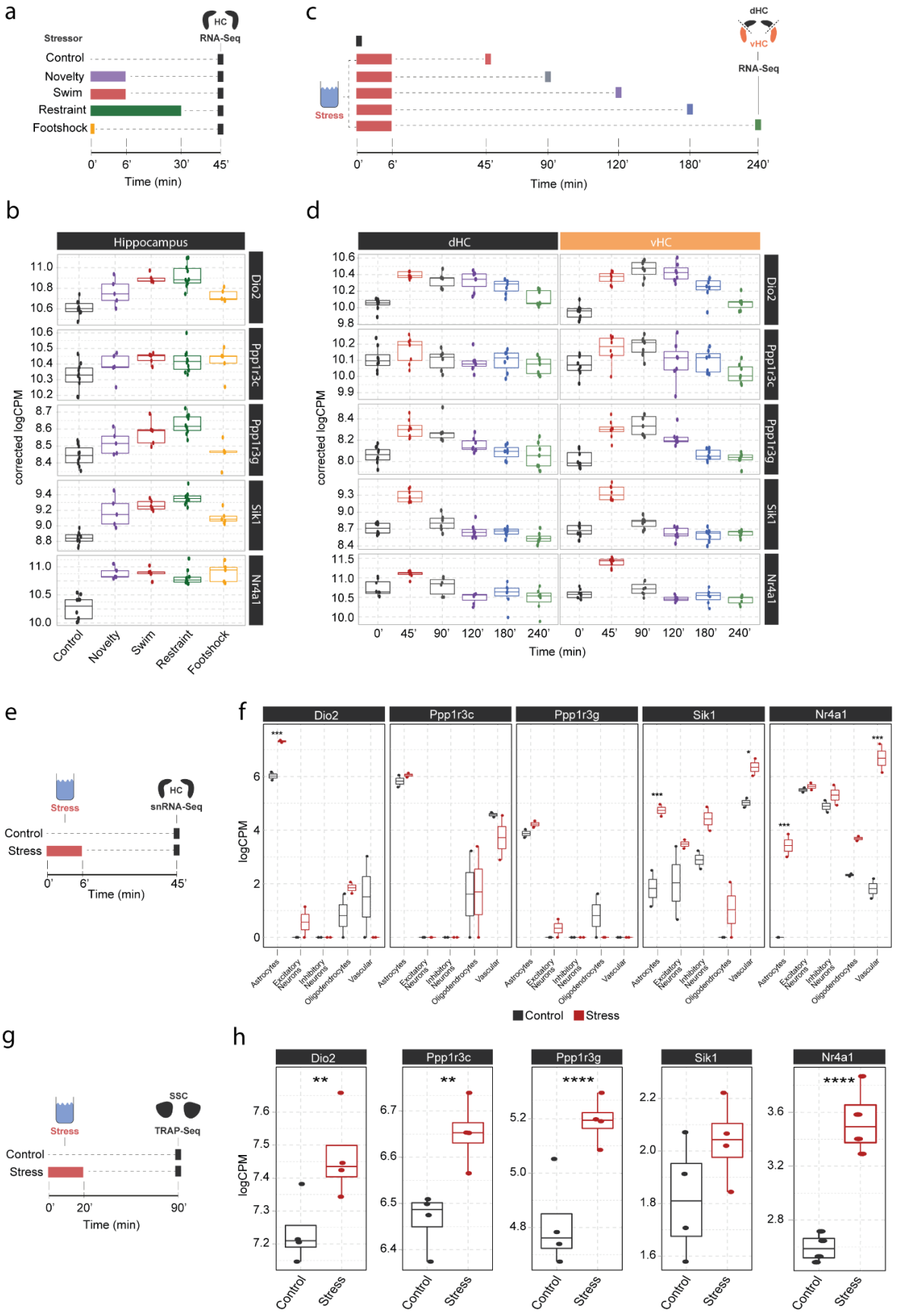

Fig 4. Screening of publicly available datasets shows that the noradrenaline-regulated genes *Dio2, Ppp1r3c, Ppp1r3g, Sik1* and *Nr4a1* are induced by various stressors predominantly in astrocytes. a, Experimental design for assessing transcriptomic changes in the hippocampus induced by different stressors as

performed by Floriou-Servou et. al [20]. These stressors included a 10 min exposure to the open field test (Novelty), a 6 min cold swim stress (Swim), a 30 min immobilization stress (Restraint) and exposure to a 1 mA footshock (Footshock). **b**, Selective boxplots of top NA-responsive genes *Dio2*, *Ppp1r3c*, *Ppp1r3g*, *Sik1* and *Nr4a1* in response to different stressors. Control $n = 10$, Novelty $n = 5$, Swim $n = 5$, Restraint $n = 10$, Footshock $n = 5$. **c**, Experimental design for assessing transcriptomic changes in the dorsal and ventral hippocampus across 4 hours following acute swim stress exposure as performed by von Ziegler et. al [18]. **d**, Selective boxplots showing expression changes of top NA-responsive genes *Dio2*, *Ppp1r3c*, *Ppp1r3g*, *Sik1* and *Nr4a1* across 4 hours following acute swim stress exposure. Control $n = 8$, 45 min $n = 8$, 90 min $n = 7$, 120 min $n = 7$, 180 min $n = 7$, 240 min $n = 7$. **e**, Experimental design for assessing single cell transcriptomic changes in the hippocampus 45 min following acute swim stress exposure by single-nucleus RNA sequencing as performed by von Ziegler et. al [18]. **f**, Selective boxplots showing expression changes of top NA-responsive genes *Dio2*, *Ppp1r3c*, *Ppp1r3g*, *Sik1* and *Nr4a1* across cell types of the hippocampus 45 min following acute swim stress exposure. Control $n = 2$, Stress $n = 2$. **g**, Experimental design for assessing actively translated RNA in the somatosensory cortex 90 min following a 20 min acute swim stress exposure by TRAP sequencing as performed by Murphy-Royal et. al [30]. **h**, Selective boxplots of top NA-responsive genes *Dio2*, *Ppp1r3c*, *Ppp1r3g*, *Sik1* and *Nr4a1* in the somatosensory cortex 90 min following a 20 min acute swim stress exposure. Acute stress increases the binding of *Dio2*, *Ppp1r3c*, *Ppp1r3g* and *Nr4a1* mRNA to the ribosome. Control $n = 4$, Stress $n = 4$. $^{*}p<0.05$, $^{**}p < 0.01$, $^{***}p < 0.001$, $^{****}p < 0.0001$.

3.4 Discussion

3.4.1 Dissecting stress with transcriptomics

The widespread molecular changes induced in the brain by an acute stress exposure [18–20,31] are part of a healthy stress response, and their dysregulation is often a hallmark of neuropsychiatric disorders [32,33]. To date, the contribution of corticosteroid signaling to stress-induced transcriptional changes has been well characterized [19,34,35], yet the contribution of other stress-mediators remains unexplored. Here, we extensively characterize the contribution of noradrenergic signaling to the transcriptomic response in the hippocampus during stress. By combining transcriptomics with circuit-specific manipulation of the LC-NA system, our unbiased approach reveals a small, but highly reproducible set of genes that are regulated directly by NA release from the LC. This gene set identifies astrocytes as a key target for NA-induced transcriptional changes.

3.4.2 Complex interactions between stress mediators

Our results indicate that the transcriptomic response to a natural stressor is more complex than the gene expression changes induced solely by NA. This is well in line with the notion that multiple stress-mediators contribute to the molecular response, and that these systems can also interact with each other. In this context, it is noteworthy that the response to LC-NA activation we observe in our experiments is short in duration. Following temporally-precise optogenetic LC activation, gene expression changes did resolve within 90 min. This is noticeably different from an actual stress response, where gene expression evolves over a 4-hour period [18]. Specifically, LC-NA regulated genes like *Ppp1r3c, Ppp1r3g* and *Dio2*, were elevated for several hours after stress exposure (Fig. 4d). This suggests that other stress-induced signals can also regulate these genes more slowly or with a greater delay. Indeed, a recent study reported that activation of the glucocorticoid receptor by dexamethasone can induce strong transcriptomic changes 4 hours after injection across multiple brain regions [36]. Analyzing their data we found that *Dio2*, *Ppp1r3c* and *Ppp1r3g* were all upregulated 4 hours after dexamethasone injection. This supports the concept that

NA can act as a rapid molecular regulator, whereas glucocorticoid signaling can extend these stress-induced changes over longer time periods [37].
In contrast to the small set of genes triggered by isolated LC-NA activation, blocking β-receptors prevents the induction of a large fraction of genes normally activated by natural stressors. This suggests that even if NA release alone is not sufficient to activate large numbers of genes, it is required to enable or enhance gene expression triggered via other mechanisms. A powerful regulator of transcription is neuronal activity linked to enhanced glutamate release [38,39]. The notion that NA release could enhance glutamate-dependent transcriptional cascades is in line with physiological evidence that NA can increase the excitability of neurons [40], and with the "glutamate amplifies noradrenergic effects" (GANE) model, which posits that NA can amplify local glutamate release to create hot-spots of activity [41].
Finally, our observation that systemic administration of the α2-adrenergic receptor antagonist yohimbine very closely recapitulates the transcriptional response to stress stands in contrast to the much more selective transcriptional changes observed after chemogenetic or optogenetic LC-NA activation. This difference could in part be due to the fact that systemic yohimbine injection will also antagonize postsynaptic α2-adrenergic receptors. This could have a more widespread impact on the hippocampus (and other brain regions) than isolated LC-NA activation, further enhancing excitability by preventing α2-mediated inhibition of cAMP production. Additionally, systemic yohimbine administration and noradrenergic activity have been shown to induce corticosterone release into the blood [42–44], while propranolol does not [45]. Thus, yohimbine injection could have broader transcriptional consequences, including corticosteroid-mediated effects on gene expression.

3.4.3 Transcriptomic fingerprinting of NA effects using LC circuit manipulation

While systemic pharmacological treatments have been a common approach in studying the effects of different stress mediators and their receptors, they lack specificity and do not provide causal evidence that the release of a given stress mediator is sufficient to trigger molecular changes. By directly combining selective chemogenetic activation of the LC with transcriptomic analyses in the hippocampus, we were able to identify a subset of stress-responsive genes that depend on β-adrenergic signaling, and which can be triggered by NA alone in the absence of a physiological stress response. Using optogenetics we were able to validate these findings and further demonstrate that the strongest NA-mediated changes are similarly affected by tonic (3 Hz and 5 Hz) and phasic (15 Hz) LC stimulation. Interestingly, this is in contrast with our previous findings that these stimulation patterns differentially affect brain network connectivity (Grimm and Duss et al, 2022). This suggests that engagement of a transcriptomic response via β-adrenergic receptors seems common across these LC activity patterns, while changes on a network level might rely more on α1-mediated effects [5].
We found that direct activation of hippocampus-projecting LC neurons (LC_{HC}) was sufficient to increase expression of our top target genes, suggesting that local LC-NA release in the hippocampus is directly contributing to these changes during stress. While we did not extensively characterize LC_{HC} neurons, our data further show that in contrast to whole LC activation with 5 Hz, LC_{HC} neurons do not seem to project to the cortex nor do they affect pupil size.

3.4.4 Differences in the noradrenergic response across the hippocampal axis and sex

Our results suggest that the transcriptomic response is independent of sex, and uniform across the dorsal and ventral hippocampus. However, due to the multivariate design and our genome-wide approach, subtle changes might not have survived multiple-testing correction, particularly given that our study was not sufficiently powered to specifically identify sex differences. An example for this is the expression of *Ctla2b*, a gene which has previously been shown to be dependent on β-adrenergic signaling and selectively increased in females after stress exposure [14]. Indeed, targeted interrogation of our dataset shows that *Ctla2b* is increased by stress only in females but not males, yet this effect fails to pass multiple testing correction (Supplementary Fig. 6). Similarly, it is possible that subtle differences exist between dHC and vHC. As our data are publicly available, they can be used for targeted hypothesis testing of individual genes to generate leads for follow-up work.

3.4.5 LC-NA targeted genes

Across experiments, our transcriptomic screening revealed a conserved set of genes (Fig. 2o, Supplementary table 1) that are selectively regulated by NA from LC projections in the hippocampus following acute stress exposure. Cross-referencing our data with publicly available single-cell databases suggests that - among the top ten LC-NA sensitive genes - most are enriched in astrocytes [18,46]. Interestingly, immediate early genes commonly upregulated during stress and associated with neuronal activation like *Fos*, *Egr1*, *Arc*, *Dusp1* and *Npas4* [38,39,47,48], are not upregulated by LC activation (Supplementary Fig. 5). Taken together, our findings further add to accumulating evidence highlighting astrocytes as a direct and major cellular target of the LC-NA system [49–51] .

Our screen revealed *Dio2* as the most prominent target influenced by LC activity. *Dio2* is selectively expressed in astrocytes and encodes for the intracellular type II iodothyronine deiodinase, which converts thyroxine (T4) to the bioactive thyroid hormone 3,3',5-triiodothyronine (T3) and therefore regulates the local availability of T3 in the brain [52]. Enzymatic activity of DIO2 has further been shown to be increased by prolonged noradrenergic transmission through desipramine treatment in LC projection areas [53]. This suggests that the LC-NA system and its widespread projections could act as a major regulator of brain-derived T3. Along the same line, we found that three subunits of the astrocytic protein phosphatase 1 (*Ppp1r3d*, *Ppp1r3g* and *Ppp1r3c*) respond strongly to LC-NA activity. All three subunits enhance protein phosphatase 1 mediated glycogen synthesis. Especially *Ppp1r3c* expression has been found to be a master regulator of astrocytic glycogen synthesis and has previously been linked to NA activity [54,55]. Another important mechanism might include regulating sodium homeostasis via the widely expressed salt-inducible kinase 1 (*Sik1*). SIK1 has been shown to respond to neuronal activity and regulate Na+/K+-ATPase activity [56–59]. It was also found to detect low glucose availability and initiate gluconeogenesis in liver cells [60], a process which could also be important for noradrenergic activity in the brain. Our findings support the idea of the LC-NA system as a major regulator of brain-wide energy metabolism, stimulating astrocytic glycogen breakdown and consequently increasing energy supply to target areas [51,61].

Another interesting molecular target is the Nuclear Receptor Subfamily 4 Group A Member 1 (Nr4a1), a widely expressed transcription factor that could trigger broader downstream

changes. Within astrocytes, Nr4a1 activity was found to reduce oxidative stress and inflammation [419,420] and might further regulate blood brain barrier integrity [421,422]. Our re-analysis of published data showed that *Dio2*, *Ppp1r3c*, *Ppp1r3g* and *Nr4a1* are actively translated in somatosensory cortical astrocytes following acute stress exposure. It remains to be tested whether protein levels, transcription factor activity or enzymatic activity of these genes are also altered in the hippocampus, and what this ultimately means mechanistically for stress-related NA signaling.

3.4.6 Summary

Overall, we provide the first genome-wide characterization of the molecular impact of NA release in vivo in the brain. The set of genes that are sensitive to NA release from the LC point to astrocytes as key molecular targets of NA during stress, and suggest that astrocytic processes involving glycogen and thyroid hormone metabolism could be key to the neuromodulatory effects of NA in the hippocampus.

3.5 Methods

3.5.1 Animals

All experiments were conducted in accordance with the Swiss federal guidelines for the use of animals in research and under licenses ZH161/17, ZH106/20 and ZH067/2022 approved by the Zurich Cantonal veterinary office. For experiments with wild type animals, 2-3 month old C57Bl/6J mice were obtained directly from Janvier (France). For experiments involving chemo- and optogenetic LC manipulations, heterozygous C57BL/6-Tg(Dbh-icre)1Gsc mice were kept in breeding trios with wild-type C57BL/6J mice at the ETH Zurich animal facility (EPIC). All mice were housed in groups of 2-5 per cage in a temperature- and humidity-controlled facility on a 12-hour reversed light-dark cycle (lights off: 9:15 am; lights on: 9:15 pm), with food and water *ad libitum*, and used for experiments at the age of 2-4 months. All experiments were conducted during the animals' active (dark) phase. For all experiments, mice were single-housed 24 hours before exposure to stress or LC activation, which reduces corticosterone levels in both sexes, and avoids confounding gene expression effects from social stressors [14,66].

3.5.2 Stereotactic Surgeries

For experiments involving hippocampal infusions, female C57BL/6-Tg(Dbh-icre)1Gsc mice at the age of 2-3 months were subjected to stereotactic surgery. The mice were anesthetized with 4% isoflurane and then placed in a stereotaxic frame with continuous anesthesia of 2% isoflurane. For analgesia, animals received a subcutaneous injection of 5 mg/kg Meloxicam and buprenorphine (0.1 mg/kg), as well as application of the local analgesics lidocaine (2 mg/kg) and bupivacaine (2 mg/kg) before and after surgery. After the skull was exposed, bregma (defined as the intersection of the coronal and sagittal suture) was located and the skull placement corrected for tilt and scaling. Bilateral holes were drilled above the hippocampus at -1.8 mm AP and +/- 1.5 mm ML from bregma, followed by the implantation of a bilateral guide cannula (62036, RWD Life Science, China) into the hippocampus (coordinates from bregma: -1.8 mm AP, +/- 1.5 mm ML, -1.5 mm DV).

For chemo- and optogenetic experiments male C57BL/6-Tg(Dbh-icre)1Gsc mice at the age of 2-3 months were subjected to stereotactic surgery. The mice were anesthetized with 4% isoflurane and then placed in a stereotaxic frame with continuous anesthesia of 2% isoflurane. For analgesia, animals received a subcutaneous injection of 5 mg/kg Meloxicam and a local anesthetic (Emla cream; 5% lidocaine, 5% prilocaine) before and after surgery. After the skull was exposed, bregma was located and the skull placement corrected for tilt and scaling. Bilateral (chemogenetics) or unilateral (Right hemisphere, optogenetics) small holes were drilled above the LC at -5.4 mm AP and 0.9 mm ML from bregma. A pneumatic injector (Narishige, IM-11-2) and calibrated microcapillaries (Sigma-Aldrich, P0549) were then used to inject 1 µL of virus to the LC (coordinates from bregma: −5.4 mm AP, ± 1.0 mm ML, −3.8 mm DV). All Viral vectors were obtained from the Viral Vector Facility (VVF) of the Neuroscience Center Zurich. For chemogenetic experiments, either ssAAV-5/2-hSyn1-dlox-hM3D(Gq)_mCherry(rev)-dlox-WPRE-hGHp(A) (hM3Dq+) or ssAAV-5/2-hSyn1-dlox-mCherry(rev)-dlox-WPRE-hGHp(A) (hM3Dq-) were injected bilaterally.
For optogenetic experiments, ssAAV-5/2-hEF1α-dlox-hChR2(H134R)_EYFP(rev)-dlox-WPRE-hGHp(A) (ChR2+) or ssAAV-5/2-hEF1a-dloxEGFP(rev)-dlox-WPRE-bGHp(A) (ChR2-) were delivered unilaterally to the right hemisphere locus coeruleus. For retrograde activation of hippocampus projecting LC neurons, animals received one injection of either ssAAV-retro/2-hEF1a-dlox-hChR2(H134R)_EYFP(rev)-dlox-WPRE-hGHp(A) (ChR2+) or ssAAV-retro/2-hEF1a-dlox-mCherry(rev)-dlox-WPRE-hGHp(A) (ChR2-) to the ipsilateral dHC (coordinates from bregma: -2.10 mm AP, 1.5 mm ML; -1.8 mm DV) and vHC (coordinates from bregma: -3.30 mm AP, 2.75 mm ML; -4.0 mm DV). Additionally, all optogenetic animals were unilaterally implanted with an optic fiber (200 µm diameter, 0.22 NA) above the LC (coordinates from bregma: -5.4 mm AP, 0.9 mm ML, -3.5 mm DV). The health of all animals was monitored over the course of 3 consecutive days post-surgery. Experiments on operated animals were conducted 4-8 weeks post-surgery to allow for recovery and sufficient virus expression. All viruses were obtained from the Viral Vector Facility of the University of Zurich and ETH Zurich.

3.5.3 Drug injections/infusions

All drugs were freshly prepared immediately before experiments and dissolved in phosphate-buffered 0.9% saline (Gibco, pH 7.4). Drugs were administered intraperitoneally at their corresponding dosages: Yohimbine-Hydrochloride (3 mg/kg, Merck, Germany), Propranolol-Hydrochloride (10 mg/kg, Merck, Germany), Prazosin-Hydrochloride (1 mg/kg, Merck, Germany) and Clozapine (0.03mg/kg, Merck, Germany).
For intra-hippocampal infusions of isoproterenol hydrochloride (Merck, Germany), animals were restrained and the guide cannula was inserted with an injector needle (62236, RWD Life Science, China) connected to an infusion pump (R462 Syringe Pump, RWD Life Science, China) via plastic tubing. Prior to attachment, the tubing was filled with sunflower seed oil (Merck, Germany) and vehicle (0.9% saline) or isoproterenol, separated by a small air bubble. Afterwards, animals were allowed to freely roam their home cage for 2 minutes followed by bilateral intra-hippocampal infusions of vehicle drug or 1 µl of isoproterenol (3 µg/µl diluted in phosphate-buffered 0.9% saline) at 50 µl/min. Diffusion of vehicle and isoproterenol was allowed for another 2 min, before the animal was detached from the infusion setup and returned to its homecage.

3.5.4 Forced swim test

For the forced cold swim stress, mice were placed for 6 min in a plastic beaker (20 cm diameter, 25 cm deep) filled with 18 ± 0.1°C water to 17 cm, in a room with dim red lighting. Immediately after stress exposure, mice returned to their assigned single-housing homecage.

3.5.5 Open field test (OFT)

Open-field testing was performed in a square 45 cm (l) × 45 cm (w) × 40 cm (h) arena, and consisted of four black Plexiglas walls and a white PVC floor. Mice were tested under dim lighting (5 lux at the center of the arena). Mice were placed directly into the center of the open field and the tracking/recording was initiated 2 seconds after the mouse was detected. The test lasted 10 min for acute stress exposed animals, 21 min for yohimbine and optogenetic stimulated animals and 30 min for chemogenetic stimulated animals. Distance, time in center, supported and unsupported rearings were tracked by the software EthoVision XT14 (Noldus, Netherlands) and manual scoring. For pharmacological and chemogenetic experiments, animals received an i.p injection of yohimbine (3 mg/kg) or clozapine (0.03 mg/kg) immediately before being placed into the arena. For optogenetic experiments, animals were attached to the optic fiber and directly placed into the arena.

3.5.6 Optogenetic stimulation

Across optogenetic experiments the LC was stimulated with either 473 nm or 635 nm light at 10 mW power and 3 Hz, 5 Hz or 15 Hz frequency (10 ms pulse width) alternating between 3 min off and on as previously described [7,29].

3.5.7 Pupillometry

Pupillometry was used to evaluate optogenetic LC stimulation as previously described [26]. At 3-4 weeks post-surgery, ChR2- and ChR2+ animals were anesthetized with 4% isoflurane and then placed in a stereotaxic frame with continuous anesthesia of 2% isoflurane. Recordings were performed of the right eye ipsilateral to the stimulated LC and consisted of an initial baseline recording of 60 seconds, followed by tonic LC stimulation (5 Hz at 10 mW for 10 s) and 1 min post stimulation recording. Pupil videos were tracked with DeepLabCut and analyzed with the Pupillometry App.

3.5.8 Tissue collection

At the appropriate time point after initiation of stress (for immediate groups within maximum 1 min after offset of stress) or LC activation, mice were euthanized by cervical dislocation and decapitation. The brain was quickly dissected on a cold glass plate and isolated hippocampi were separated by a cut at a ratio of 1:2 to divide the dHC and vHC. For experiments that were analyzed with uHPLC additionally the whole cortex was also collected. Isolated tissues were then snap-frozen in liquid nitrogen and stored at -80°C until further processing. For immunohistochemistry, the hindbrain (containing the LC) was

isolated with a single cut from a razor blade at the beginning of the cerebellum and directly transferred to a tube with 4% paraformaldehyde solution.

3.5.9 Immunohistochemistry

LC containing hindbrain samples were fixed for 2 hours in ice-cold paraformaldehyde solution (4% PFA in PBS, pH 7.4). The tissue then was rinsed with PBS and stored in a sucrose solution (30% sucrose in PBS) at 4°C, overnight. The tissue was frozen in tissue mounting medium (Tissue-Tek O.C.T Compound, Sakura Finetek Europe B.V., Netherlands), and sectioned coronally using a cryostat (Leica CM3050 S, Leica Biosystems Nussloch GmbH) into 40 µm thick sections. The sections were immediately transferred into ice-cold PBS. LC containing sections were stained in primary antibody solution with 0.05% Triton X-100, and 4% normal goat serum in PBS at 4C under continuous agitation over 2 nights. The primary antibodies used were: mouse anti-TH (22941, Immunostar, 1:1000), chicken anti-GFP (ab13970, Abcam, 1:1000) and rabbit anti-cFOS (226 003, Synaptic Systems, 1:5000). Afterwards, the sections were washed 3 times in PBS, and transferred to secondary antibody solution containing 0.05% Triton X-100, and 4% normal goat serum in PBS. The secondary antibodies used were: goat anti-mouse Alexa 488 (ab150113, Abcam, 1:300), goat anti-mouse Cy3 (115-165-003, Jackson ImmunoResearch, 1:300), goat anti-chicken Alexa 488 (A-11039, Thermo Fischer Scientific, 1:300), goat anti-rabbit Alexa 488 (A-11008 Thermo Fisher Scientific, 1:500), goat anti-rabbit Alexa 546 (A-11035, Thermo Fisher Scientific, 1:300) and donkey anti-mouse Alexa 647 (A-31571, Thermo Fisher Scientific, 1:300). Nissl was stained by NeuroTrace 640/660 Nissl stain (N21483, Thermo Fisher Scientific). After 3 more PBS washes, the sections were mounted onto glass slides (Menzel-Glaser SUPERFROST PLUS, Thermo Scientific), air-dried and coverslipped with Dako fluorescence mounting medium (Agilent Technologies). Microscopy images were acquired in a confocal laser-scanning microscope (CLSM 880, Carl Zeiss AG, Germany) with a 20x objective. Images were analyzed using FIJI and for cFos quantification TH+ and cFos+ cells were counted manually.

3.5.10 Ultra-high performance liquid chromatography (uHPLC)

To quantify noradrenergic (NA; MHPG) compounds from cortical and hippocampal tissue, a reversed-phase uHPLC system coupled with electrochemical detection (RP-uHPLC-ECD) was used (Alexys™ Neurotransmitter Analyzer, Antec Leyden, Zoeterwoude, Netherlands). In short, our previously validated RP-HPLC method with ion pairing chromatography was applied as described (Van Dam et al., 2014), albeit with minor modifications regarding the installed column (BEH C18 Waters column, 150 mm x 1 mm, 1.7 µm particle size) and pump preference (LC110S pump, 470-480 bar; flow rate of 62 L/min), achieving the most optimal separation conditions in a RP-UHPLC setting. Brain samples were defrosted to 4°C and subsequently homogenized in 800-900 µL ice-cold sample buffer (50 mM citric acid, 50 mM phosphoric acid, 0.1 mM EDTA, 8 mM KCl and 1.8 mM octane-1-sulfonic acid sodium salt (OSA), adjusted to pH = 3.6), using a Precellys® Minilys Personal Tissue Homogenizer (Bertin Technologies™, France) with CK14 1.4 mm ceramic beads (40-60 sec approximately, full speed). To remove excess proteins, 450 mL homogenate was transferred onto a 10,000 Da Amicon Ultra 0.5 Centrifugal Filter (Millipore, Ireland) that had been pre-washed twice using 450 µL sample buffer (centrifugation: 14,000 x g, 20 min, 4°C). The Amicon filter

loaded with the homogenate was then centrifuged (14,000 x g, 20 min, 4°C). Finally, the filtrate was transferred into a polypropylene vial (0.3 mL, Machery-Nagel GmbH & Co. KG, Germany) and automatically injected into the uHPLC column by the Alexys AS110 Autosampler (5 µL sample loop). Levels of the monoamines and metabolites were calculated using Clarity software™ (DataApex Ltd., v86.12.0.77208, 2015, Prague, Czech Republic).

3.5.11 RNA extraction

Dorsal and ventral hippocampal samples were homogenized in 500 µL Trizol (Invitrogen 15596026) in a tissue lyser bead mill (Qiagen, Germany) at 4°C for 2 mins, and RNA was extracted according to manufacturer's recommendations. This was followed by determining RNA purity and quantity with a UV/V spectrophotometer (Nanodrop 1000).

3.5.12 Bulk RNA sequencing and data analysis

For experiments shown in Figure 1c-e and 2, bulk mRNA sequencing was performed at the Functional Genomics Center Zurich (FGCZ) core facility. Data shown in figure 1c-e and 2c-d belong to the same experiment and were split up for better visualization of effects after sample processing and RNA sequencing analysis was performed. RNA integrity was assessed with high sensitivity RNA screen tape on an Agilent Tape Station/Bioanalyzer, according to the manufacturer's protocol. The RIN values of all samples ranged from 8.4 to 10.0. For library preparation, the TruSeq stranded RNA kit (Illumina Inc.) was used according to the manufacturer's protocol. For bulk sequencing library preparation, the TruSeq stranded RNA kit (Illumina Inc.) was used according to the manufacturer's protocol. The mRNA was purified by polyA selection, chemically fragmented and transcribed into cDNA before adapter ligation. Single-end (100nt) sequencing was performed with HiSeq 4000. Samples within experiments were each run on one or multiple lanes and demultiplexed. A sequencing depth of ~20M reads per sample was used. Bulk mRNA sequencing for experiments shown in Figure 1g-h and 3 were performed at Novogene UK. Total RNA samples were used for library preparation using NEB Next® Ultra RNA Library Prep Kit for Illumina®. Indices were included to multiplex multiple samples. Briefly, mRNA was purified from total RNA using poly-T oligo-attached magnetic beads. After fragmentation, the first strand cDNA was synthesized using random hexamer primers followed by the second strand cDNA synthesis. The library was ready after end repair, A-tailing, adapter ligation, and size selection. After amplification and purification, insert size of the library was validated on an Agilent 2100 and quantified using quantitative PCR (qPCR). Libraries were then sequenced on Illumina NovaSeq 6000 S4 flowcell with PE150 according to results from library quality control and expected data volume. Samples within experiments were each run on one or multiple lanes and demultiplexed. A sequencing depth of ~40M reads per sample was used.
For all experiments, adapters were trimmed using cutadapt [67] with a maximum error rate of 0.05 and a minimum length of 15. Kallisto (v0.44.0) [68] was used for pseudo alignment of reads on the transcriptome level using the genecode.vM17 assembly with 30 bootstrap samples and an estimated fragment length of 200 ± 20 for single-end samples. For differential gene expression (DGE) analysis we aggregated reads of protein coding transcripts and used R (v. 4.0.3) with the package "edgeR" (v 3.32.1) for analysis. A filter was used to remove genes with low expression prior to DGE analysis. EdgeR was then used to calculate the normalization factors (TMM method) and estimate the dispersion (by weighted likelihood empirical Bayes). For two group comparisons the genewise exact test

was used, for more complex designs we used a generalized linear model (GLM) with empirical Bayes quasi-likelihood F-tests. Exact specifications for each tested model can be found under https://github.com/ETHZ-INS/LC_Opto_Transcriptomics. For multiple testing correction the Benjamini-Hochberg false discovery rate (FDR) method was used. For analyses of data-sets originating from multiple experiments we further employed SVA correction to correct for processing specific effects [23]. Surrogate variables independent of experimental groups were identified using the SVA package (v3.38.0) on data after DESeq2 (v1.30.1) variance-stabilization [69], and were then included as additive terms in the GLMs. Heatmaps were produced with the SECHM (v1.5.1) package. To avoid rare extreme values from driving the scale, the color scale is linear for values within a 98% interval, and ordinal for values outside it. Unless otherwise specified, the rows were sorted using the features' angle on a two-dimensional projection of the plotted values, as implemented in SEtools (v1.9.4).
For the combined analysis of consistent effects across yohimbine injection, chemogenetic and optogenetic stimulation we first combined all three datasets and modeled batch effects using SVA correction. We then designed a combined response variable that was set to control (homecage in the injection experiment, hM3Dq- in chemogenetic and ChR2- in optogenetic) or response (yohimbine in the injection experiment, hM3Dq+ in chemogenetic and ChR2+ in optogenetic). We then fit an additive generalized linear model with the newly defined response variable and the surrogate variables from the SVA correction and tested it for the response variable coefficient.
For the cumulative rank analysis, statistical results were used from multiple analyses (Stress group vs propranolol group in vHC of the first injection experiment; Stress group vs propranolol group in dHC of the first injection experiment; Stress:Propranolol interaction in second injection experiment; effect of chemogenetic LC activation in vHC; effect of chemogenetic LC activation in dHC; effect of optogenetic LC activation after 45 minutes). Then, in each analysis the gene with the lowest p-value was set to rank 1, the one with the highest to rank N. These ranks were then summed up across all analyses to generate the cumulative rank.

3.5.13 Reverse transcription quantitative real-time polymerase chain reaction (RT-qPCR)

Reactions were conducted using SYBR green (Roche) on a CFX384 Touch Real-Time PCR Detection System (Bio-Rad) and normalized against Tubulin delta 1 (Tubd1). Cycling conditions were 5 min at 95 °C, then 50 cycles with denaturation (10 s at 95 °C), annealing (10 s at 60 °C), and elongation (10 s at 72 °C). Primers were designed using PrimerBlast [70] and tested for quality and specificity by melt-curve analysis, gel electrophoresis and appropriate negative controls. Forward (FP) and reverse (RP) primer sequences were as follows:

Tubd1:	FP: TCTCTTGCTAACTTGGTGGTCCTC / RP: GCTGGGTCTTTAAATCCCTCTACG
Apold1:	FP: ACCTCAGGCTCTCCTTCCATCATC / RP: ACCCGAGACAAAGCACCAATGC
Dio2:	FP: GCCTACAAACAGGTTAAACTGGGTG / RP: CCATCAGCGGTCTTCTCC
Sik1:	FP: ACAGCTCACTTCAGCCCTTAT / RP: CTCGCTGATAGCTGTGTCCA
Ppp1r3c:	FP: TGAGCTGCACCAGAATGATCC / RP:GGTGGTGAATGAGCCAAGCA

3.5.14 Statistics

We used a block design for experiments. Animals and samples were split into multiple blocks, containing one replicate of each condition. Experimental and processing order within these blocks was randomized. Investigators were blinded during behavior and sample processing, but not during the analysis process. However, the same algorithmic analysis methods were used for all samples within each sequencing experiment. Analysis was performed in R or GraphPad Prism 9.2.0. For statistical analyses of behavior, pupillometry, immunohistochemistry and uHPLC data, we used independent samples t tests when comparing two independent groups. When comparing more than two groups we used one-way ANOVAs if there was a single independent variable, or two-way ANOVAs for two-factorial designs (e.g., injection x group). Significant main effects and interactions were analyzed using Tukey's post hoc tests. For linear model analysis we used the function lm() from the "stats" package in R and F-statistics for significance testing. No statistical method was used to predetermine sample size. No data were excluded from the analyses.

3.6 Supplementary Figures

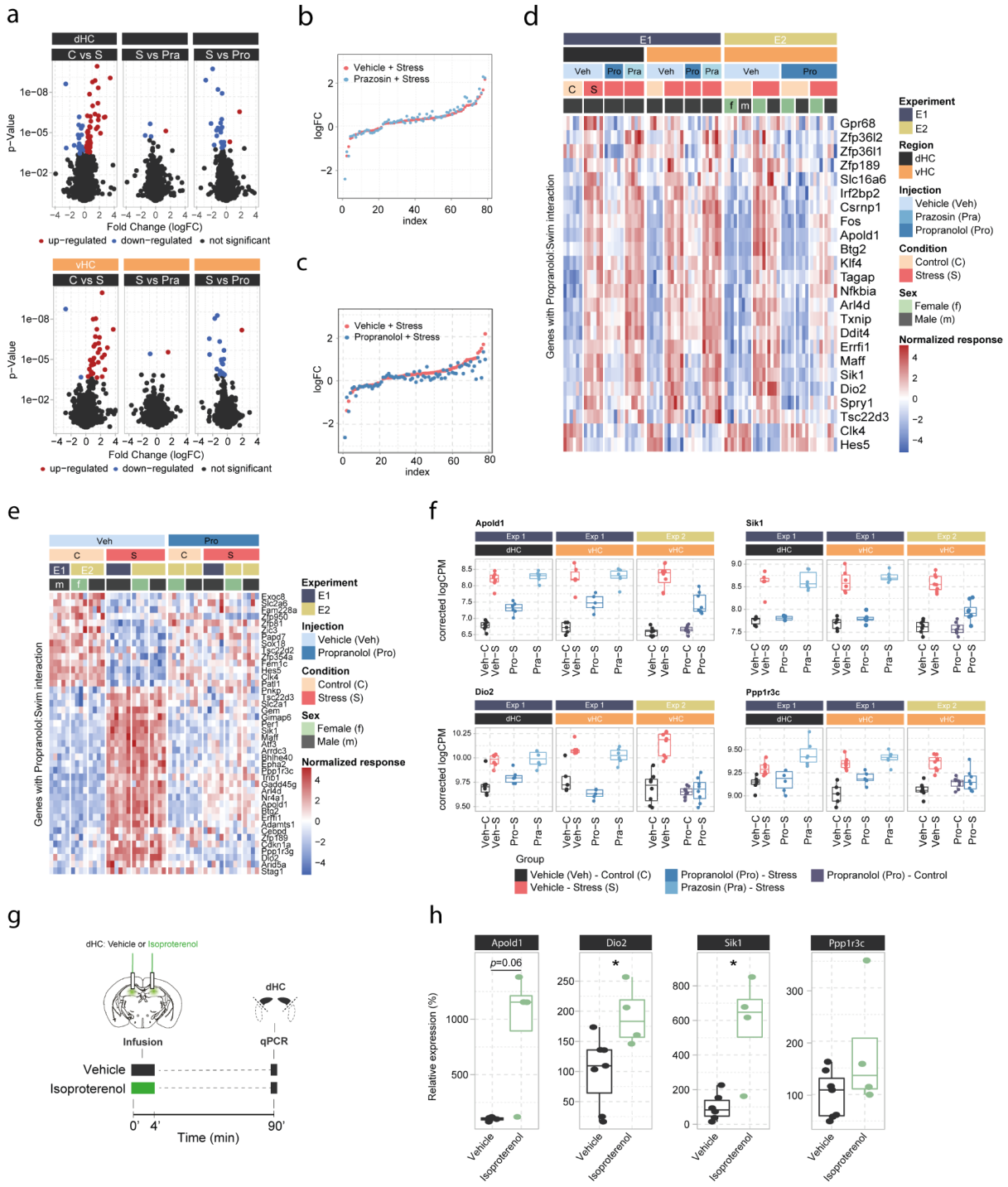

Supplementary Figure 1. In-depth analysis of noradrenergic contribution to stress-induced transcriptomic changes in the hippocampus. a, Volcano plots showing differentially expressed RNA transcripts between vehicle (Veh, i.p.), prazosin (Pra, 1 mg/kg, i.p.) and propranolol (Pro, 10 mg/kg, i.p.) injected animals 45 min after onset of acute swim stress exposure. Red and blue values represent changes with FDR-adjusted $p<0.05$ ($n = 6$ per group). **b**, Strength of the prazosin effect on the transcriptomic stress response. Data are sorted by interaction strength in the stress group (orange) and the corresponding interaction strength of the stress+prazosin group are shown in lightblue for the same gene. **c**, Strength of the propranolol effect on the transcriptomic stress response. Data are sorted by interaction strength in the stress group (orange) and the corresponding interaction strength of the stress+prazosin group are shown in dark blue for the same gene. **d**,

Heatmap showing expression of all differentially expressed genes with a stress:propranolol interaction identified in experiment 1 (as seen in Fig. 1c-f) across both experiments. **e**, Heatmap showing expression of all differentially expressed genes with a stress:propranolol interaction when re-analysed across both experiments. **f**, Selective Boxplots showing the expression of selected propranolol-responsive genes (*Apold1, Hes5, Dio2 and Per1*) across experiments. **g**, Experimental design for assessing the effect of intrahippocampal infusion of isoproterenol (3 µg/hemisphere) on expression of selected genes in the dorsal hippocampus (dHC) 90 min after infusion in the absence of stress. **h**, Boxplots showing the expression of selected stress- and propranolol-responsive genes (*Apold1, Dio2 and Sik1*) 90 min after infusion of isoproterenol (3 µg/hemisphere) into the dHC, as measured by quantitative real-time PCR. Isoproterenol increased the expression of *Dio2* (unpaired t test; t(9) = 2.637, p = 0.02706) and *Sik1* (welch unpaired t test; t(3.3) = 3.176, p = 0.04428). Vehicle, n = 7; Isoproterenol, n = 4. *p < 0.05.

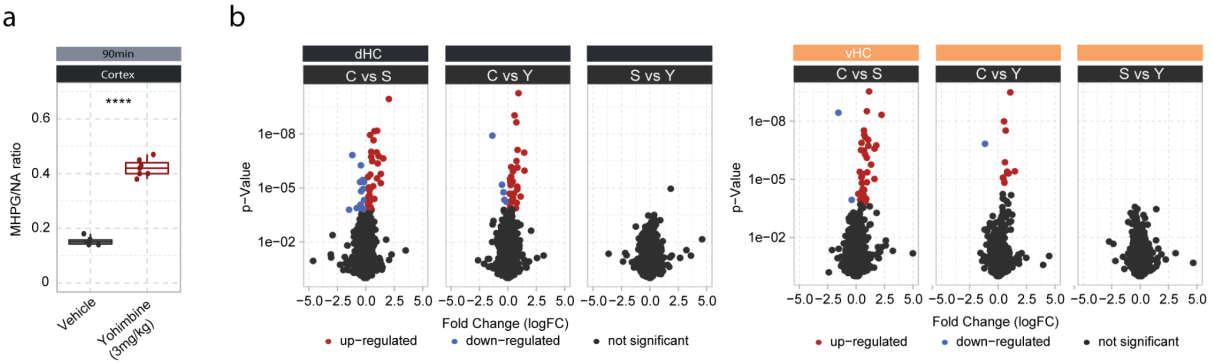

Supplementary Figure 2. Yohimbine-mediated cortical NA release and hippocampal transcriptomic changes in comparison to changes induced by acute stress. a, Quantification of cortical MHPG/NA ratio, as measured by uHPLC, 90 min after systemic injection of vehicle or yohimbine (3 mg/kg, i.p.). Yohimbine significantly increases cortical NA turnover (unpaired *t* test; t(8.9) = -20.099**,** p = 1.015e-08). Vehicle, n = 6; Yohimbine , n = 7. **b**, Volcano plots showing differentially expressed RNA transcripts between control (C) and acute stress (S) or yohimbine (Yoh) injected animals 45 min after stress or yohimbine injection in the dorsal (dHC) and ventral (vHC) hippocampus, as well as a direct comparison between the two responses. Red and blue values represent changes with FDR-adjusted p<0.05 (Veh n = 5, Yoh n = 5). ****p < 0.0001.

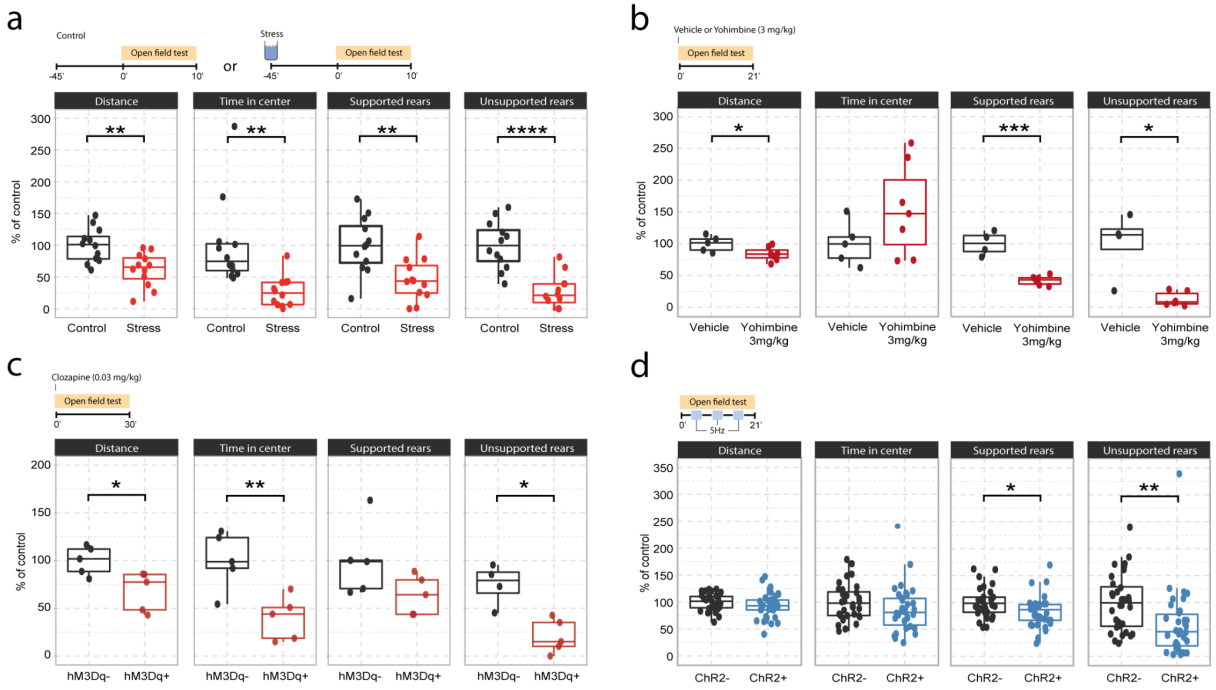

Supplementary Figure 3. Effects of acute stress and noradrenergic stimulation on anxiety-like behaviour in the open field test. **a**, Stress-induced changes in the open field test 45 min after stress onset. Stressed animals show overall reductions in distance traveled (unpaired t-test; t=3.55, df=22, *p*=0.0018), time in center (welch unpaired t-test; t=3.50, df=13.61, *p*=0.0036), supported rears (unpaired t-test; t=3.39, df=22, *p*=0.0026) and unsupported rears (unpaired t-test; t=5.53, df=22, *p* = 1.47e-05) compared to controls (Control *n* = 12; Stress *n* = 12). This data have been previously published [311]. **b**, Yohimbine (3 mg/kg, i.p.) injected animals show reduced distance traveled (unpaired t-test; t=2.39, df=10, *p*=0.03772), reduced supported rears (unpaired t-test; t=6.56, df=10, *p*=0.00006) and reduced unsupported rears (welch unpaired t-test; t=3.69, df=4.4, *p* = 0.01785) compared to vehicle injected animals (Vehicle *n* = 6; Yohimbine *n* = 7). **c**, Chemogenetic LC activation induced changes in the open field test immediately after clozapine (0.03 mg/kg, i.p.) injection. hM3Dq+ animals show reduced distance traveled (unpaired t-test; t=2.78, df=8, *p*=0.02403), reduced time in center (unpaired t-test; t=3.54, df=8, *p*=0.00759), as well as reduced unsupported rears (welch unpaired t-test; t=2.86, df=4.71, *p* = 0.03804) compared to hM3D- animals (hM3Dq- *n* = 5; hM3Dq+ *n* = 5). **d**, Optogenetic 5 Hz LC activation induced changes during the open field test. ChR2+ animals show reduced supported rears (unpaired t-test; t=2.42, df=64, *p*=0.0185) and reduced unsupported rears (unpaired t-test; t=2.91, df=64, *p* = 0.00499) compared to ChR2- animals (ChR2- *n* = 32; ChR2+ *n* = 36). Data expressed as mean ± SEM. **p* < 0.05, ***p* < 0.01, ****p* < 0.001, *****p* < 0.0001.

a

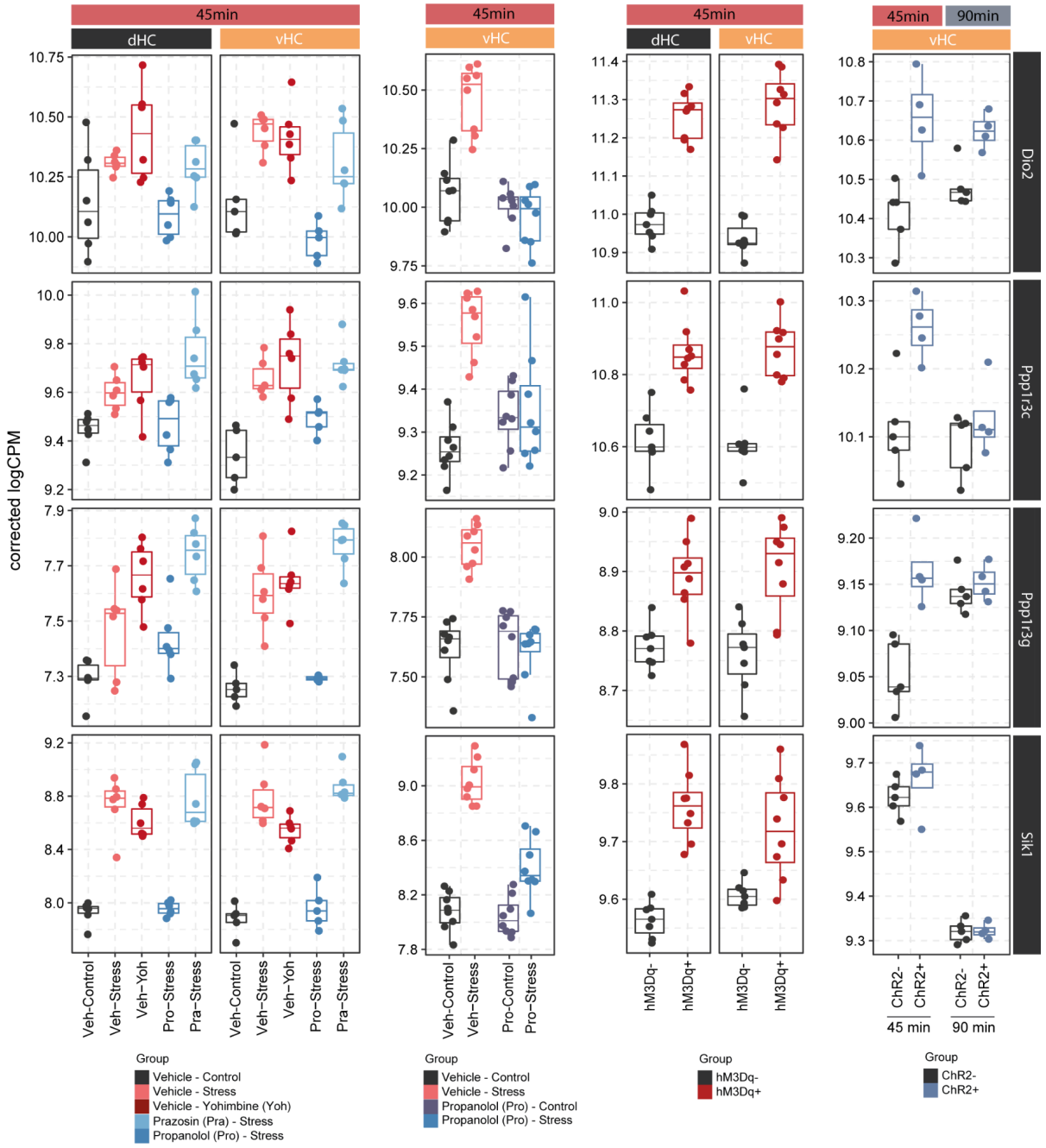

Supplementary Figure 4. Expression of *Dio2*, *Ppp1r3c*, *Ppp1r3g* and *Sik1* is consistent across pharmacological, chemogenetic and optogenetic manipulations of the noradrenergic system. a, Selective boxplots showing the expression changes of top 4 most responsive genes across all LC-NA manipulations. *Dio2, Ppp1r3c, Ppp1r3g and Sik1* are plotted across experiments in response to acute swim stress exposure, yohimbine (3 mg/kg, i.p.), swim stress and propranolol (10 mg/kg, i.p.), swim stress and prazosin (1 mg/kg, i.p.), as well as chemogenetic and optogenetic LC activation.

a

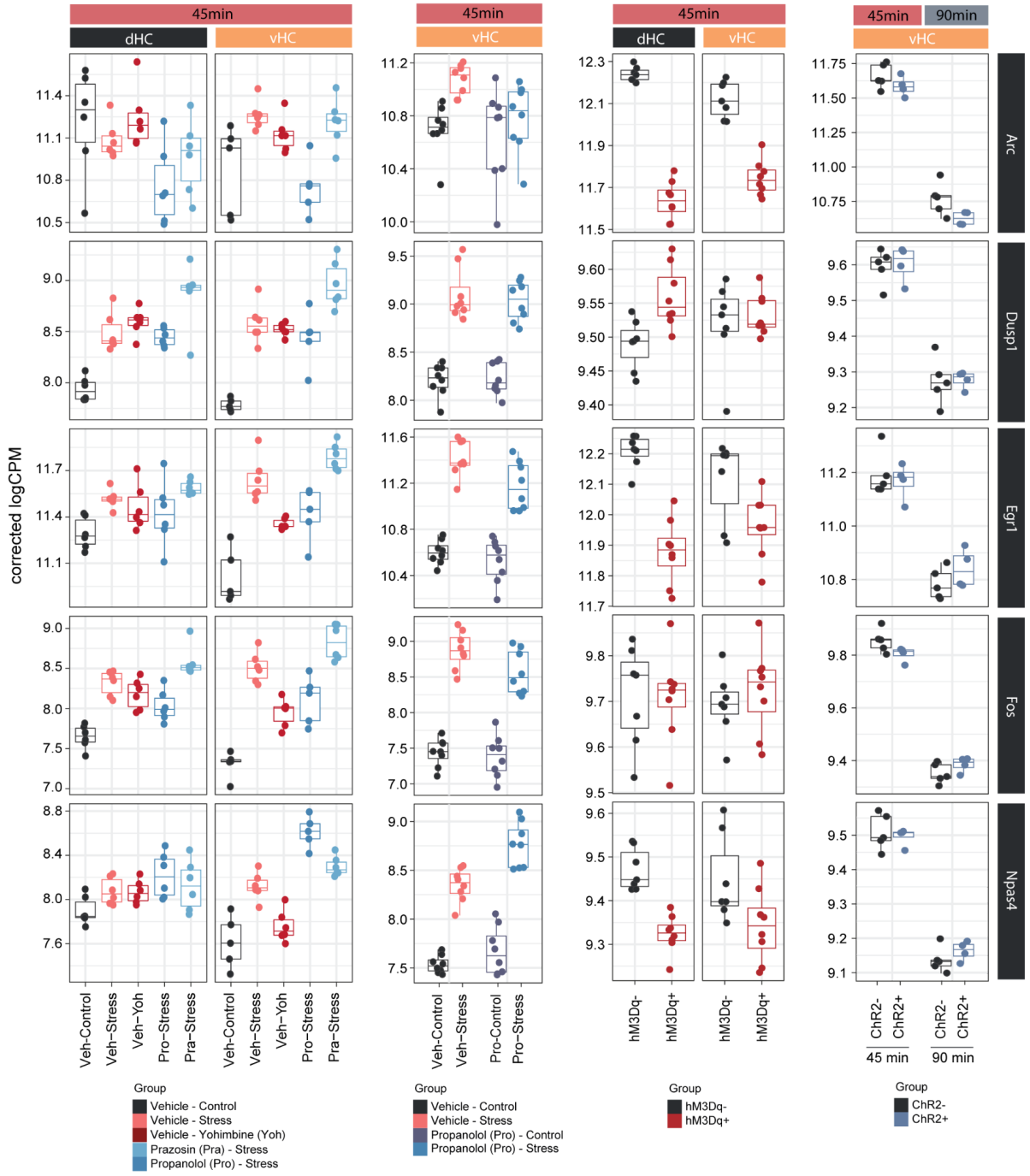

Supplementary Figure 5. Neuronal immediate early genes in the hippocampus are not regulated by noradrenaline signaling. **a**, Selective boxplots showing the expression changes of genes associated with neuronal activation (*Arc, Dusp1, Egr1, Fos* and *Npas4*) across experiments in response to acute stress and noradrenergic manipulation. Propranolol was not able to block the stress-induced expression of these genes, and locus coeruleus stimulation was not able to mimic their stress-induced upregulation.

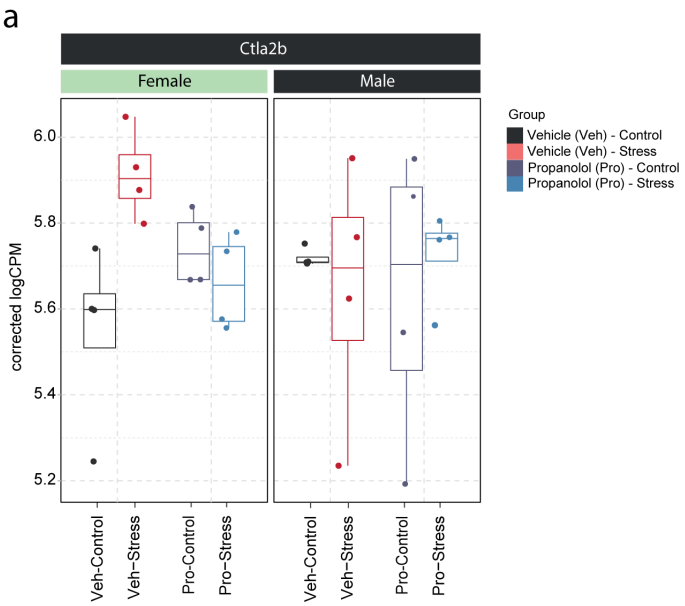

Supplementary Figure 6. Sex dependent expression of Ctla2b in the ventral hippocampus of female and male mice. a, Selective boxplot of *Ctla2b* expression - from data shown in figure 1g-h - in response to acute swim stress and propranolol 45 min after stress onset in female and male mice. *n* = 4 per group.

3.7 Data availability

The sequencing data data generated in this study has been deposited in the Gene Expression Omnibus database under accession code GSE218315 (reviewer token yhilwoocbhujjwp) for all injection experiments and GSE218313 for chemo and optogenetic experiments (reviewer token stoxiksgfhmpjiz).

3.8 Code availability

Code for all analyses (independent scripts) presented here is available on GitHub under https://github.com/ETHZ-INS/LC_Opto_Transcriptomics.

3.9 Acknowledgments

The lab of JB was supported by the ETH Zurich, ETH Project Grant ETH-20 19-1, the Swiss National Science Foundation (grants 310030_172889/1 and 310030_204372), the Forschungskredit of the University of Zurich, the Novartis Foundation for Medical-Biological Research, the Swiss Foundation for Excellence and Talent in Biomedical Research, the Vontobel Foundation, the Betty and David Koetser Foundation for Brain Research. The lab of PPDD and DVD was supported by the University of Antwerp, Research Foundation Flanders (FWO), Joint Programming Initiative Neurodegenerative Diseases (JPND) and ZonMW (HEROES 73305172), Alzheimer Nederland and Neurosearch Antwerp.
We thank the staff of the EPIC for the excellent animal care and their service to our animal facility and Prof. Isabelle Mansuy for providing support and space. We thank Han-Yu Lin for help with sample processing and Julia Bode for maintaining the animal colony.

3.10 Author Contributions

Conceptualization, M.P, A.F, S.N.D and J.B; Methodology, M.P, L.v.Z, A.F, S.N.D, R.Z, S.L, F.K.R, A.H, Y.V and D.V.D ; Investigation, M.P, L.v.Z, A.F, S.N.D, R.Z, S.L, O.S, R.W; Writing – Original Draft, M.P, L.v.Z and J.B; Writing – Review & Editing, M.P, L.v.Z, A.F, S.N.D, R.Z, S.L, O.S, R.W, F.K.R, A.H, Y.V, D.V.D, P.P.D.D and J.B; Funding Acquisition, D.V.D, P.P.D.D and J.B

3.11 References

1. Floriou-Servou A, von Ziegler LM, Waag R, Schläppi C, Germain P-L, Bohacek J. The Acute Stress Response in the Multiomic Era. Biol Psychiatry. 2021;89: 1116–1126.
2. Joëls M, Baram TZ. The neuro-symphony of stress. Nat Rev Neurosci. 2009;10: 459–466.
3. Likhtik E, Johansen JP. Neuromodulation in circuits of aversive emotional learning. Nat Neurosci. 2019;22: 1586–1597.
4. Poe GR, Foote S, Eschenko O, Johansen JP, Bouret S, Aston-Jones G, et al. Locus coeruleus: a new look at the blue spot. Nature Reviews Neuroscience. 2020. pp. 644–659. doi:10.1038/s41583-020-0360-9
5. Zerbi V, Floriou-Servou A, Markicevic M, Vermeiren Y, Sturman O, Privitera M, et al. Rapid Reconfiguration of the Functional Connectome after Chemogenetic Locus Coeruleus Activation. Neuron. 2019;103: 702–718.e5.
6. Oyarzabal EA, Hsu L-M, Das M, Chao T-HH, Zhou J, Song S, et al. Chemogenetic stimulation of tonic locus coeruleus activity strengthens the default mode network. Sci Adv. 2022;8: eabm9898.
7. McCall JG, Al-Hasani R, Siuda ER, Hong DY, Norris AJ, Ford CP, et al. CRH Engagement of the Locus Coeruleus Noradrenergic System Mediates Stress-Induced Anxiety. Neuron. 2015;87: 605–620.
8. McCall JG, Siuda ER, Bhatti DL, Lawson LA, McElligott ZA, Stuber GD, et al. Locus coeruleus to basolateral amygdala noradrenergic projections promote anxiety-like behavior. Elife. 2017;6. doi:10.7554/eLife.18247
9. Hirschberg S, Li Y, Randall A, Kremer EJ, Pickering AE. Functional dichotomy in spinal- vs prefrontal-projecting locus coeruleus modules splits descending noradrenergic analgesia from ascending aversion and anxiety in rats. Elife. 2017;6. doi:10.7554/eLife.29808
10. Uematsu A, Tan BZ, Johansen JP. Projection specificity in heterogeneous locus coeruleus cell populations: implications for learning and memory. Learn Mem. 2015;22: 444–451.
11. Hansen N. The Longevity of Hippocampus-Dependent Memory Is Orchestrated by the Locus Coeruleus-Noradrenergic System. Neural Plast. 2017;2017: 2727602.
12. Sara SJ. Locus Coeruleus in time with the making of memories. Curr Opin Neurobiol. 2015;35: 87–94.
13. Schwabe L, Hermans EJ, Joëls M, Roozendaal B. Mechanisms of memory under stress. Neuron. 2022. pp. 1450–1467. doi:10.1016/j.neuron.2022.02.020
14. Roszkowski M, Manuella F, von Ziegler L, Durán-Pacheco G, Moreau J-L, Mansuy IM, et al. Rapid stress-induced transcriptomic changes in the brain depend on beta-adrenergic signaling. Neuropharmacology. 2016;107: 329–338.
15. Loy R, Koziell DA, Lindsey JD, Moore RY. Noradrenergic innervation of the adult rat hippocampal formation. The Journal of Comparative Neurology. 1980. pp. 699–710. doi:10.1002/cne.901890406
16. Robertson SD, Plummer NW, de Marchena J, Jensen P. Developmental origins of central norepinephrine neuron diversity. Nat Neurosci. 2013;16: 1016–1023.
17. Oleskevich S, Descarries L, Lacaille JC. Quantified distribution of the noradrenaline innervation in the hippocampus of adult rat. J Neurosci. 1989;9: 3803–3815.
18. von Ziegler LM, Floriou-Servou A, Waag R, Das Gupta RR, Sturman O, Gapp K, et al. Multiomic profiling of the acute stress response in the mouse hippocampus. Nat Commun. 2022;13: 1824.
19. Mifsud KR, Kennedy CLM, Salatino S, Sharma E, Price EM, Haque SN, et al. Distinct regulation of hippocampal neuroplasticity and ciliary genes by corticosteroid receptors. Nat Commun. 2021;12: 1–23.
20. Floriou-Servou A, von Ziegler L, Stalder L, Sturman O, Privitera M, Rassi A, et al. Distinct Proteomic, Transcriptomic, and Epigenetic Stress Responses in Dorsal and Ventral Hippocampus. Biol Psychiatry. 2018;84: 531–541.
21. Strange BA, Witter MP, Lein ES, Moser EI. Functional organization of the hippocampal longitudinal axis. Nat Rev Neurosci. 2014;15: 655–669.
22. Cembrowski MS, Bachman JL, Wang L, Sugino K, Shields BC, Spruston N. Spatial Gene-Expression Gradients Underlie Prominent Heterogeneity of CA1 Pyramidal Neurons. Neuron. 2016;89: 351–368.
23. Leek JT, Evan Johnson W, Parker HS, Jaffe AE, Storey JD. The sva package for removing batch effects and other unwanted variation in high-throughput experiments. Bioinformatics. 2012. pp. 882–883. doi:10.1093/bioinformatics/bts034
24. Sturman O, Germain P-L, Bohacek J. Exploratory rearing: a context- and stress-sensitive behavior recorded in the open-field test. Stress. 2018;21: 443–452.
25. Zhu H, Aryal DK, Olsen RHJ, Urban DJ, Swearingen A, Forbes S, et al. Cre-dependent DREADD (Designer Receptors Exclusively Activated by Designer Drugs) mice. Genesis. 2016;54: 439–446.
26. Privitera M, Ferrari KD, von Ziegler LM, Sturman O, Duss SN, Floriou-Servou A, et al. A complete

pupillometry toolbox for real-time monitoring of locus coeruleus activity in rodents. Nat Protoc. 2020;15: 2301–2320.
27. Harley CW, Yuan Q. Locus Coeruleus Optogenetic Modulation: Lessons Learned from Temporal Patterns. Brain Sci. 2021;11. doi:10.3390/brainsci11121624
28. Ghosh A, Massaeli F, Power KD, Omoluabi T, Torraville SE, Pritchett JB, et al. Locus Coeruleus Activation Patterns Differentially Modulate Odor Discrimination Learning and Odor Valence in Rats. Cereb Cortex Commun. 2021;2: tgab026.
29. Grimm C, Duss SN, Privitera M, Munn BR, Frässle S, Chernysheva M, et al. Locus Coeruleus firing patterns selectively modulate brain activity and dynamics. bioRxiv. 2022. p. 2022.08.29.505672. doi:10.1101/2022.08.29.505672
30. Murphy-Royal C, Johnston AD, Boyce AKJ, Diaz-Castro B, Institoris A, Peringod G, et al. Stress gates an astrocytic energy reservoir to impair synaptic plasticity. Nat Commun. 2020;11: 2014.
31. Stankiewicz AM, Goscik J, Majewska A, Swiergiel AH, Juszczak GR. The Effect of Acute and Chronic Social Stress on the Hippocampal Transcriptome in Mice. PLoS One. 2015;10: e0142195.
32. Girgenti MJ, Pothula S, Newton SS. Stress and Its Impact on the Transcriptome. Biol Psychiatry. 2021;90: 102–108.
33. Rubin TG, Gray JD, McEwen BS. Experience and the ever-changing brain: what the transcriptome can reveal. Bioessays. 2014;36: 1072–1081.
34. Gray JD, Rubin TG, Hunter RG, McEwen BS. Hippocampal gene expression changes underlying stress sensitization and recovery. Mol Psychiatry. 2013;19: 1171–1178.
35. Meijer OC, Buurstede JC, Viho EMG, Amaya JM, Koning A-SCAM, van der Meulen M, et al. Transcriptional glucocorticoid effects in the brain: Finding the relevant target genes. J Neuroendocrinol. 2022; e13213.
36. Gerstner N, Krontira AC, Cruceanu C, Roeh S, Pütz B, Sauer S, et al. DiffBrainNet: differential analyses add new insights into the response to glucocorticoids at the level of genes, networks and brain regions. 2022. doi:10.1101/2022.04.21.489034
37. Hermans EJ, Henckens MJAG, Joëls M, Fernández G. Dynamic adaptation of large-scale brain networks in response to acute stressors. Trends Neurosci. 2014;37: 304–314.
38. Fernandez-Albert J, Lipinski M, Lopez-Cascales MT, Rowley MJ, Martin-Gonzalez AM, Del Blanco B, et al. Immediate and deferred epigenomic signatures of in vivo neuronal activation in mouse hippocampus. Nat Neurosci. 2019;22. doi:10.1038/s41593-019-0476-2
39. Tyssowski KM, DeStefino NR, Cho JH, Dunn CJ, Carty CE, Jones RD, et al. Different Neuronal Activity Patterns Induce Different Gene Expression Programs. Neuron. 2018;98. doi:10.1016/j.neuron.2018.04.001
40. Bouret S, Sara SJ. Locus coeruleus activation modulates firing rate and temporal organization of odour-induced single-cell responses in rat piriform cortex. Eur J Neurosci. 2002;16: 2371–2382.
41. Mather M, Clewett D, Sakaki M, Harley CW. GANEing traction: The broad applicability of NE hotspots to diverse cognitive and arousal phenomena. Behav Brain Sci. 2016;39: e228.
42. Johnston AL, Baldwin HA, File SE. Measures of anxiety and stress in the rat following chronic treatment with yohimbine. J Psychopharmacol. 1988;2: 33–38.
43. Leibowitz SF, Sladek C, Spencer L, Tempel D. Neuropeptide Y, epinephrine and norepinephrine in the paraventricular nucleus: stimulation of feeding and the release of corticosterone, vasopressin and glucose. Brain Res Bull. 1988;21: 905–912.
44. Fink G. Stress: Neuroendocrinology and Neurobiology: Handbook of Stress Series. Academic Press; 2016.
45. Villain H, Benkahoul A, Birmes P, Ferry B, Roullet P. Influence of early stress on memory reconsolidation: Implications for post-traumatic stress disorder treatment. PLoS One. 2018;13: e0191563.
46. Endo F, Kasai A, Soto JS, Yu X, Qu Z, Hashimoto H, et al. Molecular basis of astrocyte diversity and morphology across the CNS in health and disease. Science. 2022. doi:10.1126/science.adc9020
47. Smith MA, Banerjee S, Gold PW, Glowa J. Induction of c-fos mRNA in rat brain by conditioned and unconditioned stressors. Brain Res. 1992;578: 135–141.
48. Benito E, Barco A. The neuronal activity-driven transcriptome. Mol Neurobiol. 2015;51: 1071–1088.
49. Zenger M, Burlet-Godinot S, Petit J-M, Magistretti PJ. Chapter 9 - Noradrenergic System and Memory: The Role of Astrocytes. In: Vardjan N, Zorec R, editors. Noradrenergic Signaling and Astroglia. Academic Press; 2017. pp. 183–200.
50. O'Donnell J, Ding F, Nedergaard M. Distinct functional states of astrocytes during sleep and wakefulness: Is norepinephrine the master regulator? Curr Sleep Med Rep. 2015;1: 1–8.
51. Dienel GA. The metabolic trinity, glucose-glycogen-lactate, links astrocytes and neurons in brain energetics, signaling, memory, and gene expression. Neurosci Lett. 2017;637: 18–25.
52. Bianco AC, Dumitrescu A, Gereben B, Ribeiro MO, Fonseca TL, Fernandes GW, et al. Paradigms of Dynamic Control of Thyroid Hormone Signaling. Endocr Rev. 2019;40: 1000–1047.
53. Campos-Barros A, Meinhold H, Stula M, Müller F, Köhler R, Eravci M, et al. The influence of desipramine on thyroid hormone metabolism in rat brain. J Pharmacol Exp Ther. 1994;268: 1143–1152.
54. Allaman I, Pellerin L, Magistretti PJ. Protein targeting to glycogen mRNA expression is stimulated by noradrenaline in mouse cortical astrocytes. Glia. 2000;30: 382–391.
55. Petit J-M, Eren-Koçak E, Karatas H, Magistretti P, Dalkara T. Brain glycogen metabolism: A possible link between sleep disturbances, headache and depression. Sleep Med Rev. 2021;59: 101449.
56. Jaitovich A, Bertorello AM. Intracellular sodium sensing: SIK1 network, hormone action and high blood pressure. Biochim Biophys Acta. 2010;1802: 1140–1149.
57. Huang BS, White RA, Leenen FHH. Possible role of brain salt-inducible kinase 1 in responses to central

sodium in Dahl rats. American Journal of Physiology-Regulatory, Integrative and Comparative Physiology. 2012 [cited 1 Nov 2022]. doi:10.1152/ajpregu.00381.2011
58. Feldman JD, Vician L, Crispino M, Hoe W, Baudry M, Herschman HR. The salt-inducible kinase, SIK, is induced by depolarization in brain. J Neurochem. 2000;74: 2227–2238.
59. Bertorello AM, Zhu J-K. SIK1/SOS2 networks: decoding sodium signals via calcium-responsive protein kinase pathways. Pflugers Arch. 2009;458: 613–619.
60. Wang C, Song D, Fu J, Wen X. SIK1 Regulates CRTC2-Mediated Gluconeogenesis Signaling Pathway in Human and Mouse Liver Cells. Front Endocrinol . 2020;11. doi:10.3389/fendo.2020.00580
61. Coggan JS, Keller D, Calì C, Lehväslaiho H, Markram H, Schürmann F, et al. Norepinephrine stimulates glycogenolysis in astrocytes to fuel neurons with lactate. PLoS Comput Biol. 2018;14: e1006392.
62. Xu L, Dan M, Shao A, Cheng X, Zhang C, Yokel RA, et al. Silver nanoparticles induce tight junction disruption and astrocyte neurotoxicity in a rat blood-brain barrier primary triple coculture model. Int J Nanomedicine. 2015;10: 6105–6118.
63. Popichak KA, Hammond SL, Moreno JA, Afzali MF, Backos DS, Slayden RD, et al. Compensatory Expression of Nur77 and Nurr1 Regulates NF-κB-Dependent Inflammatory Signaling in Astrocytes. Mol Pharmacol. 2018;94: 1174–1186.
64. Pan J, Ma N, Zhong J, Yu B, Wan J, Zhang W. Age-associated changes in microglia and astrocytes ameliorate blood-brain barrier dysfunction. Mol Ther Nucleic Acids. 2021;26: 970–986.
65. Paillasse MR, de Medina P. The NR4A nuclear receptors as potential targets for anti-aging interventions. Med Hypotheses. 2015;84: 135–140.
66. Bohacek J, Manuella F, Roszkowski M, Mansuy IM. Hippocampal gene expression induced by cold swim stress depends on sex and handling. Psychoneuroendocrinology. 2015;52: 1–12.
67. Martin M. Cutadapt removes adapter sequences from high-throughput sequencing reads. EMBnet.journal. 2011;17: 10–12.
68. Bray NL, Pimentel H, Melsted P, Pachter L. Near-optimal probabilistic RNA-seq quantification. Nat Biotechnol. 2016;34: 525–527.
69. Love MI, Huber W, Anders S. Moderated estimation of fold change and dispersion for RNA-seq data with DESeq2. Genome Biol. 2014;15: 550.
70. Kozyreva AA, Zlotina AM, Golovkin AS, Kalinina OV, Kostareva AA. Primer designing in Primer-BLAST. Translational Medicine. 2021. pp. 37–52. doi:10.18705/2311-4495-2021-8-3-37-52
71. Roman C., Elena V. Fuior, Violeta G. Trusca, Dimitris Kardassis, Maya Simionescu, Anca V. Gafencu, 2015. “Thyroid hormones upregulate apolipoprotein E gene expression in astrocytes.” *Biochemical and Biophysical Research Communications*, Volume 468, 190-195.

Chapter 4. Discussion

4.1 A new era of LC research: Insights from technological advances

For many decades, the small size and location of the LC has made it a very difficult brain region to investigate. Studying the LC was thus reserved for a few laboratories with highly specialized skills in electrophysiology. However, neuroscience research has witnessed technical revolutions both on the level of circuit neuroscience, as well as on the level of molecular neuroscience. On the side of circuit neuroscience, the advent of optogenetics has revolutionized the field of neuroscience since its first appearance in 2005 [423]. For the first time, precise temporal control over the firing of specific neuronal populations was possible *in vivo*. In 2010, the first paper using optogenetics to study the LC was published [96], since then a large number of studies have leveraged optogenetics and viral tracing technologies to study new aspects of LC function. Amongst other things, one particularly important discovery resulted from this: The insight that the LC is organized in ensembles to regulate different aspects of behavior in an activity dependent manner. Insights from neuropsychiatric diseases further highlight the need for a better understanding of LC firing patterns, as these contribute to the heterogeneous effects of the LC-NA system. Recent work has demonstrated that LC tonic and phasic firing patterns can be mimicked to induce distinct effects across the brain, including differential engagement of neuronal networks and behavior [100,424,425], hence, optogenetics finally allows to study the precise effects of diverse LC firing patterns and potentially mimic physiological LC activation in more detail. We have further demonstrated that optogenetic LC stimulation can mimic stress-induced behavioral phenotypes and, when combined with other methods, can be used to study molecular changes specific to its firing patterns. However, this also comes with some limitations, for once, the common practice of simultaneous activation of the whole LC does not likely resemble physiological engagement of LC neurons. Physiological afferent stimulation instead most likely only recruits targeted ensembles within the LC. Thus, to fully mimic LC activity it is essential to understand which specific subpopulations respond to physiological situations, and target these. Especially the combined use with photometry and retrograde viral constructs, alongside the continuous development of new light-sensitive receptors and sensors, will allow us to target these issues and further advance our knowledge of LC firing patterns and their physiological release of NA and co-transmitters in target areas.

In contrast to optogenetics, pupillometry has long been neglected in animal research of the noradrenergic system. Our work presented here has demonstrated that pupillometry offers a simple and cheap alternative to validate LC activation as induced by optogenetics. Thus, pupillometry complements LC manipulations and can improve everyday experimental work in contrast to traditional methods. This approach can further be adapted to other brain areas that either influence the pupil directly or alter LC activity [426,427]. Due to the translational potential of pupillometry, it could also bridge aspects between human disorders of the noradrenergic system and corresponding animal models [394,396,428,429]. However, direct association of pupil size with LC activity has to be done carefully, as various other neurotransmitter systems, such as the cholinergic system, can modulate pupil size directly or through LC stimulation [426,429–431]. Thus changes in pupil size might therefore better be considered as a proxy for alterations in general arousal instead of direct LC function.

On the molecular level, LC research is about to be transformed as well. This is important, because pathophysiological changes in the LC manifest on the molecular level by altering LC activity and NA responsiveness. Most recently, next generation sequencing methods were used to molecularly define both LC and peri-LC cell types in detail and assess differences of LC neurons between sexes [432,433]. This work has demonstrated that the LC seems to be sexually dimorphic, with great differences in gene expression between the LC of male and female mice, and its activity is regulated by diverse molecular and spatial populations of GABAergic peri-LC neurons. Rapid advances in molecular sequencing methods finally also allow the investigation of the noradrenergic response on a cellular level in target areas. With further development of these methods, it will eventually be possible to fully resolve the noradrenergic impact on a single-cell population level across the brain, including effects on gene expression (transcriptomics), protein translation (translatomics), phosphorylation cascades (proteomics), and epigenetic mechanisms (DNA methylation and protein interaction analysis).
What we have tried here - for the first time - is to bring the advances in circuit and molecular neuroscience together, to investigate the effects of the LC-NA system. As a first step we have demonstrated that it is possible to combine specific chemo- and optogenetic manipulation with transcriptomics to characterize LC-mediated changes on hippocampal gene expression and identify specific molecular pathways potentially mediating stress responses. Next generation sequencing techniques will also be able to tackle some other open questions in LC research. As an example, visual and pharmacological methods have so far not been able to reliably assess adrenergic receptor distribution in a cell-type specific manner, which is now possible through single-cell sequencing data across brain structures. In summary, combining targeted manipulations of the LC with these technological advances in sequencing technology has the potential to drastically improve our understanding of the molecular impact the LC-NA system mediates.

4.2 Astrocytes: The major target of the LC-NA system

In contrast to classical neurotransmitters, the LC-NA system mostly performs volume transmission, suggesting that NA targets various cells of the CNS and not only neurons. Adrenergic receptors are found across neurons, microglia, oligodendrocytes, and astrocytes and mediate various noradrenergic functions within these cell types. These actions ultimately modulate neuronal output, especially through enhancing the signal-to-noise ratio. Hence, early research focused exclusively on the neuronal effects of NA. However, astrocytes have long been known to be a direct target of NA release and are strategically placed between blood vessels and synapses, form interconnected networks, and are crucial for energy metabolism and neuronal activity [434,435]. Astrocytes send out a mesh of fine stellar processes governing distinct domains, which are further connected between astrocytes through gap junctions and form large astrocytic networks. A single astrocytic domain can contain 300-600 neuronal dendrites and regulate up to 10^5 synapses within the cortex and hippocampus [436,437]. Therefore, astrocytes offer an ideal target for the LC-NA system to amplify its effects across widespread astrocytic networks to alter whole brain environments and brain states, a feature that is unlikely to be achieved by 1 on 1 synaptic connections across the brain.
Unsurprisingly, astrocytes express the largest variety and density of α1-, α2- and β-adrenergic receptors among CNS cells [435,438,439]. LC activity and consequent activation of α1-adrenergic receptors have further been shown to induce profound astrocytic

Ca^{2+} waves across brain areas in various vertebrate species [440–445]. Intracellular Ca^{2+} waves are known to alter the activity of several Ca^{2+}-dependent membrane proteins, elements of the cytoskeleton, enzymes, and induce gliotransmission [446–449]. These mechanisms mediate various changes in neuronal activity as well as local blood flow [450–454]. Evidence also suggests a key role of the β-adrenergic receptors in astrocyte function, including glycogen metabolism, regulation of immune responses, release of neurotrophic factors, and morphological changes [455–457]. Morphological changes in astrocytes could further influence the stabilization and maturation of dendritic spines, and thus potentially alter how astrocytes integrate and modify synaptic transmission and plasticity [458–462]. Within the hippocampus, astrocytic pathways are especially important for memory consolidation during stress exposure [463,464]. In fact, noradrenergic regulation of memory consolidation seems to be mediated through astrocytic and not neuronal β-adrenergic receptors in the hippocampus and anterior cingulate cortex [465,466]. In addition, our own work shows how stress and the LC-NA system affects astrocytic gene expression and highlights energy and thyroid hormone metabolism as important molecular mediators of astrocytic function in the hippocampus.

4.3 The LC as a major regulator of astrocytic energy metabolism

The brain requires huge amounts of energy to power the activity of neurons, especially when exposed to stressful situations. Astrocytes are the major source of energy substrates - including adenosine triphosphate (ATP), glucose, and lactate - to the brain. Astrocytes commonly manage the glucose uptake from the blood and store it as glycogen. Upon demand, astrocytic glycogen is broken down, processed, and distributed to other cells [467].
Astrocytic glucose and lactate fuel neuronal ATP production [468,469]. Astrocytic glycogenolysis is therefore essential for proper neuronal functioning, as ATP is required for neuronal survival and powers a multitude of cellular mechanisms.
Astrocytic glycogenolysis is heavily stimulated through astrocytic β-adrenergic receptors [470–472], suggesting that the LC-NA system anticipates and sources high energy demands in the CNS through immediate astrocytic glycogen break down. Accumulating evidence also suggests that after NA-mediated breakdown, slower mechanisms mediated by α1- and β-adrenergic receptors, replenish astrocytic glycogen through enhanced glucose uptake and activity of protein phosphatase 1 [473–475]. This is further supported by our own findings, which show a slow transcriptomic increase in glycogen binding subunits of protein phosphatase 1. Especially long-term memory consolidation and underlying neuronal adaptations seem to depend on astrocytic energy substrates [465,476–480], suggesting that this energy cycle is essential to facilitate memory formation through the LC-NA system under stress.

4.4 The LC as a major regulator of brain derived triiodothyronine

Apart from promoting the shuttling of glucose and lactate to neurons, evidence suggests that the LC-NA system might govern local astrocytic production of triiodothyronine (T3) [481,482]. Our own data supports these findings and shows that NA is essential for the stress-dependent upregulation of Dio2. This is of special interest, as, in fact, astrocyte derived T3 contributes to 50-70% of the total T3 concentration in the adult brain [483]. Astrocytes do not only synthesize T3 from thyroxine (T4), but also release it locally through

paracrine signaling, which affects cells nearby via binding of intracellular thyroid hormone receptors [484,485]. Aside from astrocytic T3 release, evidence also suggests that T3 is accumulated within neurons of the LC and transported to axonal terminals [486,487], implying that the LC-NA system may release T3 as a co-transmitter [488]. LC axons were also found to innervate thyrotropin-releasing hormone (TRH)-containing neurons of the PVN [489,490] and thus potentially stimulate peripheral release of thyroid hormones through activation of the hypothalamic–pituitary–thyroid axis. Evidence further shows that hippocampal T3 concentrations are drastically diminished after treatment with the LC-specific neurotoxin DSP-4 [486], indicating that the LC-NA system and its widespread projections could act as a major regulator and source of brain-derived T3. However, research into brain-derived T3 is still difficult, due to a lack of reliable methods to directly manipulate thyroid metabolism in the brain, as well as detect low concentrations of T3 and T4 within brain areas.

4.4.1 T3 facilitates neuronal signaling and plasticity

Neuronal function, in particular, seems to be regulated by the antagonistic signaling of T3 and its prohormone T4. Whereas T3 overall facilitates neuronal functions and T4 hinders them [491]. This effect is especially prominent during embryonic development, where T3 concentrations are kept high and promote proper development of the CNS [492–496]. However, in the adult brain, T4 is the predominant thyroid hormone, and thus activation of the LC-NA system could induce a local and temporal switch to promote T3 signaling.

Through genomic and non-genomic effects, T3 mediates changes in neuronal gene expression, chromatin remodeling, energy metabolism, neurogenesis, myelination, neurotransmission, and synaptic plasticity [497–508]. In particular, T3 seems to enhance the responsiveness of neurons to serotonin and NA [509–514]. This includes increased expression, translocation, and binding of active β-adrenergic receptors [511,515,516]. In contrast to T4, T3 is therefore able to increase local responsiveness to NA and potentiate consecutive noradrenergic excitation and inhibition of neurons in a positive feedback loop [517–519]. This bimodal control over neurotransmission could underlie effects on neuronal plasticity; as T4 has been found to promote synaptic LTD, while T3 instead promotes LTP [520–523]. This "thyroidergic switch" in neuronal plasticity further seems to directly affect memory formation, as local infusion of T3 has been shown to enhance hippocampal memory consolidation, while T4 had the opposite effect [524–526]. Thus, increases in T3 in the hippocampal region, in particular, could enhance the LC-NA system's effect on memory formation.

The actions of T3 are also locally regulated by the expression of the type III iodothyronine deiodinase (Dio3) in neurons. Dio3 is commonly located at the membrane of neurons and is capable of inactivating T3 before it enters the cell [527]. CNS expression of Dio3 is however very low at baseline, but is significantly upregulated in a state of hyperthyroidism [528]. Dio3 is also found among neurons of the hippocampus, amygdala and cortex, suggesting that it might play a role in regulating excessive actions of T3 in stress-related circuits. Single-cell sequencing of neuronal populations in the hippocampus further indicates that baseline expression of Dio3 is very specific and restricted to the vHC, in particular neurons of the ventral CA1 [319]. Thus, while LC-mediated increase of Dio2 activity occurs across the hippocampal axis, T3 might only affect the function of neurons within the dHC. This suggests that neuronal responses to NA can be quite heterogeneous depending on local thyroid

hormone regulation and might explain differences in noradrenergic regulation of LTP found in dorsal versus ventral hippocampus [529,530].

4.4.2 The LC-T3 link as a potential disease mechanism

Due to the crucial actions of T3 in the brain it potentially offers an important mechanism in the propagation of neurological disorders related to the LC-NA system. This is supported by the fact that impairment LC activity and reciprocal alterations in thyroid hormones are often comorbidities across various diseases and disorders.
In particular, neurodegenerative pathologies, such as AD, where early LC degeneration and lower T3 levels are prominent [357,362,531–538]. T3 has further been shown to suppress the expression of the potent AD mediators β-amyloid precursor protein (APP) and apolipoprotein E (ApoE), as well as improve cognitive AD symptoms [522,539–543]. Accordingly, patients with hypothyroidism have an increased risk of developing AD [544,545]. This suggests that early loss of LC neurons in AD and consequential decrease of local thyroid hormone availability could play a prominent role in the propagation of AD and especially its aspects of memory impairment. A specific state of T3 scarcity in the brain, in the absence of thyroid dysfunction, was also hypothesized to underlie major depression disorder [546]. This could be promoted by the decreased activity of the LC-NA system in depression, which would lead to a diminished peripheral conversion of T3 in astrocytes. A similar relationship between LC activity and thyroid hormones has also been seen in stress-related disorders. PTSD, for example, is not only marked by an increased LC activity but also elevated levels of T3 [547,548]. Thyroid hormone alterations have been associated with the formation of anxiety [549–551], and 60% of patients with hyperthyroidism do indeed develop anxiety disorders [546]. Abnormally high T3 levels could thus potentiate noradrenergic signaling and facilitate the consolidation and reinforcement of traumatic memories. In summary, various neurological diseases and disorders share reciprocal alterations in thyroid hormones and noradrenergic signaling, which could point to some shared underlying disease mechanism. However, research in this direction is still very limited, due the lack of reliable tools to study thyroid hormones in the brain. Thus, it remains to be explored how LC-mediated T3 production contributes to molecular LC function in health and disease.

4.6 An updated model of the LC-NA system

Aston Jones and Cohen [97], first proposed a profound role of the LC-NA system in optimizing behavior, due to its wide-range regulation of cognitive functions. Based on the theory of Aston-Jones and Cohen, Mather and colleagues have more recently brought forward the “glutamate amplifies noradrenergic effects” (GANE) model to underlie LC mediated optimization of behavior [98]. The GANE model proposes that increased glutamatergic transmission at the site of prioritized representations increases local NA release from the LC to generate “NA hotspots”. Within these hotspots, glutamate and NA synergistically enhance and amplify neuronal gain to promote attention and memory under arousal. In accordance with the GANE model and accumulating molecular evidence, I propose that enhancement and amplification of neuronal gain - mediated by the LC-NA system - is achieved mostly through engagement of astrocytic pathways. In particular, NA-mediated astrocytic release of energy substrates and T3 creates a temporal environment

or “hotspot” within target regions, which is highly favorable for neurotransmission and synaptic plasticity. This could lead to the simultaneous optimization of connections between the PFC, amygdala and hippocampus, whilst especially facilitating memory consolidation of arousing experiences across these regions, to improve future responses to stress. This is further supported by recent findings in the hippocampus and anterior cingulate cortex, which demonstrated that astrocytic β-adrenergic receptor signaling is essential for memory consolidation in these regions [465,466].
Moreover, noradrenergic control over Dio2-mediated T3 production is also regulated by glucocorticoids in a dose- and time-dependent manner [552]. Whereas low levels of glucocorticoids were found to enhance NA-mediated increase in Dio2 activity in adipocytes, but high levels had the opposite effect. This would further fit with current models of stress-dependent memory consolidation in the amygdala [553], suggesting that the LC-NA system and glucocorticoids could act together to create a restricted time window for T3-mediated actions in the brain after stress exposure. The proposed molecular pathway would thus fit current models of the LC and memory consolidation. With the advance of improved molecular methods in neuroscience, this offers an ideal starting point to further investigate the molecular workings of the LC in health and disease.

Acknowledgments

2801 Days. From start to finish. For 2801 days I walked the path of an explorer, a pioneer, a scientist. I would like to take a moment to thank those who have shared this path alongside me. Foremost, Johannes, 8 years ago we set out together to investigate the LC and out of an idea grew all that is now. I have learned a lot from you in this time and it was a pleasure working for you. I hope you keep succeeding in all of your future endeavors too. I would also like to thank my thesis committee members Denis Burdakov and Benno Roozendaal for their valued feedback and input throughout this journey. Next, I would like to thank all current and previous members of the Bohacek, Gapp and Schratt lab. It was a pleasure to work alongside all of you and I will cherish the fond memories we created within and outside of our labs. I want to specially thank all the original members of our lab Amalia Floriou-Servou, Oliver Sturman and Lukas von Ziegler, together we built a whole Lab and the scientific foundation for success. Special thanks also goes to all the students I had the pleasure to train and guide, foremost, Sian Duss, Rebecca Waag, Letizia Giovagnoli and Rhunzong Zhang. They have become great scientists and I am humbled to have played a small part in their journey. I would also like to thank all the admin and support staff: Sonja Bamert, Han-Yu Lin, Julia Bode, Jens Weissman, Roger Staub and Sanja Vasic. In addition, I would like to thank Isabelle Mansuy and her lab for the early support in our endeavors and all scientific collaborators I had the pleasure of working with, especially Kim David Ferrari and Yannick Vermeiren. Last but not least, I would like to thank my family, girlfriend and friends who supported me at every step of my journey no matter what.

Bibliography

References of chapter 1 and 4.

1. Darwin C. On the Origin of Species by Means of Natural Selection, Or The Preservation of Favoured Races in the Struggle for Life. 1859.
2. Cannon WB. Bodily Changes in Pain, Hunger, Fear and Rage: An Account of Recent Researches Into the Function of Emotional Excitement. 1915.
3. The Fight-or-Flight Response: A Cornerstone of Stress Research. Stress: Concepts, Cognition, Emotion, and Behavior. Academic Press; 2016. pp. 33–37.
4. Joëls M, Baram TZ. The neuro-symphony of stress. Nat Rev Neurosci. 2009;10: 459–466.
5. Koolhaas JM, Meerlo P, De Boer SF, Strubbe JH, Bohus B. The temporal dynamics of the stress response. Neurosci Biobehav Rev. 1997;21: 775–782.
6. Larzelere MM, Jones GN. Stress and health. Prim Care. 2008;35: 839–856.
7. Burchfield SR. The stress response: a new perspective. Psychosom Med. 1979;41: 661–672.
8. Chrousos GP. Stress and disorders of the stress system. Nat Rev Endocrinol. 2009;5: 374–381.
9. Pfau ML, Russo SJ. Peripheral and Central Mechanisms of Stress Resilience. Neurobiol Stress. 2015;1: 66–79.
10. Marin M-F, Lord C, Andrews J, Juster R-P, Sindi S, Arsenault-Lapierre G, et al. Chronic stress, cognitive functioning and mental health. Neurobiol Learn Mem. 2011;96: 583–595.
11. McEwen BS, Stellar E. Stress and the individual. Mechanisms leading to disease. Arch Intern Med. 1993;153: 2093–2101.
12. de Kloet ER, Joëls M, Holsboer F. Stress and the brain: from adaptation to disease. Nat Rev Neurosci. 2005;6: 463–475.
13. Sapolsky RM. Glucocorticoids, stress, and their adverse neurological effects: relevance to aging. Exp Gerontol. 1999;34: 721–732.
14. Tsigos C, Chrousos GP. Hypothalamic-pituitary-adrenal axis, neuroendocrine factors and stress. J Psychosom Res. 2002;53: 865–871.
15. Nicolaides NC, Chrousos G, Kino T. Glucocorticoid Receptor. MDText.com, Inc.; 2020.
16. Gomez-Sanchez E, Gomez-Sanchez CE. The multifaceted mineralocorticoid receptor. Compr Physiol. 2014;4: 965–994.
17. Munck A, Guyre PM, Holbrook NJ. Physiological Functions of Glucocorticoids in Stress and Their Relation to Pharmacological Actions*. Endocr Rev. 1984;5: 25–44.
18. Pardridge WM, Mietus LJ. Transport of steroid hormones through the rat blood-brain barrier. Primary role of albumin-bound hormone. J Clin Invest. 1979;64: 145–154.
19. McEwen BS, Weiss JM, Schwartz LS. Selective retention of corticosterone by limbic structures in rat brain. Nature. 1968;220: 911–912.
20. Herman JP. Regulation of adrenocorticosteroid receptor mRNA expression in the central nervous system. Cell Mol Neurobiol. 1993;13: 349–372.
21. Mora F, Segovia G, Del Arco A, de Blas M, Garrido P. Stress, neurotransmitters, corticosterone and body-brain integration. Brain Res. 2012;1476: 71–85.
22. Thoeringer CK, Sillaber I, Roedel A, Erhardt A, Mueller MB, Ohl F, et al. The temporal dynamics of intrahippocampal corticosterone in response to stress-related stimuli with different emotional and physical load: An in vivo microdialysis study in C57BL/6 and DBA/2 inbred mice. Psychoneuroendocrinology. 2007;32: 746–757.
23. Linthorst ACE. Chapter 4.1 Microdialysis to study the effects of stress on serotonin, corticosterone and

behaviour. Handbook of Microdialysis - Methods, Applications and Perspectives. 2006. pp. 301–315. doi:10.1016/s1569-7339(06)16017-8

24. Imperato A, Puglisi-Allegra S, Casolini P, Zocchi A, Angelucci L. Stress-induced enhancement of dopamine and acetylcholine release in limbic structures: role of corticosterone. Eur J Pharmacol. 1989;165: 337–338.

25. Karst H, Berger S, Turiault M, Tronche F, Schütz G, Joëls M. Mineralocorticoid receptors are indispensable for nongenomic modulation of hippocampal glutamate transmission by corticosterone. Proc Natl Acad Sci U S A. 2005;102: 19204–19207.

26. Musazzi L, Milanese M, Farisello P, Zappettini S, Tardito D, Barbiero VS, et al. Acute Stress Increases Depolarization-Evoked Glutamate Release in the Rat Prefrontal/Frontal Cortex: The Dampening Action of Antidepressants. PLoS ONE. 2010. p. e8566. doi:10.1371/journal.pone.0008566

27. Venero C, Borrell J. Rapid glucocorticoid effects on excitatory amino acid levels in the hippocampus: a microdialysis study in freely moving rats. Eur J Neurosci. 1999;11: 2465–2473.

28. Nahar J, Haam J, Chen C, Jiang Z, Glatzer NR, Muglia LJ, et al. Rapid Nongenomic Glucocorticoid Actions in Male Mouse Hypothalamic Neuroendocrine Cells Are Dependent on the Nuclear Glucocorticoid Receptor. Endocrinology. 2015;156: 2831–2842.

29. Makara GB, Haller J. Non-genomic effects of glucocorticoids in the neural system. Evidence, mechanisms and implications. Prog Neurobiol. 2001;65: 367–390.

30. Fan Y, Chen P, Li Y, Cui K, Noel DM, Cummins ED, et al. Corticosterone administration up-regulated expression of norepinephrine transporter and dopamine β-hydroxylase in rat locus coeruleus and its terminal regions. J Neurochem. 2014;128: 445–458.

31. Chaouloff F, Groc L. Temporal modulation of hippocampal excitatory transmission by corticosteroids and stress. Front Neuroendocrinol. 2011;32: 25–42.

32. Groc L, Choquet D, Chaouloff F. The stress hormone corticosterone conditions AMPAR surface trafficking and synaptic potentiation. Nat Neurosci. 2008;11: 868–870.

33. Gerstner N, Krontira AC, Cruceanu C, Roeh S, Pütz B, Sauer S, et al. DiffBrainNet: Differential analyses add new insights into the response to glucocorticoids at the level of genes, networks and brain regions. Neurobiol Stress. 2022;21: 100496.

34. Droste SK, de Groote L, Atkinson HC, Lightman SL, Reul JMHM, Linthorst ACE. Corticosterone levels in the brain show a distinct ultradian rhythm but a delayed response to forced swim stress. Endocrinology. 2008;149: 3244–3253.

35. Spencer RL, Deak T. A users guide to HPA axis research. Physiol Behav. 2017;178: 43–65.

36. Krugers H, Karst H, Joels M. Interactions between noradrenaline and corticosteroids in the brain: from electrical activity to cognitive performance. Front Cell Neurosci. 2012;6. doi:10.3389/fncel.2012.00015

37. de Kloet ER, Karst H, Joëls M. Corticosteroid hormones in the central stress response: quick-and-slow. Front Neuroendocrinol. 2008;29: 268–272.

38. Roozendaal B, Okuda S, Van der Zee EA, McGaugh JL. Glucocorticoid enhancement of memory requires arousal-induced noradrenergic activation in the basolateral amygdala. Proc Natl Acad Sci U S A. 2006;103: 6741–6746.

39. Joëls M, de Kloet ER. Effects of glucocorticoids and norepinephrine on the excitability in the hippocampus. Science. 1989;245: 1502–1505.

40. Vogel S, Fernández G, Joëls M, Schwabe L. Cognitive Adaptation under Stress: A Case for the Mineralocorticoid Receptor. Trends Cogn Sci. 2016;20: 192–203.

41. Basarrate S, Monzel AS, Smith J, Marsland A, Trumpff C, Picard M. Glucocorticoid and adrenergic receptor distribution across human organs and tissues: a map for stress transduction. bioRxiv. 2022. p. 2022.12.29.520757. doi:10.1101/2022.12.29.520757

42. Jhanwar-Uniyal M, Leibowitz SF. Impact of circulating corticosterone on alpha 1- and alpha 2-noradrenergic receptors in discrete brain areas. Brain Res. 1986;368: 404–408.

43. Buurstede JC, van Weert LTCM, Colucci P, Gentenaar M, Viho EMG, Koorneef LL, et al. Hippocampal glucocorticoid target genes associated with enhancement of memory consolidation. Eur J Neurosci. 2022;55: 2666–2683.

44. Roozendaal B, McEwen BS, Chattarji S. Stress, memory and the amygdala. Nat Rev Neurosci. 2009;10: 423–433.

45. Sandi C. Glucocorticoids act on glutamatergic pathways to affect memory processes. Trends Neurosci. 2011;34: 165–176.

46. Ulrich-Lai YM, Herman JP. Neural regulation of endocrine and autonomic stress responses. Nature Reviews Neuroscience. 2009. pp. 397–409. doi:10.1038/nrn2647

47. Joëls M, Pu Z, Wiegert O, Oitzl MS, Krugers HJ. Learning under stress: how does it work? Trends Cogn Sci. 2006;10: 152–158.

48. Alberini CM, Kandel ER. The regulation of transcription in memory consolidation. Cold Spring Harb Perspect Biol. 2014;7: a021741.

49. Jansen ASP, Van Nguyen X, Karpitskiy V, Mettenleiter TC, Loewy AD. Central Command Neurons of the Sympathetic Nervous System: Basis of the Fight-or-Flight Response. Science. 1995. pp. 644–646. doi:10.1126/science.270.5236.644

50. Goldstein DS. Stress-induced activation of the sympathetic nervous system. Baillière's Clinical Endocrinology and Metabolism. 1987. pp. 253–278. doi:10.1016/s0950-351x(87)80063-0

51. Nakamura K, Morrison SF. Central sympathetic network for thermoregulatory responses to psychological stress. Auton Neurosci. 2022;237: 102918.

52. Alshak MN, M Das J. Neuroanatomy, Sympathetic Nervous System. StatPearls. Treasure Island (FL): StatPearls Publishing; 2022.

53. Lu FC, Allmark MG. A Comparison of the Bronchodilator Activities of Adrenaline and Noradrenaline: A Proposed Procedure for the Biological Assay of Adrenaline Solutions Containing Noradrenaline*. J Pharm Pharmacol. 2011;6: 513–521.

54. McCulloch MW, Proctor C, Rand MJ. Evidence for an adrenergic homeostatic bronchodilator reflex mechanism. Eur J Pharmacol. 1967;2: 214–223.

55. Zaglia T, Mongillo M. Cardiac sympathetic innervation, from a different point of (re)view. J Physiol. 2017;595: 3919–3930.

56. Triposkiadis F, Karayannis G, Giamouzis G, Skoularigis J, Louridas G, Butler J. The sympathetic nervous system in heart failure physiology, pathophysiology, and clinical implications. J Am Coll Cardiol. 2009;54: 1747–1762.

57. Wang Q, Sharma VP, Shen H, Xiao Y, Zhu Q, Xiong X, et al. The hepatokine Tsukushi gates energy expenditure via brown fat sympathetic innervation. Nat Metab. 2019;1: 251–260.

58. Landsberg L, Saville ME, Young JB. Sympathoadrenal system and regulation of thermogenesis. Am J Physiol. 1984;247: E181–9.

59. Landsberg L, Young JB. The role of the sympathetic nervous system and catecholamines in the regulation of energy metabolism. Am J Clin Nutr. 1983;38: 1018–1024.

60. Szabadi E. Modulation of physiological reflexes by pain: role of the locus coeruleus. Front Integr Neurosci. 2012;6: 94.

61. Christensen NJ. The biochemical assessment of sympathoadrenal activity in man. Clin Auton Res. 1991;1: 167–172.

62. Meston CM. Sympathetic nervous system activity and female sexual arousal. Am J Cardiol. 2000;86: 30F–34F.

63. Lomax AE, Sharkey KA, Furness JB. The participation of the sympathetic innervation of the gastrointestinal tract in disease states. Neurogastroenterol Motil. 2010;22: 7–18.

64. Weaver LC. Organization of sympathetic responses to distension of urinary bladder. Am J Physiol. 1985;248: R236–40.

65. Hardebo JE, Edvinsson L, Mackenzie ET, Owman C. Regional brain uptake of noradrenaline following mechanical or osmotic opening of the blood-brain barrier. Acta Physiol Scand. 1977;101: 342–350.

66. Manger PR, Eschenko O. The Mammalian Locus Coeruleus Complex-Consistencies and Variances in

Nuclear Organization. Brain Sci. 2021;11. doi:10.3390/brainsci11111486

67. Stanford SC. Central noradrenergic neurones and stress. Pharmacol Ther. 1995;68: 297–242.

68. Poe GR, Foote S, Eschenko O, Johansen JP, Bouret S, Aston-Jones G, et al. Locus coeruleus: a new look at the blue spot. Nature Reviews Neuroscience. 2020. pp. 644–659. doi:10.1038/s41583-020-0360-9

69. Vicq-d'Azyr F, François-Ambroise Didot,) AB. Traité d'anatomie et de physiologie, avec des planches coloriées représentant au naturel les divers organes de l'homme et des animaux. Dédié au Roi par M. Vicq d'Azyr,... Tome premier. de l'imprimerie de Franc. Amb. Didot l'ainé; 1786.

70. Dahlström A, Fuxe K. Localization of monoamines in the lower brain stem. Experientia. 1964;20: 398–399.

71. Wang S, Wang Z, Mu Y. Locus Coeruleus in Non-Mammalian Vertebrates. Brain Sci. 2022;12. doi:10.3390/brainsci12020134

72. Sharma Y, Xu T, Graf WM, Fobbs A, Sherwood CC, Hof PR, et al. Comparative anatomy of the locus coeruleus in humans and nonhuman primates. J Comp Neurol. 2010;518: 963–971.

73. Ma PM. Catecholaminergic systems in the zebrafish. I. Number, morphology, and histochemical characteristics of neurons in the locus coeruleus. J Comp Neurol. 1994;344: 242–255.

74. Loughlin SE, Foote SL, Grzanna R. Efferent projections of nucleus locus coeruleus: morphologic subpopulations have different efferent targets. Neuroscience. 1986;18: 307–319.

75. Swanson LW. The locus coeruleus: a cytoarchitectonic, Golgi and immunohistochemical study in the albino rat. Brain Res. 1976;110: 39–56.

76. Shimizu N, Imamoto K. Fine structure of the locus coeruleus in the rat. Arch Histol Jpn. 1970;31: 229–246.

77. Cintra L, Díaz-Cintra S, Kemper T, Morgane PJ. Nucleus locus coeruleus: a morphometric Golgi study in rats of three age groups. Brain Res. 1982;247: 17–28.

78. Grzanna R, Molliver ME. The locus coeruleus in the rat: An immunohistochemical delineation. Neuroscience. 1980. pp. 21–40. doi:10.1016/0306-4522(80)90068-8

79. Aston-Jones G, Shipley MT, Chouvet G, Ennis M, van Bockstaele E, Pieribone V, et al. Afferent regulation of locus coeruleus neurons: anatomy, physiology and pharmacology. Prog Brain Res. 1991;88: 47–75.

80. Jin X, Li S, Bondy B, Zhong W, Oginsky MF, Wu Y, et al. Identification of a Group of GABAergic Neurons in the Dorsomedial Area of the Locus Coeruleus. PLoS One. 2016;11: e0146470.

81. Aston-Jones G, Zhu Y, Card JP. Numerous GABAergic afferents to locus ceruleus in the pericerulear dendritic zone: possible interneuronal pool. J Neurosci. 2004;24: 2313–2321.

82. Samuels ER, Szabadi E. Functional neuroanatomy of the noradrenergic locus coeruleus: its roles in the regulation of arousal and autonomic function part I: principles of functional organisation. Curr Neuropharmacol. 2008;6: 235–253.

83. Samuels ER, Szabadi E. Functional neuroanatomy of the noradrenergic locus coeruleus: its roles in the regulation of arousal and autonomic function part II: physiological and pharmacological manipulations and pathological alterations of locus coeruleus activity in humans. Curr Neuropharmacol. 2008;6: 254–285.

84. Schwarz LA, Miyamichi K, Gao XJ, Beier KT, Weissbourd B, DeLoach KE, et al. Viral-genetic tracing of the input–output organization of a central noradrenaline circuit. Nature. 2015;524: 88–92.

85. Valentino RJ, Van Bockstaele E. Convergent regulation of locus coeruleus activity as an adaptive response to stress. Eur J Pharmacol. 2008;583: 194–203.

86. Valentino RJ, Foote SL, Aston-Jones G. Corticotropin-releasing factor activates noradrenergic neurons of the locus coeruleus. Brain Res. 1983;270: 363–367.

87. Valentino RJ, Van Bockstaele E. Opposing regulation of the locus coeruleus by corticotropin-releasing factor and opioids. Potential for reciprocal interactions between stress and opioid sensitivity. Psychopharmacology . 2001;158: 331–342.

88. Snyder K, Wang W-W, Han R, McFadden K, Valentino RJ. Corticotropin-releasing factor in the norepinephrine nucleus, locus coeruleus, facilitates behavioral flexibility. Neuropsychopharmacology. 2012;37: 520–530.

89. Butler PD, Weiss JM, Stout JC, Nemeroff CB. Corticotropin-releasing factor produces fear-enhancing and behavioral activating effects following infusion into the locus coeruleus. J Neurosci. 1990;10: 176–183.

90. Reyes BAS, Valentino RJ, Xu G, Van Bockstaele EJ. Hypothalamic projections to locus coeruleus neurons in rat brain. Eur J Neurosci. 2005;22: 93–106.

91. Valentino RJ, Page M, Van Bockstaele E, Aston-Jones G. Corticotropin-releasing factor innervation of the locus coeruleus region: distribution of fibers and sources of input. Neuroscience. 1992;48: 689–705.

92. Van Bockstaele EJ, Colago EEO. Amygdaloid corticotropin‐releasing factor targets locus coeruleus dendrites: substrate for the co‐ordination of emotional and cognitive limbs of the stress response. Journal of. 1998. Available: https://onlinelibrary.wiley.com/doi/abs/10.1046/j.1365-2826.1998.00254.x?casa_token=uFgqrs3u0icAAAAA:enXHngdIwtyNYA60NsMTmDolmySX23L_AKBJiywApbGfBq-ErZhF4lz-UY1zbTdIlXk_9ijYVpghkWo

93. Tomycz ND, Friedlander RM. Neuromodulation of the Locus Coeruleus: A Key to Controlling Wakefulness. Neurosurgery. 2011. pp. N14–N15. doi:10.1227/01.neu.0000393589.31014.61

94. Hayat H, Regev N, Matosevich N, Sales A, Paredes-Rodriguez E, Krom AJ, et al. Locus coeruleus norepinephrine activity mediates sensory-evoked awakenings from sleep. Sci Adv. 2020;6: eaaz4232.

95. Aston-Jones G. Behavioral functions of locus coeruleus derived from cellular attributes. Physiological Psychology. 1985;13: 118–126.

96. Carter ME, Yizhar O, Chikahisa S, Nguyen H, Adamantidis A, Nishino S, et al. Tuning arousal with optogenetic modulation of locus coeruleus neurons. Nat Neurosci. 2010;13: 1526–1533.

97. Aston-Jones G, Cohen JD. An integrative theory of locus coeruleus-norepinephrine function: adaptive gain and optimal performance. Annu Rev Neurosci. 2005;28: 403–450.

98. Mather M, Clewett D, Sakaki M, Harley CW. Norepinephrine ignites local hotspots of neuronal excitation: How arousal amplifies selectivity in perception and memory. Behav Brain Sci. 2016;39: e200.

99. McCall JG, Al-Hasani R, Siuda ER, Hong DY, Norris AJ, Ford CP, et al. CRH Engagement of the Locus Coeruleus Noradrenergic System Mediates Stress-Induced Anxiety. Neuron. 2015;87: 605–620.

100. Grimm C, Duss SN, Privitera M, Munn BR, Frässle S, Chernysheva M, et al. Locus Coeruleus firing patterns selectively modulate brain activity and dynamics. bioRxiv. 2022. p. 2022.08.29.505672. doi:10.1101/2022.08.29.505672

101. Loughlin SE, Foote SL, Bloom FE. Efferent projections of nucleus locus coeruleus: topographic organization of cells of origin demonstrated by three-dimensional reconstruction. Neuroscience. 1986;18: 291–306.

102. Sara SJ, Bouret S. Orienting and reorienting: the locus coeruleus mediates cognition through arousal. Neuron. 2012;76: 130–141.

103. Schwarz LA, Luo L. Organization of the locus coeruleus-norepinephrine system. Curr Biol. 2015;25: R1051–R1056.

104. Chandler DJ, Gao W-J, Waterhouse BD. Heterogeneous organization of the locus coeruleus projections to prefrontal and motor cortices. Proc Natl Acad Sci U S A. 2014;111: 6816–6821.

105. Kebschull JM, Garcia da Silva P, Reid AP, Peikon ID, Albeanu DF, Zador AM. High-Throughput Mapping of Single-Neuron Projections by Sequencing of Barcoded RNA. Neuron. 2016;91: 975–987.

106. McNaughton N, Mason ST. The neuropsychology and neuropharmacology of the dorsal ascending noradrenergic bundle--a review. Prog Neurobiol. 1980;14: 157–219.

107. Kostowski W. Two noradrenergic systems in the brain and their interactions with other monoaminergic neurons. Pol J Pharmacol Pharm. 1979;31: 425–436.

108. Szabadi E. Functional neuroanatomy of the central noradrenergic system. J Psychopharmacol. 2013;27: 659–693.

109. Ungerstedt U. Stereotaxic mapping of the monoamine pathways in the rat brain. Acta Physiol Scand Suppl. 1971;367: 1–48.

110. Mejías-Aponte CA, Drouin C, Aston-Jones G. Adrenergic and noradrenergic innervation of the midbrain ventral tegmental area and retrorubral field: prominent inputs from medullary homeostatic centers. J

Neurosci. 2009;29: 3613–3626.

111. Hirschberg S, Li Y, Randall A, Kremer EJ, Pickering AE. Functional dichotomy in spinal- vs prefrontal-projecting locus coeruleus modules splits descending noradrenergic analgesia from ascending aversion and anxiety in rats. eLife. 2017. doi:10.7554/elife.29808

112. Kalaria RN, Stockmeier CA, Harik SI. Brain microvessels are innervated by locus ceruleus noradrenergic neurons. Neurosci Lett. 1989;97: 203–208.

113. Kalinin S, Feinstein DL, Xu H-L, Huesa G, Pelligrino DA, Galea E. Degeneration of noradrenergic fibres from the locus coeruleus causes tight-junction disorganisation in the rat brain. Eur J Neurosci. 2006;24: 3393–3400.

114. Geffen LB, Livett BG. Synaptic vesicles in sympathetic neurons. Physiol Rev. 1971;51: 98–157.

115. Livett BG. Histochemical visualization of peripheral and central adrenergic neurones. Br Med Bull. 1973;29: 93–99.

116. Chiti Z, Teschemacher AG. Exocytosis of norepinephrine at axon varicosities and neuronal cell bodies in the rat brain. FASEB J. 2007;21: 2540–2550.

117. Hökfelt T. In vitro studies on central and peripheral monoamine neurons at the ultrastructural level. Z Zellforsch Mikrosk Anat. 1968;91: 1–74.

118. Descarries L, Watkins KC, Lapierre Y. Noradrenergic axon terminals in the cerebral cortex of rat. III. Topometric ultrastructural analysis. Brain Res. 1977;133: 197–222.

119. Lapierre Y, Beaudet A, Demianczuk N, Descarries L. Noradrenergic axon terminals in the cerebral cortex of rat. II. Quantitative data revealed by light and electron microscope radioautography of the frontal cortex. Brain Res. 1973;63: 175–182.

120. Descarries L, Lapierre Y. Noradrenergic axon terminals in the cerebral cortex of rat. I. Radioautographic visualization after topical application of dl-[3H]norepinephrine. Brain Res. 1973;51: 141–160.

121. Beaudet A, Descarries L. The monoamine innervation of rat cerebral cortex: synaptic and nonsynaptic axon terminals. Neuroscience. 1978;3: 851–860.

122. Descarries L, Mechawar N. Ultrastructural evidence for diffuse transmission by monoamine and acetylcholine neurons of the central nervous system. Prog Brain Res. 2000;125: 27–47.

123. Fuxe K, Agnati LF, Marcoli M, Borroto-Escuela DO. Volume Transmission in Central Dopamine and Noradrenaline Neurons and Its Astroglial Targets. Neurochem Res. 2015;40: 2600–2614.

124. Del Cid-Pellitero E, Garzón M. Hypocretin1/OrexinA-containing axons innervate locus coeruleus neurons that project to the Rat medial prefrontal cortex. Implication in the sleep-wakefulness cycle and cortical activation. Synapse. 2011;65: 843–857.

125. Devoto P, Flore G. On the origin of cortical dopamine: is it a co-transmitter in noradrenergic neurons? Curr Neuropharmacol. 2006;4: 115–125.

126. Smith CC, Greene RW. CNS dopamine transmission mediated by noradrenergic innervation. J Neurosci. 2012;32: 6072–6080.

127. Devoto P, Flore G, Saba P, Fà M, Gessa GL. Stimulation of the locus coeruleus elicits noradrenaline and dopamine release in the medial prefrontal and parietal cortex. J Neurochem. 2005;92: 368–374.

128. Kempadoo KA, Mosharov EV, Choi SJ, Sulzer D, Kandel ER. Dopamine release from the locus coeruleus to the dorsal hippocampus promotes spatial learning and memory. Proc Natl Acad Sci U S A. 2016;113: 14835–14840.

129. Holets VR, Hökfelt T, Rökaeus A, Terenius L, Goldstein M. Locus coeruleus neurons in the rat containing neuropeptide Y, tyrosine hydroxylase or galanin and their efferent projections to the spinal cord, cerebral cortex and hypothalamus. Neuroscience. 1988;24: 893–906.

130. Poelchen W, Sieler D, Wirkner K, Illes P. Co-transmitter function of ATP in central catecholaminergic neurons of the rat. Neuroscience. 2001;102: 593–602.

131. Fung SJ, Reddy VK, Liu RH, Wang Z, Barnes CD. Existence of glutamate in noradrenergic locus coeruleus neurons of rodents. Brain Res Bull. 1994;35: 505–512.

132. Fung SJ, Reddy VK, Zhuo H, Liu RH, Wang Z, Barnes CD. Anatomical evidence for the presence of glutamate or enkephalin in noradrenergic projection neurons of the locus coeruleus. Microsc Res Tech. 1994;29: 219–225.

133. Kvetnansky R, Sabban EL, Palkovits M. Catecholaminergic systems in stress: structural and molecular genetic approaches. Physiol Rev. 2009;89: 535–606.

134. Bylund DB, Bylund KC. Norepinephrine. In: Aminoff MJ, Daroff RB, editors. Encyclopedia of the Neurological Sciences (Second Edition). Oxford: Academic Press; 2014. pp. 614–616.

135. Glavin GB. Stress and brain noradrenaline: a review. Neurosci Biobehav Rev. 1985;9: 233–243.

136. Axelrod J, Kopin IJ. The uptake, storage, release and metabolism of noradrenaline in sympathetic nerves. Prog Brain Res. 1969;31: 21–32.

137. Iversen LL. Role of Transmitter Uptake Mechanisms in Synaptic Neurotransmission. British Journal of Pharmacology. 1971. pp. 571–591. doi:10.1111/j.1476-5381.1971.tb07066.x

138. Zahniser NR, Doolen S. Chronic and acute regulation of Na+/Cl- -dependent neurotransmitter transporters: drugs, substrates, presynaptic receptors, and signaling systems. Pharmacol Ther. 2001;92: 21–55.

139. Mandela P, Ordway GA. The norepinephrine transporter and its regulation. J Neurochem. 2006;97: 310–333.

140. Takeda H, Inazu M, Matsumiya T. Astroglial dopamine transport is mediated by norepinephrine transporter. Naunyn Schmiedebergs Arch Pharmacol. 2002;366: 620–623.

141. Xu F, Gainetdinov RR, Wetsel WC, Jones SR, Bohn LM, Miller GW, et al. Mice lacking the norepinephrine transporter are supersensitive to psychostimulants. Nat Neurosci. 2000;3: 465–471.

142. Bönisch H, Brüss M. The norepinephrine transporter in physiology and disease. Handb Exp Pharmacol. 2006; 485–524.

143. Ramos BP, Arnsten AFT. Adrenergic pharmacology and cognition: focus on the prefrontal cortex. Pharmacol Ther. 2007;113: 523–536.

144. Day HE, Campeau S, Watson SJ Jr, Akil H. Distribution of alpha 1a-, alpha 1b- and alpha 1d-adrenergic receptor mRNA in the rat brain and spinal cord. J Chem Neuroanat. 1997;13: 115–139.

145. Perez DM. The Adrenergic Receptors: In the 21st Century. Springer Science & Business Media; 2006.

146. Graham RM. Adrenergic receptors: structure and function. Cleve Clin J Med. 1990;57: 481–491.

147. MacDonald E, Kobilka BK, Scheinin M. Gene targeting — homing in on α2-adrenoceptor-subtype function. Trends Pharmacol Sci. 1997;18: 211–219.

148. Saunders C, Limbird LE. Localization and trafficking of alpha2-adrenergic receptor subtypes in cells and tissues. Pharmacol Ther. 1999;84: 193–205.

149. Nicholas AP, Pieribone V, Hökfelt T. Distributions of mRNAs for alpha-2 adrenergic receptor subtypes in rat brain: an in situ hybridization study. J Comp Neurol. 1993;328: 575–594.

150. Limbird LE. Receptors linked to inhibition of adenylate cyclase: additional signaling mechanisms. FASEB J. 1988;2: 2686–2695.

151. Duzic E, Coupry I, Downing S, Lanier SM. Factors determining the specificity of signal transduction by guanine nucleotide-binding protein-coupled receptors. I. Coupling of alpha 2-adrenergic receptor subtypes to distinct G-proteins. J Biol Chem. 1992;267: 9844–9851.

152. Perez DM. Localization of Adrenergic Receptor Subtypes and Transgenic Expression of Fluorescent-Tagged Receptors. In: Perez DM, editor. The Adrenergic Receptors: In the 21st Century. Totowa, NJ: Humana Press; 2006. pp. 173–204.

153. Rodriguez M, Carillon C, Coquerel A, Le Fur G, Ferrara P, Caput D, et al. Evidence for the presence of β3-adrenergic receptor mRNA in the human brain. Molecular Brain Research. 1995;29: 369–375.

154. Nicholas AP, Pieribone VA, Hökfelt T. Cellular localization of messenger RNA for beta-1 and beta-2 adrenergic receptors in rat brain: an in situ hybridization study. Neuroscience. 1993;56: 1023–1039.

155. Grimm LJ, Blendy JA, Kellar KJ, Perry DC. Chronic reserpine administration selectively up-regulates β1- and α1b-adrenergic receptors in rat brain: An autoradiographic study. Neuroscience. 1992;47: 77–86.

156. Asanuma M, Ogawa N, Mizukawa K, Haba K, Hirata H, Mori A. Distribution of the beta-2 adrenergic receptor messenger RNA in the rat brain by in situ hybridization histochemistry: effects of chronic reserpine treatment. Neurochem Res. 1991;16: 1253–1256.

157. Prielipp RC, MacGregor DA, Butterworth JF, Meredith JW, Levy JH, Wood KE, et al. Pharmacodynamics and Pharmacokinetics of Milrinone Administration to Increase Oxygen Delivery in Critically Ill Patients. Chest. 1996;109: 1291–1301.

158. Minneman KP, Pittman RN, Molinoff PB. Beta-adrenergic receptor subtypes: properties, distribution, and regulation. Annu Rev Neurosci. 1981;4: 419–461.

159. Gelinas JN, Banko JL, Hou L, Sonenberg N, Weeber EJ, Klann E, et al. ERK and mTOR signaling couple β-adrenergic receptors to translation initiation machinery to gate induction of protein synthesis-dependent long-term potentiation. J Biol Chem. 2007;282: 27527–27535.

160. Hagena H, Hansen N, Manahan-Vaughan D. β-Adrenergic Control of Hippocampal Function: Subserving the Choreography of Synaptic Information Storage and Memory. Cereb Cortex. 2016;26: 1349–1364.

161. Hieble JP, Bondinell W, Ruffolo RR. From the gene to the clinic. 1. Molecular biology and adrenoceptor classification. J Med Chem.

162. Strosberg AD. Structure, function, and regulation of adrenergic receptors. Protein Sci. 1993;2: 1198–1209.

163. Wallukat G. The beta-adrenergic receptors. Herz. 2002;27: 683–690.

164. Maity S, Jarome TJ, Blair J, Lubin FD, Nguyen PV. Noradrenaline goes nuclear: epigenetic modifications during long-lasting synaptic potentiation triggered by activation of β-adrenergic receptors. The Journal of Physiology. 2016. pp. 863–881. doi:10.1113/jp271432

165. Siuda ER, McCall JG, Al-Hasani R, Shin G, Il Park S, Schmidt MJ, et al. Optodynamic simulation of β-adrenergic receptor signalling. Nat Commun. 2015;6: 8480.

166. Kaupp UB, Benjamin Kaupp U, Seifert R. Cyclic Nucleotide-Gated Ion Channels. Physiological Reviews. 2002. pp. 769–824. doi:10.1152/physrev.00008.2002

167. Cotecchia S. The α1-adrenergic receptors: diversity of signaling networks and regulation. J Recept Signal Transduct Res. 2010;30: 410–419.

168. Molinoff PB. ??- and ??-Adrenergic Receptor Subtypes Properties, Distribution and Regulation. Drugs. 1984. pp. 1–15. doi:10.2165/00003495-198400282-00002

169. Hein P, Michel MC. Signal transduction and regulation: Are all α1-adrenergic receptor subtypes created equal? Biochemical Pharmacology. 2007. pp. 1097–1106. doi:10.1016/j.bcp.2006.11.001

170. Han C, Abel PW, Minneman KP. α1Adrenoceptor subtypes linked to different mechanisms for increasing intracellular Ca2 in smooth muscle. Nature. 1987. pp. 333–335. doi:10.1038/329333a0

171. Xing M, Insel PA. Protein kinase C-dependent activation of cytosolic phospholipase A2 and mitogen-activated protein kinase by alpha 1-adrenergic receptors in Madin-Darby canine kidney cells. Journal of Clinical Investigation. 1996. pp. 1302–1310. doi:10.1172/jci118546

172. Ruan Y, Kan H, Parmentier JH, Fatima S, Allen LF, Malik KU. Alpha-1A adrenergic receptor stimulation with phenylephrine promotes arachidonic acid release by activation of phospholipase D in rat-1 fibroblasts: inhibition by protein kinase A. J Pharmacol Exp Ther. 1998;284: 576–585.

173. Hague C, Chen Z, Uberti M, Minneman KP. α1-Adrenergic receptor subtypes: non-identical triplets with different dancing partners? Life Sciences. 2003. pp. 411–418. doi:10.1016/j.lfs.2003.07.008

174. Woo AYH, Xiao R-P. β-Adrenergic receptor subtype signaling in heart: From bench to bedside. Acta Pharmacologica Sinica. 2012. pp. 335–341. doi:10.1038/aps.2011.201

175. Rybin VO, Xu X, Lisanti MP, Steinberg SF. Differential Targeting of β-Adrenergic Receptor Subtypes and Adenylyl Cyclase to Cardiomyocyte Caveolae: A MECHANISM TO FUNCTIONALLY REGULATE THE cAMP SIGNALING PATHWAY *. J Biol Chem. 2000;275: 41447–41457.

176. Birk A, Rinne A, Bünemann M. Membrane Potential Controls the Efficacy of Catecholamine-induced β1-Adrenoceptor Activity. J Biol Chem. 2015;290: 27311–27320.

177. Cell Trafficking and Function of G Protein-coupled Receptors. Arch Med Res. 2022;53: 451–460.

178. Chalothorn D, McCune DF, Edelmann SE, García-Cazarín ML, Tsujimoto G, Piascik MT. Differences in the Cellular Localization and Agonist-Mediated Internalization Properties of the α1-Adrenoceptor Subtypes. Mol Pharmacol. 2002;61: 1008–1016.

179. Toews ML, Prinster SC, Schulte NA. Regulation of alpha-1B adrenergic receptor localization, trafficking, function, and stability. Life Sci. 2003;74: 379–389.

180. Daunt DA, Hurt C, Hein L, Kallio J, Feng F, Kobilka BK. Subtype-specific intracellular trafficking of alpha2-adrenergic receptors. Mol Pharmacol. 1997;51: 711–720.

181. Boivin B, Lavoie C, Vaniotis G, Baragli A, Villeneuve L, Ethier N, et al. Functional β-adrenergic receptor signalling on nuclear membranes in adult rat and mouse ventricular cardiomyocytes. Cardiovascular Research. 2006. pp. 69–78. doi:10.1016/j.cardiores.2006.03.015

182. Pupo AS, Minneman KP. Specific interactions between gC1qR and alpha1-adrenoceptor subtypes. J Recept Signal Transduct Res. 2003;23: 185–195.

183. Walther C, Ferguson SSG, editors. Arrestins: Role in the Desensitization, Sequestration, and Vesicular Trafficking of G Protein-Coupled Receptors. Progress in Molecular Biology and Translational Science. Academic Press; 2013. pp. 93–113.

184. Lavoie C, Mercier J-F, Salahpour A, Umapathy D, Breit A, Villeneuve L-R, et al. β1/β2-Adrenergic Receptor Heterodimerization Regulates β2-Adrenergic Receptor Internalization and ERK Signaling Efficacy *. J Biol Chem. 2002;277: 35402–35410.

185. Zhu W-Z, Chakir K, Zhang S, Yang D, Lavoie C, Bouvier M, et al. Heterodimerization of beta1- and beta2-adrenergic receptor subtypes optimizes beta-adrenergic modulation of cardiac contractility. Circ Res. 2005;97: 244–251.

186. Mercier J-F, Salahpour A, Angers S, Breit A, Bouvier M. Quantitative assessment of β1- and β2-adrenergic re- receptor homo- and heterodimerization by bioluminescence resonance energy transfer. Journal of Biological Chemistry. 2003. p. 18704. doi:10.1016/s0021-9258(19)54982-1

187. Aston-Jones G, Rajkowski J, Cohen J. Role of locus coeruleus in attention and behavioral flexibility. Biol Psychiatry. 1999;46: 1309–1320.

188. McEwen BS. Physiology and neurobiology of stress and adaptation: central role of the brain. Physiol Rev. 2007;87: 873–904.

189. Pacák K, Palkovits M. Stressor specificity of central neuroendocrine responses: implications for stress-related disorders. Endocr Rev. 2001;22: 502–548.

190. Berridge CW, Waterhouse BD. The locus coeruleus–noradrenergic system: modulation of behavioral state and state-dependent cognitive processes. Brain Res Rev. 2003;42: 33–84.

191. Lee S-H, Dan Y. Neuromodulation of brain states. Neuron. 2012;76: 209–222.

192. McCormick DA, Nestvogel DB, He BJ. Neuromodulation of Brain State and Behavior. Annu Rev Neurosci. 2020;43: 391–415.

193. Berridge CW. Noradrenergic modulation of arousal. Brain Res Rev. 2008;58: 1–17.

194. Chandler DJ. Evidence for a specialized role of the locus coeruleus noradrenergic system in cortical circuitries and behavioral operations. Brain Res. 2016;1641: 197–206.

195. Coradazzi M, Gulino R, Fieramosca F, Falzacappa LV, Riggi M, Leanza G. Selective noradrenaline depletion impairs working memory and hippocampal neurogenesis. Neurobiol Aging. 2016;48: 93–102.

196. Sara SJ. The locus coeruleus and noradrenergic modulation of cognition. Nat Rev Neurosci. 2009;10: 211–223.

197. Troadec JD, Marien M, Darios F, Hartmann A, Ruberg M, Colpaert F, et al. Noradrenaline provides long-term protection to dopaminergic neurons by reducing oxidative stress. J Neurochem. 2001;79: 200–210.

198. Tait DS, Brown VJ, Farovik A, Theobald DE, Dalley JW, Robbins TW. Lesions of the dorsal noradrenergic bundle impair attentional set-shifting in the rat. Eur J Neurosci. 2007;25: 3719–3724.

199. Plotsky PM, Cunningham ET Jr, Widmaier EP. Catecholaminergic modulation of corticotropin-releasing factor and adrenocorticotropin secretion. Endocr Rev. 1989;10: 437–458.

200. al-Damluji S. Adrenergic mechanisms in the control of corticotrophin secretion. J Endocrinol. 1988;119: 5–14.

201. Goddard AW, Ball SG, Martinez J, Robinson MJ, Yang CR, Russell JM, et al. Current perspectives of the roles of the central norepinephrine system in anxiety and depression. Depress Anxiety. 2010;27: 339–350.

202. Pacák K, Baffi JS, Kvetňanský R, Goldstein DS, Palkovits M. Stressor-Specific Activation of Catecholaminergic Systems: Implications for Stress-Related Hypothalamic-Pituitary-Adrenocortical Responses. Advances in Pharmacology. 1997. pp. 561–564. doi:10.1016/s1054-3589(08)60812-1

203. Dunn AJ, Swiergiel AH. The role of corticotropin-releasing factor and noradrenaline in stress-related responses, and the inter-relationships between the two systems. Eur J Pharmacol. 2008;583: 186–193.

204. Ziegler DR, Cass WA, Herman JP. Excitatory influence of the locus coeruleus in hypothalamic-pituitary-adrenocortical axis responses to stress. J Neuroendocrinol. 1999;11: 361–369.

205. Bromek E, Wójcikowski J, Daniel WA. Involvement of the paraventricular (PVN) and arcuate (ARC) nuclei of the hypothalamus in the central noradrenergic regulation of liver cytochrome P450. Biochem Pharmacol. 2013;86: 1614–1620.

206. Bromek E, Danek PJ, Wójcikowski J, Basińska-Ziobroń A, Pukło R, Solich J, et al. The impact of noradrenergic neurotoxin DSP-4 and noradrenaline transporter knockout (NET-KO) on the activity of liver cytochrome P450 3A (CYP3A) in male and female mice. Pharmacol Rep. 2022;74: 1107–1114.

207. Burk O, Wojnowski L. Cytochrome P450 3A and their regulation. Naunyn Schmiedebergs Arch Pharmacol. 2004;369: 105–124.

208. Kot M, Daniel WA. Cytochrome P450 is regulated by noradrenergic and serotonergic systems. Pharmacol Res. 2011;64: 371–380.

209. Bruinstroop E, Cano G, Vanderhorst VGJM, Cavalcante JC, Wirth J, Sena-Esteves M, et al. Spinal projections of the A5, A6 (locus coeruleus), and A7 noradrenergic cell groups in rats. J Comp Neurol. 2012;520: 1985–2001.

210. Proudfit HK, Clark FM. Chapter 8 - The projections of locus coeruleus neurons to the spinal cord. In: Barnes CD, Pompeiano O, editors. Progress in Brain Research. Elsevier; 1991. pp. 123–141.

211. Shahar T, Palkovits M. Cross over of forebrain and brainstem neuronal projections to spinal cord sympathetic preganglionic neurons in the rat. Stress. 2007;10: 145–152.

212. Miyawaki T, Kawamura H, Komatsu K, Yasugi T. Chemical stimulation of the locus coeruleus: inhibitory effects on hemodynamics and renal sympathetic nerve activity. Brain Res. 1991;568: 101–108.

213. Fung SJ, Manzoni D, Chan JYH, Pompeiano O, Barnes CD. Chapter 30 - Locus coeruleus control of spinal motor output. In: Barnes CD, Pompeiano O, editors. Progress in Brain Research. Elsevier; 1991. pp. 395–409.

214. Liu Y, Rodenkirch C, Moskowitz N, Schriver B, Wang Q. Dynamic Lateralization of Pupil Dilation Evoked by Locus Coeruleus Activation Results from Sympathetic, Not Parasympathetic, Contributions. Cell Rep. 2017;20: 3099–3112.

215. Chan JY, Fung SJ, Chan SH, Barnes CD. Facilitation of lumbar monosynaptic reflexes by locus coeruleus in the rat. Brain Res. 1986;369: 103–109.

216. Szabadi E. Functional Organization of the Sympathetic Pathways Controlling the Pupil: Light-Inhibited and Light-Stimulated Pathways. Front Neurol. 2018;9: 1069.

217. Yoshimura N, Sasa M, Yoshida O, Takaori S. Alpha 1-adrenergic receptor-mediated excitation from the locus coeruleus of the sacral parasympathetic preganglionic neuron. Life Sci. 1990;47: 789–797.

218. Lewis DI, Coote JH. Excitation and inhibition of rat sympathetic preganglionic neurones by catecholamines. Brain Res. 1990;530: 229–234.

219. Arnsten AFT. Stress signalling pathways that impair prefrontal cortex structure and function. Nat Rev Neurosci. 2009;10: 410–422.

220. Dalley JW, Cardinal RN, Robbins TW. Prefrontal executive and cognitive functions in rodents: neural and neurochemical substrates. Neurosci Biobehav Rev. 2004;28: 771–784.

221. Maier SF, Amat J, Baratta MV, Paul E, Watkins LR. Behavioral control, the medial prefrontal cortex, and resilience. Dialogues Clin Neurosci. 2006;8: 397–406.

222. Lewis DA, Morrison JH. Noradrenergic innervation of monkey prefrontal cortex: A dopamine-?-hydroxylase immunohistochemical study. The Journal of Comparative Neurology. 1989. pp. 317–330. doi:10.1002/cne.902820302

223. Carboni E, Tanda GL, Frau R, Di Chiara G. Blockade of the noradrenaline carrier increases extracellular dopamine concentrations in the prefrontal cortex: evidence that dopamine is taken up in vivo by noradrenergic terminals. J Neurochem. 1990;55: 1067–1070.

224. Sara SJ. Locus Coeruleus in time with the making of memories. Curr Opin Neurobiol. 2015;35: 87–94.

225. Aoki C, Venkatesan C, Go CG, Forman R, Kurose H. Cellular and subcellular sites for noradrenergic action in the monkey dorsolateral prefrontal cortex as revealed by the immunocytochemical localization of noradrenergic receptors and axons. Cereb Cortex. 1998;8: 269–277.

226. Aoki C, Go CG, Venkatesan C, Kurose H. Perikaryal and synaptic localization of alpha 2A-adrenergic receptor-like immunoreactivity. Brain Res. 1994;650: 181–204.

227. Goldman-Rakic PS, Lidow MS, Gallager DW. Overlap of dopaminergic, adrenergic, and serotoninergic receptors and complementarity of their subtypes in primate prefrontal cortex. J Neurosci. 1990;10: 2125–2138.

228. Santana N, Artigas F. Laminar and Cellular Distribution of Monoamine Receptors in Rat Medial Prefrontal Cortex. Front Neuroanat. 2017;11: 87.

229. Santana N, Mengod G, Artigas F. Expression of α(1)-adrenergic receptors in rat prefrontal cortex: cellular co-localization with 5-HT(2A) receptors. Int J Neuropsychopharmacol. 2013;16: 1139–1151.

230. Jackson WJ, Buccafusco JJ. Clonidine enhances delayed matching-to-sample performance by young and aged monkeys. Pharmacol Biochem Behav. 1991;39: 79–84.

231. Arnsten AFT, Contant TA. Alpha-2 adrenergic agonists decrease distractibility in aged monkeys performing the delayed response task. Psychopharmacology. 1992. pp. 159–169. doi:10.1007/bf02245302

232. Caetano MS, Jin LE, Harenberg L, Stachenfeld KL, Arnsten AFT, Laubach M. Noradrenergic control of error perseveration in medial prefrontal cortex. Front Integr Neurosci. 2013;6. doi:10.3389/fnint.2012.00125

233. Florin-Lechner SM, Druhan JP, Aston-Jones G, Valentino RJ. Enhanced norepinephrine release in prefrontal cortex with burst stimulation of the locus coeruleus. Brain Res. 1996;742: 89–97.

234. Shimizu N, Nakane H, Hori T, Hayashi Y. CRF receptor antagonist attenuates stress-induced noradrenaline release in the medial prefrontal cortex of rats. Brain Res. 1994;654: 145–148.

235. Berridge CW, Spencer RC. Differential cognitive actions of norepinephrine a2 and a1 receptor signaling in the prefrontal cortex. Brain Res. 2016;1641: 189–196.

236. Lapiz MDS, Morilak DA. Noradrenergic modulation of cognitive function in rat medial prefrontal cortex as measured by attentional set shifting capability. Neuroscience. 2006;137: 1039–1049.

237. Bari A, Xu S, Pignatelli M, Takeuchi D, Feng J, Li Y, et al. Differential attentional control mechanisms by two distinct noradrenergic coeruleo-frontal cortical pathways. Proc Natl Acad Sci U S A. 2020;117: 29080–29089.

238. Mansouri FA, Tanaka K, Buckley MJ. Conflict-induced behavioural adjustment: a clue to the executive functions of the prefrontal cortex. Nat Rev Neurosci. 2009;10: 141–152.

239. Shima K, Isoda M, Mushiake H, Tanji J. Categorization of behavioural sequences in the prefrontal cortex. Nature. 2007;445: 315–318.

240. Seu E, Lang A, Rivera RJ, Jentsch JD. Inhibition of the norepinephrine transporter improves behavioral flexibility in rats and monkeys. Psychopharmacology . 2009;202: 505–519.

241. Tronel S, Feenstra MGP, Sara SJ. Noradrenergic action in prefrontal cortex in the late stage of memory consolidation. Learn Mem. 2004;11: 453–458.

242. Do-Monte FHM, Kincheski GC, Pavesi E, Sordi R, Assreuy J, Carobrez AP. Role of beta-adrenergic receptors in the ventromedial prefrontal cortex during contextual fear extinction in rats. Neurobiol Learn Mem. 2010;94: 318–328.

243. Zhou H-C, Sun Y-Y, Cai W, He X-T, Yi F, Li B-M, et al. Activation of β2-adrenoceptor enhances synaptic potentiation and behavioral memory via cAMP-PKA signaling in the medial prefrontal cortex of rats. Learn Mem. 2013;20: 274–284.

244. Reyes-López J, Nuñez-Jaramillo L, Morán-Guel E, Miranda MI. Differential effects of beta-adrenergic receptor blockade in the medial prefrontal cortex during aversive and incidental taste memory formation. Neuroscience. 2010;169: 195–202.

245. LeDoux JE. Emotion circuits in the brain. Annu Rev Neurosci. 2000;23: 155–184.

246. McGaugh JL. The amygdala modulates the consolidation of memories of emotionally arousing experiences. Annu Rev Neurosci. 2004;27: 1–28.

247. Galvez R, Mesches MH, McGaugh JL. Norepinephrine release in the amygdala in response to footshock stimulation. Neurobiol Learn Mem. 1996;66: 253–257.

248. Tanaka T, Yokoo H, Mizoguchi K, Yoshida M, Tsuda A, Tanaka M. Noradrenaline release in the rat amygdala is increased by stress: studies with intracerebral microdialysis. Brain Res. 1991;544: 174–176.

249. Kawahara H, Yoshida M, Yokoo H, Nishi M, Tanaka M. Psychological stress increases serotonin release in the rat amygdala and prefrontal cortex assessed by in vivo microdialysis. Neurosci Lett. 1993;162: 81–84.

250. Mo B, Feng N, Renner K, Forster G. Restraint stress increases serotonin release in the central nucleus of the amygdala via activation of corticotropin-releasing factor receptors. Brain Res Bull. 2008;76: 493–498.

251. Inglis FM, Moghaddam B. Dopaminergic innervation of the amygdala is highly responsive to stress. J Neurochem. 1999;72: 1088–1094.

252. Stevenson CW, Sullivan RM, Gratton A. Effects of basolateral amygdala dopamine depletion on the nucleus accumbens and medial prefrontal cortical dopamine responses to stress. Neuroscience. 2003;116: 285–293.

253. Berretta S. Cortico-amygdala circuits: role in the conditioned stress response. Stress. 2005;8: 221–232.

254. Herman JP, Figueiredo H, Mueller NK, Ulrich-Lai Y, Ostrander MM, Choi DC, et al. Central mechanisms of stress integration: hierarchical circuitry controlling hypothalamo-pituitary-adrenocortical responsiveness. Front Neuroendocrinol. 2003;24: 151–180.

255. Krettek JE, Price JL. Amygdaloid projections to subcortical structures within the basal forebrain and brainstem in the rat and cat. The Journal of Comparative Neurology. 1978. pp. 225–253. doi:10.1002/cne.901780204

256. Petrovich GD, Swanson LW. Projections from the lateral part of the central amygdalar nucleus to the postulated fear conditioning circuit. Brain Res. 1997;763: 247–254.

257. Rosen JB, Hitchcock JM, Sananes CB, Miserendino MJD, Davis M. A direct projection from the central nucleus of the amygdala to the acoustic startle pathway: Anterograde and retrograde tracing studies. Behavioral Neuroscience. 1991. pp. 817–825. doi:10.1037/0735-7044.105.6.817

258. Zhang X, Cui J, Tan Z, Jiang C, Fogel R. The central nucleus of the amygdala modulates gut-related neurons in the dorsal vagal complex in rats. J Physiol. 2003;553: 1005–1018.

259. Veening JG, Swanson LW, Sawchenko PE. The organization of projections from the central nucleus of the amygdala to brainstem sites involved in central autonomic regulation: a combined retrograde transport-immunohistochemical study. Brain Res. 1984;303: 337–357.

260. Barros DM, Pereira P, Medina JH, Izquierdo I. Modulation of working memory and of long- but not short-term memory by cholinergic mechanisms in the basolateral amygdala. Behav Pharmacol. 2002;13: 163–167.

261. Bianchin M, Mello e Souza T, Medina JH, Izquierdo I. The amygdala is involved in the modulation of long-term memory, but not in working or short-term memory. Neurobiol Learn Mem. 1999;71: 127–131.

262. Lalumiere RT, Nguyen LT, McGaugh JL. Post-training intrabasolateral amygdala infusions of dopamine modulate consolidation of inhibitory avoidance memory: involvement of noradrenergic and cholinergic systems. Eur J Neurosci. 2004;20: 2804–2810.

263. Schafe GE, LeDoux JE. Memory consolidation of auditory pavlovian fear conditioning requires protein synthesis and protein kinase A in the amygdala. J Neurosci. 2000;20: RC96.

264. Liang KC, McGaugh JL. Lesions of the stria terminalis attenuate the enhancing effect of post-training epinephrine on retention of an inhibitory avoidance response. Behav Brain Res. 1983;9: 49–58.

265. Miranda MI, McGaugh JL. Enhancement of inhibitory avoidance and conditioned taste aversion memory with insular cortex infusions of 8-Br-cAMP: involvement of the basolateral amygdala. Learn Mem. 2004;11: 312–317.

266. Roesler R, Roozendaal B, McGaugh JL. Basolateral amygdala lesions block the memory-enhancing effect of 8-Br-cAMP infused into the entorhinal cortex of rats after training. Eur J Neurosci. 2002;15: 905–910.

267. Setlow B, Roozendaal B, McGaugh JL. Involvement of a basolateral amygdala complex-nucleus accumbens pathway in glucocorticoid-induced modulation of memory consolidation. Eur J Neurosci. 2000;12: 367–375.

268. Zhang J, Muller JF, McDonald AJ. Noradrenergic innervation of pyramidal cells in the rat basolateral amygdala. Neuroscience. 2013;228: 395–408.

269. Fallon JH, Koziell DA, Moore RY. Catecholamine innervation of the basal forebrain. II. Amygdala, suprarhinal cortex and entorhinal cortex. J Comp Neurol. 1978;180: 509–532.

270. Asan E. The catecholaminergic innervation of the rat amygdala. Adv Anat Embryol Cell Biol. 1998;142: 1–118.

271. Amaral DG. The primate amygdala and the neurobiology of social behavior: implications for understanding social anxiety. Biol Psychiatry. 2002;51: 11–17.

272. Sharp BM. Basolateral amygdala and stress-induced hyperexcitability affect motivated behaviors and addiction. Transl Psychiatry. 2017;7: e1194.

273. Ghods-Sharifi S, St Onge JR, Floresco SB. Fundamental contribution by the basolateral amygdala to different forms of decision making. J Neurosci. 2009;29: 5251–5259.

274. Skelly MJ, Snyder AE, Silberman Y. Chapter 9 - Noradrenergic regulation of the basolateral amygdala. In: Urban JH, Rosenkranz JA, editors. Handbook of Behavioral Neuroscience. Elsevier; 2020. pp. 213–226.

275. Giustino TF, Ramanathan KR, Totty MS, Miles OW, Maren S. Locus Coeruleus Norepinephrine Drives Stress-Induced Increases in Basolateral Amygdala Firing and Impairs Extinction Learning. J Neurosci. 2020;40: 907–916.

276. Llorca-Torralba M, Suárez-Pereira I, Bravo L, Camarena-Delgado C, Garcia-Partida JA, Mico JA, et al. Chemogenetic Silencing of the Locus Coeruleus-Basolateral Amygdala Pathway Abolishes Pain-Induced Anxiety and Enhanced Aversive Learning in Rats. Biol Psychiatry. 2019;85: 1021–1035.

277. McCall JG, Siuda ER, Bhatti DL, Lawson LA, McElligott ZA, Stuber GD, et al. Locus coeruleus to basolateral amygdala noradrenergic projections promote anxiety-like behavior. Elife. 2017;6. doi:10.7554/eLife.18247

278. Schwabe L, Hermans EJ, Joëls M, Roozendaal B. Mechanisms of memory under stress. Neuron. 2022;110: 1450–1467.

279. Liang KC, McGaugh JL, Yao HY. Involvement of amygdala pathways in the influence of post-training intra-amygdala norepinephrine and peripheral epinephrine on memory storage. Brain Res. 1990;508: 225–233.

280. Meftahi GH, Jangravi Z, Taghdir M, Sepandi M, Bahari Z. Micro-injection of propranolol within basolateral amygdala impaired fear and spatial memory and dysregulated evoked responses of CA1 neurons following foot shock stress in rats. Brain Res Bull. 2021;177: 12–21.

281. Ferry B, Roozendaal B, McGaugh JL. Basolateral amygdala noradrenergic influences on memory storage are mediated by an interaction between beta- and alpha1-adrenoceptors. J Neurosci. 1999;19: 5119–5123.

282. Roozendaal B, McGaugh JL. Glucocorticoid receptor agonist and antagonist administration into the basolateral but not central amygdala modulates memory storage. Neurobiol Learn Mem. 1997;67: 176–179.

283. Donley MP, Schulkin J, Rosen JB. Glucocorticoid receptor antagonism in the basolateral amygdala and ventral hippocampus interferes with long-term memory of contextual fear. Behav Brain Res. 2005;164: 197–205.

284. McReynolds JR, Donowho K, Abdi A, McGaugh JL, Roozendaal B, McIntyre CK. Memory-enhancing corticosterone treatment increases amygdala norepinephrine and Arc protein expression in hippocampal synaptic fractions. Neurobiol Learn Mem. 2010;93: 312–321.

285. Roozendaal B, Quirarte GL, McGaugh JL. Glucocorticoids interact with the basolateral amygdala beta-adrenoceptor--cAMP/cAMP/PKA system in influencing memory consolidation. Eur J Neurosci. 2002;15: 553–560.

286. Roozendaal B, Schelling G, McGaugh JL. Corticotropin-releasing factor in the basolateral amygdala enhances memory consolidation via an interaction with the beta-adrenoceptor-cAMP pathway: dependence on glucocorticoid receptor activation. J Neurosci. 2008;28: 6642–6651.

287. Happe HK, Coulter CL, Gerety ME, Sanders JD, O'Rourke M, Bylund DB, et al. Alpha-2 adrenergic receptor development in rat CNS: an autoradiographic study. Neuroscience. 2004;123: 167–178.

288. Talley EM, Rosin DL, Lee A, Guyenet PG, Lynch KR. Distribution of alpha 2A-adrenergic receptor-like immunoreactivity in the rat central nervous system. J Comp Neurol. 1996;372: 111–134.

289. Buffalari DM, Grace AA. Noradrenergic modulation of basolateral amygdala neuronal activity: opposing influences of α-2 and β receptor activation. Journal of Neuroscience. 2007. Available: https://www.jneurosci.org/content/27/45/12358.short

290. Braga MFM, Aroniadou-Anderjaska V, Manion ST, Hough CJ, Li H. Stress impairs alpha(1A) adrenoceptor-mediated noradrenergic facilitation of GABAergic transmission in the basolateral amygdala. Neuropsychopharmacology. 2004;29: 45–58.

291. Myers EA, Rinaman L. Viscerosensory activation of noradrenergic inputs to the amygdala in rats. Physiol Behav. 2002;77: 723–729.

292. Cecchi M, Khoshbouei H, Morilak DA. Modulatory effects of norepinephrine, acting on alpha 1 receptors in the central nucleus of the amygdala, on behavioral and neuroendocrine responses to acute immobilization stress. Neuropharmacology. 2002;43: 1139–1147.

293. Silberman Y, Winder DG. Corticotropin releasing factor and catecholamines enhance glutamatergic neurotransmission in the lateral subdivision of the central amygdala. Neuropharmacology. 2013;70: 316–323.

294. Koob GF. Brain stress systems in the amygdala and addiction. Brain Res. 2009;1293: 61–75.

295. Belujon P, Grace AA. Hippocampus, amygdala, and stress: interacting systems that affect susceptibility to addiction. Ann N Y Acad Sci. 2011;1216: 114–121.

296. Fadok JP, Markovic M, Tovote P, Lüthi A. New perspectives on central amygdala function. Curr Opin Neurobiol. 2018;49: 141–147.

297. Bird CM, Burgess N. The hippocampus and memory: insights from spatial processing. Nat Rev Neurosci. 2008;9: 182–194.

298. Eichenbaum H. Hippocampus: cognitive processes and neural representations that underlie declarative memory. Neuron. 2004;44: 109–120.

299. McNaughton BL, Morris RGM. Hippocampal synaptic enhancement and information storage within a distributed memory system. Trends Neurosci. 1987;10: 408–415.

300. Moser EI, Kropff E, Moser M-B. Place cells, grid cells, and the brain's spatial representation system. Annu Rev Neurosci. 2008;31: 69–89.

301. McEwen BS. Plasticity of the hippocampus: adaptation to chronic stress and allostatic load. Ann N Y Acad Sci. 2001;933: 265–277.

302. Fanselow MS, Dong H-W. Are the dorsal and ventral hippocampus functionally distinct structures? Neuron. 2010;65: 7–19.

303. Strange BA, Witter MP, Lein ES, Moser EI. Functional organization of the hippocampal longitudinal axis. Nat Rev Neurosci. 2014;15: 655–669.

304. Bannerman DM, Grubb M, Deacon RMJ, Yee BK, Feldon J, Rawlins JNP. Ventral hippocampal lesions affect anxiety but not spatial learning. Behav Brain Res. 2003;139: 197–213.

305. Jacobson L, Sapolsky R. The role of the hippocampus in feedback regulation of the hypothalamic-pituitary-adrenocortical axis. Endocr Rev. 1991;12: 118–134.

306. Kheirbek MA, Drew LJ, Burghardt NS, Costantini DO, Tannenholz L, Ahmari SE, et al. Differential control of learning and anxiety along the dorsoventral axis of the dentate gyrus. Neuron. 2013;77: 955–968.

307. Trivedi MA, Coover GD. Lesions of the ventral hippocampus, but not the dorsal hippocampus, impair conditioned fear expression and inhibitory avoidance on the elevated T-maze. Neurobiol Learn Mem. 2004;81: 172–184.

308. McEwen BS, Bowles NP, Gray JD, Hill MN, Hunter RG, Karatsoreos IN, et al. Mechanisms of stress in the brain. Nat Neurosci. 2015;18: 1353–1363.

309. van Steensel B, van Haarst AD, de Kloet ER, van Driel R. Binding of corticosteroid receptors to rat hippocampus nuclear matrix. FEBS Lett. 1991;292: 229–231.

310. Nasca C, Bigio B, Zelli D, Nicoletti F, McEwen BS. Mind the gap: glucocorticoids modulate hippocampal glutamate tone underlying individual differences in stress susceptibility. Mol Psychiatry. 2015;20: 755–763.

311. von Ziegler LM, Floriou-Servou A, Waag R, Das Gupta RR, Sturman O, Gapp K, et al. Multiomic profiling of the acute stress response in the mouse hippocampus. Nat Commun. 2022;13: 1824.

312. Kim JJ, Song EY, Kim JJ, Song EY, Kosten TA. Stress effects in the hippocampus: Synaptic plasticity and memory. Stress. 2006;9: 1–11.

313. Kim JJ, Koo JW, Lee HJ, Han J-S. Amygdalar inactivation blocks stress-induced impairments in hippocampal long-term potentiation and spatial memory. J Neurosci. 2005;25: 1532–1539.

314. David A, Pierre L. Hippocampal Neuroanatomy. The Hippocampus Book. 2006. pp. 37–114. doi:10.1093/acprof:oso/9780195100273.003.0003

315. Loy R, Koziell DA, Lindsey JD, Moore RY. Noradrenergic innervation of the adult rat hippocampal formation. J Comp Neurol. 1980;189: 699–710.

316. Oleskevich S, Descarries L, Lacaille JC. Quantified distribution of the noradrenaline innervation in the hippocampus of adult rat. J Neurosci. 1989;9: 3803–3815.

317. Gage FH, Thompson RG. Differential distribution of norepinephrine and serotonin along the dorsal-ventral axis of the hippocampal formation. Brain Res Bull. 1980;5: 771–773.

318. Nalepa I, Kreiner G, Bielawski A, Rafa-Zabłocka K, Roman A. α1-Adrenergic receptor subtypes in the central nervous system: insights from genetically engineered mouse models. Pharmacol Rep. 2013;65: 1489–1497.

319. Cembrowski MS, Wang L, Sugino K, Shields BC, Spruston N. Hipposeq: a comprehensive RNA-seq database of gene expression in hippocampal principal neurons. Elife. 2016;5: e14997.

320. Saunders A, Macosko EZ, Wysoker A, Goldman M, Krienen FM, de Rivera H, et al. Molecular Diversity and Specializations among the Cells of the Adult Mouse Brain. Cell. 2018;174: 1015–1030.e16.

321. Hansen N. The Longevity of Hippocampus-Dependent Memory Is Orchestrated by the Locus Coeruleus-Noradrenergic System. Neural Plast. 2017;2017: 2727602.

322. Tully K, Bolshakov VY. Emotional enhancement of memory: how norepinephrine enables synaptic plasticity. Mol Brain. 2010;3: 15.

323. Madison DV, Nicoll RA. Noradrenaline blocks accommodation of pyramidal cell discharge in the hippocampus. Nature. 1982;299: 636–638.

324. Madison DV, Nicoll RA. Actions of noradrenaline recorded intracellularly in rat hippocampal CA1 pyramidal neurones, in vitro. J Physiol. 1986;372: 221–244.

325. Bacon TJ, Pickering AE, Mellor JR. Noradrenaline Release from Locus Coeruleus Terminals in the Hippocampus Enhances Excitation-Spike Coupling in CA1 Pyramidal Neurons Via β-Adrenoceptors. Cereb

Cortex. 2020;30: 6135–6151.

326. Pang K, Rose GM. Differential effects of norepinephrine on hippocampal complex-spike and theta-neurons. Brain Res. 1987;425: 146–158.

327. Bergles DE, Doze VA, Madison DV, Smith SJ. Excitatory actions of norepinephrine on multiple classes of hippocampal CA1 interneurons. J Neurosci. 1996;16: 572–585.

328. Madison DV, Nicoll RA. Norepinephrine decreases synaptic inhibition in the rat hippocampus. Brain Res. 1988;442: 131–138.

329. Hansen N, Manahan-Vaughan D. Locus Coeruleus Stimulation Facilitates Long-Term Depression in the Dentate Gyrus That Requires Activation of β-Adrenergic Receptors. Cereb Cortex. 2015;25: 1889–1896.

330. Nguyen PV, Connor SA. Noradrenergic Regulation of Hippocampus-Dependent Memory. Cent Nerv Syst Agents Med Chem. 2019;19: 187–196.

331. Lim EP, Tan CH, Jay TM, Dawe GS. Locus coeruleus stimulation and noradrenergic modulation of hippocampo-prefrontal cortex long-term potentiation. Int J Neuropsychopharmacol. 2010;13: 1219–1231.

332. Lemon N, Aydin-Abidin S, Funke K, Manahan-Vaughan D. Locus coeruleus activation facilitates memory encoding and induces hippocampal LTD that depends on beta-adrenergic receptor activation. Cereb Cortex. 2009;19: 2827–2837.

333. Schutsky K, Ouyang M, Thomas SA. Xamoterol impairs hippocampus-dependent emotional memory retrieval via Gi/o-coupled β2-adrenergic signaling. Learn Mem. 2011;18: 598–604.

334. Murchison CF, Schutsky K, Jin S-H, Thomas SA. Norepinephrine and ß1-adrenergic signaling facilitate activation of hippocampal CA1 pyramidal neurons during contextual memory retrieval. Neuroscience. 2011;181: 109–116.

335. Maity S, Rah S, Sonenberg N, Gkogkas CG, Nguyen PV. Norepinephrine triggers metaplasticity of LTP by increasing translation of specific mRNAs. Learn Mem. 2015;22: 499–508.

336. Takeuchi T, Duszkiewicz AJ, Sonneborn A, Spooner PA, Yamasaki M, Watanabe M, et al. Locus coeruleus and dopaminergic consolidation of everyday memory. Nature. 2016;537: 357–362.

337. Yamasaki M, Takeuchi T. Locus Coeruleus and Dopamine-Dependent Memory Consolidation. Neural Plast. 2017;2017: 8602690.

338. Schwabe L, Wolf OT. Stress and multiple memory systems: from “thinking” to “doing.” Trends Cogn Sci. 2013;17: 60–68.

339. Wagatsuma A, Okuyama T, Sun C, Smith LM, Abe K, Tonegawa S. Locus coeruleus input to hippocampal CA3 drives single-trial learning of a novel context. Proc Natl Acad Sci U S A. 2018;115: E310–E316.

340. Harley CW. A role for norepinephrine in arousal, emotion and learning?: limbic modulation by norepinephrine and the Kety hypothesis. Prog Neuropsychopharmacol Biol Psychiatry. 1987;11: 419–458.

341. Seo D-O, Zhang ET, Piantadosi SC, Marcus DJ, Motard LE, Kan BK, et al. A locus coeruleus to dentate gyrus noradrenergic circuit modulates aversive contextual processing. Neuron. 2021;109: 2116–2130.e6.

342. Ishida Y, Shirokawa T, Miyaishi O. Age-dependent changes in projections from locus coeruleus to hippocampus dentate gyrus and frontal cortex. European Journal of. 2000. Available: https://onlinelibrary.wiley.com/doi/abs/10.1046/j.1460-9568.2000.00017.x

343. Ishida Y, Shirokawa T, Komatsu Y, Isobe K. Changes in cortical noradrenergic axon terminals of locus coeruleus neurons in aged F344 rats. Neurosci Lett. 2001;307: 197–199.

344. Shirokawa T, Ishida Y, Isobe K-I. Age-related changes in the release and uptake activity of presynaptic axon terminals of rat locus coeruleus neurons. Neurosci Lett. 2003;344: 212–214.

345. Grudzien A, Shaw P, Weintraub S, Bigio E, Mash DC, Mesulam MM. Locus coeruleus neurofibrillary degeneration in aging, mild cognitive impairment and early Alzheimer’s disease. Neurobiol Aging. 2007;28: 327–335.

346. Manaye KF, McIntire DD, Mann DM, German DC. Locus coeruleus cell loss in the aging human brain: a non-random process. J Comp Neurol. 1995;358: 79–87.

347. Insel PA. Adrenergic receptors, G proteins, and cell regulation: implications for aging research. Exp Gerontol. 1993;28: 341–348.

348. Mather M, Harley CW. The Locus Coeruleus: Essential for Maintaining Cognitive Function and the Aging Brain. Trends Cogn Sci. 2016;20: 214–226.

349. Zecca L, Stroppolo A, Gatti A, Tampellini D, Toscani M, Gallorini M, et al. The role of iron and copper molecules in the neuronal vulnerability of locus coeruleus and substantia nigra during aging. Proc Natl Acad Sci U S A. 2004;101: 9843–9848.

350. Matchett BJ, Grinberg LT, Theofilas P, Murray ME. The mechanistic link between selective vulnerability of the locus coeruleus and neurodegeneration in Alzheimer's disease. Acta Neuropathol. 2021;141: 631–650.

351. German DC, Manaye KF, White CL 3rd, Woodward DJ, McIntire DD, Smith WK, et al. Disease-specific patterns of locus coeruleus cell loss. Ann Neurol. 1992;32: 667–676.

352. Del Tredici K, Braak H. Dysfunction of the locus coeruleus–norepinephrine system and related circuitry in Parkinson's disease-related dementia. J Neurol Neurosurg Psychiatry. 2013;84: 774–783.

353. Tilley BS, Patel SR, Goldfinger MH, Pearce RKB, Gentleman SM. Locus Coeruleus Pathology Indicates a Continuum of Lewy Body Dementia. J Parkinsons Dis. 2021;11: 1641–1650.

354. Bari BA, Chokshi V, Schmidt K. Locus coeruleus-norepinephrine: basic functions and insights into Parkinson's disease. Neural Regeneration Res. 2020;15: 1006–1013.

355. Tomlinson BE, Irving D, Blessed G. Cell loss in the locus coeruleus in senile dementia of Alzheimer type. J Neurol Sci. 1981;49: 419–428.

356. Kelly SC, He B, Perez SE, Ginsberg SD, Mufson EJ, Counts SE. Locus coeruleus cellular and molecular pathology during the progression of Alzheimer's disease. Acta Neuropathol Commun. 2017;5: 8.

357. Jacobs HIL, Becker JA, Kwong K, Engels-Domínguez N, Prokopiou PC, Papp KV, et al. In vivo and neuropathology data support locus coeruleus integrity as indicator of Alzheimer's disease pathology and cognitive decline. Sci Transl Med. 2021;13. doi:10.1126/scitranslmed.abj2511

358. Mercan D, Heneka MT. The Contribution of the Locus Coeruleus-Noradrenaline System Degeneration during the Progression of Alzheimer's Disease. Biology . 2022;11. doi:10.3390/biology11121822

359. Braak H, Rüb U, Gai WP, Del Tredici K. Idiopathic Parkinson's disease: possible routes by which vulnerable neuronal types may be subject to neuroinvasion by an unknown pathogen. J Neural Transm. 2003;110: 517–536.

360. Harley CW, Walling SG, Yuan Q, Martin GM. The "a, b, c"s of pretangle tau and their relation to aging and the risk of Alzheimer's Disease. Semin Cell Dev Biol. 2021;116: 125–134.

361. Kelly SC, McKay EC, Beck JS, Collier TJ, Dorrance AM, Counts SE. Locus coeruleus degeneration induces forebrain vascular pathology in a transgenic rat model of Alzheimer's disease. J Alzheimers Dis. 2019;70: 371–388.

362. Giorgi FS, Galgani A, Puglisi-Allegra S, Busceti CL, Fornai F. The connections of Locus Coeruleus with hypothalamus: potential involvement in Alzheimer's disease. J Neural Transm. 2021;128: 589–613.

363. Dordevic M, Müller-Fotti A, Müller P, Schmicker M, Kaufmann J, Müller NG. Optimal Cut-Off Value for Locus Coeruleus-to-Pons Intensity Ratio as Clinical Biomarker for Alzheimer's Disease: A Pilot Study. J Alzheimers Dis Rep. 2017;1: 159–167.

364. Rorabaugh JM, Chalermpalanupap T, Botz-Zapp CA, Fu VM, Lembeck NA, Cohen RM, et al. Chemogenetic locus coeruleus activation restores reversal learning in a rat model of Alzheimer's disease. Brain. 2017;140: 3023–3038.

365. Robertson IH. A noradrenergic theory of cognitive reserve: implications for Alzheimer's disease. Neurobiol Aging. 2013;34: 298–308.

366. Heneka MT, Nadrigny F, Regen T, Martinez-Hernandez A, Dumitrescu-Ozimek L, Terwel D, et al. Locus ceruleus controls Alzheimer's disease pathology by modulating microglial functions through norepinephrine. Proc Natl Acad Sci U S A. 2010;107: 6058–6063.

367. Porterfield VM, Gabella KM, Simmons MA, Johnson JD. Repeated stressor exposure regionally enhances beta-adrenergic receptor-mediated brain IL-1β production. Brain Behav Immun. 2012;26:

1249–1255.

368. Cancela LM, Volosin M, Molina VA. Chronic stress attenuation of α2-adrenoceptor reactivity is reversed by naltrexone. Pharmacol Biochem Behav. 1988;31: 33–35.

369. Meyer H, Palchaudhuri M, Scheinin M, Flügge G. Regulation of alpha(2A)-adrenoceptor expression by chronic stress in neurons of the brain stem. Brain Res. 2000;880: 147–158.

370. Stone EA, Platt JE. Brain adrenergic receptors and resistance to stress. Brain Res. 1982;237: 405–414.

371. Hipólide DC, Tufik S, Raymond R, Nobrega JN. Heterogeneous effects of rapid eye movement sleep deprivation on binding to alpha- and beta-adrenergic receptor subtypes in rat brain. Neuroscience. 1998;86: 977–987.

372. Pavcovich LA, Cancela LM, Volosin M, Molina VA, Ramirez OA. Chronic stress-induced changes in locus coeruleus neuronal activity. Brain Res Bull. 1990;24: 293–296.

373. Brady LS. Stress, antidepressant drugs, and the locus coeruleus. Brain Res Bull. 1994;35: 545–556.

374. Borodovitsyna O, Joshi N, Chandler D. Persistent Stress-Induced Neuroplastic Changes in the Locus Coeruleus/Norepinephrine System. Neural Plast. 2018;2018: 1892570.

375. Jedema HP, Finlay JM, Sved AF, Grace AA. Chronic cold exposure potentiates CRH-evoked increases in electrophysiologic activity of locus coeruleus neurons. Biol Psychiatry. 2001;49: 351–359.

376. Jedema HP, Gold SJ, Gonzalez-Burgos G, Sved AF, Tobe BJ, Wensel T, et al. Chronic cold exposure increases RGS7 expression and decreases alpha(2)-autoreceptor-mediated inhibition of noradrenergic locus coeruleus neurons. Eur J Neurosci. 2008;27: 2433–2443.

377. Makino S, Smith MA, Gold PW. Regulatory role of glucocorticoids and glucocorticoid receptor mRNA levels on tyrosine hydroxylase gene expression in the locus coeruleus during repeated immobilization stress. Brain Res. 2002;943: 216–223.

378. Morris LS, McCall JG, Charney DS, Murrough JW. The role of the locus coeruleus in the generation of pathological anxiety. Brain Neurosci Adv. 2020;4: 2398212820930321.

379. Krystal JH, Abdallah CG, Pietrzak RH, Averill LA, Harpaz-Rotem I, Levy I, et al. Locus Coeruleus Hyperactivity in Posttraumatic Stress Disorder: Answers and Questions. Biological psychiatry. 2018. pp. 197–199.

380. Sabban EL, Serova LI, Newman E, Aisenberg N, Akirav I. Changes in Gene Expression in the Locus Coeruleus-Amygdala Circuitry in Inhibitory Avoidance PTSD Model. Cell Mol Neurobiol. 2018;38: 273–280.

381. Naegeli C, Zeffiro T, Piccirelli M, Jaillard A, Weilenmann A, Hassanpour K, et al. Locus Coeruleus Activity Mediates Hyperresponsiveness in Posttraumatic Stress Disorder. Biol Psychiatry. 2018;83: 254–262.

382. Arnsten AFT, Raskind MA, Taylor FB, Connor DF. The Effects of Stress Exposure on Prefrontal Cortex: Translating Basic Research into Successful Treatments for Post-Traumatic Stress Disorder. Neurobiol Stress. 2015;1: 89–99.

383. Nisenbaum LK, Zigmond MJ, Sved AF, Abercrombie ED. Prior exposure to chronic stress results in enhanced synthesis and release of hippocampal norepinephrine in response to a novel stressor. J Neurosci. 1991;11: 1478–1484.

384. Bremner JD, Krystal JH, Southwick SM, Charney DS. Noradrenergic mechanisms in stress and anxiety: I. Preclinical studies. Synapse. 1996;23: 28–38.

385. Simson PE, Weiss JM. Altered activity of the locus coeruleus in an animal model of depression. Neuropsychopharmacology. 1988;1: 287–295.

386. Zhu MY, Klimek V, Dilley GE, Haycock JW, Stockmeier C, Overholser JC, et al. Elevated levels of tyrosine hydroxylase in the locus coeruleus in major depression. Biol Psychiatry. 1999;46: 1275–1286.

387. Moret C, Briley M. The importance of norepinephrine in depression. Neuropsychiatr Dis Treat. 2011;7: 9–13.

388. Harro J, Oreland L. Depression as a spreading adjustment disorder of monoaminergic neurons: a case for primary implication of the locus coeruleus. Brain Res Brain Res Rev. 2001;38: 79–128.

389. Weiss JM, Simson PG. Depression in an animal model: focus on the locus ceruleus. Ciba Found Symp.

1986;123: 191–215.

390. Weiss JM, Stout JC, Aaron MF, Quan N, Owens MJ, Butler PD, et al. Depression and anxiety: role of the locus coeruleus and corticotropin-releasing factor. Brain Res Bull. 1994;35: 561–572.

391. Aston-Jones G, Rajkowski J, Cohen J. Locus coeruleus and regulation of behavioral flexibility and attention. Progress in Brain Research. Elsevier; 2000. pp. 165–182.

392. Halperin JM, Schulz KP. Revisiting the role of the prefrontal cortex in the pathophysiology of attention-deficit/hyperactivity disorder. Psychol Bull. 2006;132: 560–581.

393. Bast N, Poustka L, Freitag CM. The locus coeruleus-norepinephrine system as pacemaker of attention - a developmental mechanism of derailed attentional function in autism spectrum disorder. Eur J Neurosci. 2018;47: 115–125.

394. Shirama A, Takeda T, Ohta H, Iwanami A, Toda S, Kato N. Atypical alert state control in adult patients with ADHD: A pupillometry study. PLoS One. 2020;15: e0244662.

395. Bast N, Boxhoorn S, Supér H, Helfer B, Polzer L, Klein C, et al. Atypical Arousal Regulation in Children With Autism but Not With Attention-Deficit/Hyperactivity Disorder as Indicated by Pupillometric Measures of Locus Coeruleus Activity. Biol Psychiatry Cogn Neurosci Neuroimaging. 2023;8: 11–20.

396. Kim Y, Kadlaskar G, Keehn RM, Keehn B. Measures of tonic and phasic activity of the locus coeruleus-norepinephrine system in children with autism spectrum disorder: An event-related potential and pupillometry study. Autism Res. 2022;15: 2250–2264.

397. Mehler MF, Purpura DP. Autism, fever, epigenetics and the locus coeruleus. Brain Res Rev. 2009;59: 388–392.

398. Igata S, Hayashi T, Itoh M, Akasu T, Takano M, Ishimatsu M. Persistent α1-adrenergic receptor function in the nucleus locus coeruleus causes hyperexcitability in AD/HD model rats. J Neurophysiol. 2014;111: 777–786.

399. Privitera CM, Renninger LW, Carney T, Klein S, Aguilar M. The pupil dilation response to visual detection. SPIE Proceedings. 2008. doi:10.1117/12.772844

400. Mathôt S. Pupillometry: Psychology, Physiology, and Function. J Cogn. 2018;1: 16.

401. Joshi S, Li Y, Kalwani RM, Gold JI. Relationships between Pupil Diameter and Neuronal Activity in the Locus Coeruleus, Colliculi, and Cingulate Cortex. Neuron. 2016;89: 221–234.

402. Larsen RS, Waters J. Neuromodulatory Correlates of Pupil Dilation. Front Neural Circuits. 2018;12: 21.

403. David M, Malhotra PA. New approaches for the quantification and targeting of noradrenergic dysfunction in Alzheimer's disease. Ann Clin Transl Neurol. 2022;9: 582–596.

404. Wainstein G, Rojas-Líbano D, Crossley NA, Carrasco X, Aboitiz F, Ossandón T. Pupil Size Tracks Attentional Performance In Attention-Deficit/Hyperactivity Disorder. Scientific Reports. 2017. doi:10.1038/s41598-017-08246-w

405. Rubin TG, Gray JD, McEwen BS. Experience and the ever-changing brain: what the transcriptome can reveal. Bioessays. 2014;36: 1072–1081.

406. Floriou-Servou A, von Ziegler L, Waag R, Schläppi C, Germain P-L, Bohacek J. The Acute Stress Response in the Multiomic Era. Biol Psychiatry. 2021;89: 1116–1126.

407. Girgenti MJ, Pothula S, Newton SS. Stress and Its Impact on the Transcriptome. Biol Psychiatry. 2021;90: 102–108.

408. Sullivan KE, Kendrick RM, Cembrowski MS. Elucidating memory in the brain via single-cell transcriptomics. J Neurochem. 2021;157: 982–992.

409. Fuentes-Ramos M, Alaiz-Noya M, Barco A. Transcriptome and epigenome analysis of engram cells: Next-generation sequencing technologies in memory research. Neurosci Biobehav Rev. 2021;127: 865–875.

410. Conrad CD. Chronic stress-induced hippocampal vulnerability: the glucocorticoid vulnerability hypothesis. Rev Neurosci. 2008;19: 395–411.

411. Joëls M, Karst H, Alfarez D, Heine VM, Qin Y, van Riel E, et al. Effects of chronic stress on structure and cell function in rat hippocampus and hypothalamus. Stress. 2004;7: 221–231.

412. Girgenti MJ, Duman RS. Transcriptome Alterations in Posttraumatic Stress Disorder. Biol Psychiatry. 2018;83: 840–848.

413. Reshetnikov VV, Kisaretova PE, Bondar NP. Transcriptome Alterations Caused by Social Defeat Stress of Various Durations in Mice and Its Relevance to Depression and Posttraumatic Stress Disorder in Humans: A Meta-Analysis. Int J Mol Sci. 2022;23. doi:10.3390/ijms232213792

414. Gormanns P, Mueller NS, Ditzen C, Wolf S, Holsboer F, Turck CW. Phenome-transcriptome correlation unravels anxiety and depression related pathways. J Psychiatr Res. 2011;45: 973–979.

415. Bagot RC, Cates HM, Purushothaman I, Lorsch ZS, Walker DM, Wang J, et al. Circuit-wide Transcriptional Profiling Reveals Brain Region-Specific Gene Networks Regulating Depression Susceptibility. Neuron. 2016;90: 969–983.

416. Larosa A, Wong TP. The hippocampus in stress susceptibility and resilience: Reviewing molecular and functional markers. Prog Neuropsychopharmacol Biol Psychiatry. 2022;119: 110601.

417. Gray JD, Rubin TG, Hunter RG, McEwen BS. Hippocampal gene expression changes underlying stress sensitization and recovery. Mol Psychiatry. 2014;19: 1171–1178.

418. Davson H, editor. 18 - The pupil. Physiology of the Eye (Fourth Edition). Academic Press; 1980. pp. 468–477.

419. Xu L, Dan M, Shao A, Cheng X, Zhang C, Yokel RA, et al. Silver nanoparticles induce tight junction disruption and astrocyte neurotoxicity in a rat blood-brain barrier primary triple coculture model. Int J Nanomedicine. 2015;10: 6105–6118.

420. Popichak KA, Hammond SL, Moreno JA, Afzali MF, Backos DS, Slayden RD, et al. Compensatory Expression of Nur77 and Nurr1 Regulates NF-κB-Dependent Inflammatory Signaling in Astrocytes. Mol Pharmacol. 2018;94: 1174–1186.

421. Pan J, Ma N, Zhong J, Yu B, Wan J, Zhang W. Age-associated changes in microglia and astrocytes ameliorate blood-brain barrier dysfunction. Mol Ther Nucleic Acids. 2021;26: 970–986.

422. Paillasse MR, de Medina P. The NR4A nuclear receptors as potential targets for anti-aging interventions. Med Hypotheses. 2015;84: 135–140.

423. Boyden ES, Zhang F, Bamberg E, Nagel G, Deisseroth K. Millisecond-timescale, genetically targeted optical control of neural activity. Nat Neurosci. 2005;8: 1263–1268.

424. Harley CW, Yuan Q. Locus Coeruleus Optogenetic Modulation: Lessons Learned from Temporal Patterns. Brain Sci. 2021;11. doi:10.3390/brainsci11121624

425. Grella SL, Neil JM, Edison HT, Strong VD, Odintsova IV, Walling SG, et al. Locus Coeruleus Phasic, But Not Tonic, Activation Initiates Global Remapping in a Familiar Environment. J Neurosci. 2019;39: 445–455.

426. Grujic N, Tesmer A, Bracey EF, Peleg-Raibstein D, Burdakov D. Control and coding of pupil size by hypothalamic orexin neurons. bioRxiv. 2022. p. 2022.04.12.488026. doi:10.1101/2022.04.12.488026

427. Cazettes F, Reato D, Morais JP, Renart A, Mainen ZF. Phasic Activation of Dorsal Raphe Serotonergic Neurons Increases Pupil Size. Curr Biol. 2021;31: 192–197.e4.

428. Singh AK, Verma S. Use of ocular biomarkers as a potential tool for early diagnosis of Alzheimer's disease. Indian J Ophthalmol. 2020;68: 555–561.

429. Reimer J, McGinley MJ, Liu Y, Rodenkirch C, Wang Q, McCormick DA, et al. Pupil fluctuations track rapid changes in adrenergic and cholinergic activity in cortex. Nat Commun. 2016;7: 13289.

430. Megemont M, McBurney-Lin J, Yang H. Pupil diameter is not an accurate real-time readout of locus coeruleus activity. Elife. 2022;11. doi:10.7554/eLife.70510

431. Joshi S. Pupillometry: Arousal State or State of Mind? Current biology: CB. 2021. pp. R32–R34.

432. Luskin AT, Li L, Fu X, Barcomb K, Blackburn T, Li EM, et al. A diverse network of pericoerulear neurons control arousal states. bioRxiv. 2022. p. 2022.06.30.498327. doi:10.1101/2022.06.30.498327

433. Mulvey B, Bhatti DL, Gyawali S, Lake AM, Kriaucionis S, Ford CP, et al. Molecular and Functional Sex Differences of Noradrenergic Neurons in the Mouse Locus Coeruleus. Cell Rep. 2018;23: 2225–2235.

434. Verkhratsky A, Nedergaard M, Hertz L. Why are astrocytes important? Neurochem Res. 2015;40:

389–401.

435. Salm AK, McCarthy KD. The evidence for astrocytes as a target for central noradrenergic activity: expression of adrenergic receptors. Brain Res Bull. 1992;29: 265–275.

436. Nag S. Morphology and Properties of Astrocytes. In: Nag S, editor. The Blood-Brain and Other Neural Barriers: Reviews and Protocols. Totowa, NJ: Humana Press; 2011. pp. 69–100.

437. Halassa MM, Fellin T, Takano H, Dong J-H, Haydon PG. Synaptic islands defined by the territory of a single astrocyte. J Neurosci. 2007;27: 6473–6477.

438. Hertz L, Lovatt D, Goldman SA, Nedergaard M. Adrenoceptors in brain: cellular gene expression and effects on astrocytic metabolism and [Ca(2+)]i. Neurochem Int. 2010;57: 411–420.

439. Shao Y, McCarthy KD. Plasticity of astrocytes. Glia. 1994;11: 147–155.

440. Paukert M, Agarwal A, Cha J, Doze VA, Kang JU, Bergles DE. Norepinephrine controls astroglial responsiveness to local circuit activity. Neuron. 2014;82: 1263–1270.

441. Bekar LK, He W, Nedergaard M. Locus coeruleus α-adrenergic–mediated activation of cortical astrocytes in vivo. Cereb Cortex. 2008. Available: https://academic.oup.com/cercor/article-abstract/18/12/2789/361704

442. Orts-Del'Immagine A, Dhanasekar M, Lejeune F-X, Roussel J, Wyart C. A norepinephrine-dependent glial calcium wave travels in the spinal cord upon acoustovestibular stimuli. Glia. 2022;70: 491–507.

443. Schnell C, Negm M, Driehaus J, Scheller A, Hülsmann S. Norepinephrine-induced calcium signaling in astrocytes in the respiratory network of the ventrolateral medulla. Respir Physiol Neurobiol. 2016;226: 18–23.

444. Nuriya M, Takeuchi M, Yasui M. Background norepinephrine primes astrocytic calcium responses to subsequent norepinephrine stimuli in the cerebral cortex. Biochem Biophys Res Commun. 2017;483: 732–738.

445. Rupprecht P, Lewis CM, Helmchen F. Centripetal integration of past events by hippocampal astrocytes. bioRxiv. 2022. Available: https://www.biorxiv.org/content/10.1101/2022.08.16.504030.abstract

446. Scemes E, Giaume C. Astrocyte calcium waves: what they are and what they do. Glia. 2006;54: 716–725.

447. Durkee CA, Araque A. Diversity and Specificity of Astrocyte-neuron Communication. Neuroscience. 2019;396: 73–78.

448. Kofuji P, Araque A. G-Protein-Coupled Receptors in Astrocyte-Neuron Communication. Neuroscience. 2021;456: 71–84.

449. Buskila Y, Bellot-Saez A, Morley JW. Generating Brain Waves, the Power of Astrocytes. Front Neurosci. 2019;13: 1125.

450. Fellin T, Carmignoto G. Neurone-to-astrocyte signalling in the brain represents a distinct multifunctional unit. J Physiol. 2004. Available: https://physoc.onlinelibrary.wiley.com/doi/abs/10.1113/jphysiol.2004.063214

451. Haydon PG. GLIA: listening and talking to the synapse. Nat Rev Neurosci. 2001;2: 185–193.

452. Volterra A, Meldolesi J. Astrocytes, from brain glue to communication elements: the revolution continues. Nat Rev Neurosci. 2005;6: 626–640.

453. Takano T, Tian G-F, Peng W, Lou N, Libionka W, Han X, et al. Astrocyte-mediated control of cerebral blood flow. Nat Neurosci. 2006;9: 260–267.

454. Pankratov Y, Lalo U. Role for astroglial α1-adrenoreceptors in gliotransmission and control of synaptic plasticity in the neocortex. Front Cell Neurosci. 2015;9: 230.

455. Laureys G, Clinckers R, Gerlo S, Spooren A, Wilczak N, Kooijman R, et al. Astrocytic beta(2)-adrenergic receptors: from physiology to pathology. Prog Neurobiol. 2010;91: 189–199.

456. Sherpa AD, Xiao F, Joseph N, Aoki C, Hrabetova S. Activation of β-adrenergic receptors in rat visual cortex expands astrocytic processes and reduces extracellular space volume. Synapse. 2016;70: 307–316.

457. Vardjan N, Kreft M, Zorec R. Dynamics of β-adrenergic/cAMP signaling and morphological changes in

cultured astrocytes. Glia. 2014;62: 566–579.

458. Perea G, Navarrete M, Araque A. Tripartite synapses: astrocytes process and control synaptic information. Trends Neurosci. 2009;32: 421–431.

459. Ventura R, Harris KM. Three-dimensional relationships between hippocampal synapses and astrocytes. J Neurosci. 1999;19: 6897–6906.

460. Ullian EM, Sapperstein SK, Christopherson KS, Barres BA. Control of synapse number by glia. Science. 2001;291: 657–661.

461. Liu C-Y, Yang Y, Ju W-N, Wang X, Zhang H-L. Emerging Roles of Astrocytes in Neuro-Vascular Unit and the Tripartite Synapse With Emphasis on Reactive Gliosis in the Context of Alzheimer's Disease. Front Cell Neurosci. 2018;12: 193.

462. Lee J-H, Kim J-Y, Noh S, Lee H, Lee SY, Mun JY, et al. Astrocytes phagocytose adult hippocampal synapses for circuit homeostasis. Nature. 2021;590: 612–617.

463. Gibbs ME, Hutchinson D, Hertz L. Astrocytic involvement in learning and memory consolidation. Neurosci Biobehav Rev. 2008;32: 927–944.

464. Pearson-Leary J, Osborne DM, McNay EC. Role of Glia in Stress-Induced Enhancement and Impairment of Memory. Front Integr Neurosci. 2015;9: 63.

465. Gao V, Suzuki A, Magistretti PJ, Lengacher S, Pollonini G, Steinman MQ, et al. Astrocytic β_2-adrenergic receptors mediate hippocampal long-term memory consolidation. Proc Natl Acad Sci U S A. 2016;113: 8526–8531.

466. Iqbal Z, Lei Z, Ramkrishnan AS, Liu S, Hasan M, Akter M, et al. Adrenergic signalling to astrocytes in anterior cingulate cortex contributes to pain-related aversive memory in rats. Commun Biol. 2023;6: 10.

467. Dienel GA, Cruz NF. Contributions of glycogen to astrocytic energetics during brain activation. Metab Brain Dis. 2015;30: 281–298.

468. Dienel GA. The metabolic trinity, glucose-glycogen-lactate, links astrocytes and neurons in brain energetics, signaling, memory, and gene expression. Neurosci Lett. 2017;637: 18–25.

469. Powell CL, Davidson AR, Brown AM. Universal Glia to Neurone Lactate Transfer in the Nervous System: Physiological Functions and Pathological Consequences. Biosensors. 2020;10. doi:10.3390/bios10110183

470. Dienel GA, Cruz NF. Aerobic glycolysis during brain activation: adrenergic regulation and influence of norepinephrine on astrocytic metabolism. J Neurochem. 2016;138: 14–52.

471. DiNuzzo M, Giove F, Maraviglia B, Mangia S. Monoaminergic Control of Cellular Glucose Utilization by Glycogenolysis in Neocortex and Hippocampus. Neurochem Res. 2015;40: 2493–2504.

472. Zuend M, Saab AS, Wyss MT, Ferrari KD, Hösli L, Looser ZJ, et al. Arousal-induced cortical activity triggers lactate release from astrocytes. Nat Metab. 2020;2: 179–191.

473. Newgard CB, Brady MJ, O'Doherty RM, Saltiel AR. Organizing glucose disposal: emerging roles of the glycogen targeting subunits of protein phosphatase-1. Diabetes. 2000;49: 1967–1977.

474. Allaman I, Pellerin L, Magistretti PJ. Protein targeting to glycogen mRNA expression is stimulated by noradrenaline in mouse cortical astrocytes. Glia. 2000;30: 382–391.

475. Yu N, Martin JL, Stella N, Magistretti PJ. Arachidonic acid stimulates glucose uptake in cerebral cortical astrocytes. Proc Natl Acad Sci U S A. 1993;90: 4042–4046.

476. Newman LA, Korol DL, Gold PE. Lactate produced by glycogenolysis in astrocytes regulates memory processing. PLoS One. 2011;6: e28427.

477. Duran J, Saez I, Gruart A, Guinovart JJ, Delgado-García JM. Impairment in long-term memory formation and learning-dependent synaptic plasticity in mice lacking glycogen synthase in the brain. J Cereb Blood Flow Metab. 2013;33: 550–556.

478. Gibbs ME. Role of Glycogenolysis in Memory and Learning: Regulation by Noradrenaline, Serotonin and ATP. Front Integr Neurosci. 2015;9: 70.

479. Vezzoli E, Calì C, De Roo M, Ponzoni L, Sogne E, Gagnon N, et al. Ultrastructural Evidence for a Role

of Astrocytes and Glycogen-Derived Lactate in Learning-Dependent Synaptic Stabilization. Cereb Cortex. 2020;30: 2114–2127.

480. Veloz Castillo MF, Magistretti PJ, Calì C. l-Lactate: Food for Thoughts, Memory and Behavior. Metabolites. 2021;11. doi:10.3390/metabo11080548

481. Campos-Barros A, Meinhold H, Stula M, Müller F, Köhler R, Eravci M, et al. The influence of desipramine on thyroid hormone metabolism in rat brain. J Pharmacol Exp Ther. 1994;268: 1143–1152.

482. Kundu S, Biswas A, Roy S, De J, Pramanik M, Ray AK. Thyroid hormone homeostasis in brain: possible involvement of adrenergic phenomenon in adult rat. Neuroendocrinology. 2009;89: 140–151.

483. Crantz FR, Silva JE, Larsen PR. An analysis of the sources and quantity of 3,5,3'-triiodothyronine specifically bound to nuclear receptors in rat cerebral cortex and cerebellum. Endocrinology. 1982;110: 367–375.

484. Freitas BCG, Gereben B, Castillo M, Kalló I, Zeöld A, Egri P, et al. Paracrine signaling by glial cell-derived triiodothyronine activates neuronal gene expression in the rodent brain and human cells. J Clin Invest. 2010;120: 2206–2217.

485. Morte B, Bernal J. Thyroid hormone action: astrocyte-neuron communication. Front Endocrinol . 2014;5: 82.

486. Gordon JT, Kaminski DM, Rozanov CB, Dratman MB. Evidence that 3,3',5-triiodothyronine is concentrated in and delivered from the locus coeruleus to its noradrenergic targets via anterograde axonal transport. Neuroscience. 1999;93: 943–954.

487. Rozanov CB, Dratman MB. Immunohistochemical mapping of brain triiodothyronine reveals prominent localization in central noradrenergic systems. Neuroscience. 1996;74: 897–915.

488. Dratman MB, Gordon JT. Thyroid hormones as neurotransmitters. Thyroid. 1996;6: 639–647.

489. Füzesi T, Wittmann G, Lechan RM, Liposits Z, Fekete C. Noradrenergic innervation of hypophysiotropic thyrotropin-releasing hormone-synthesizing neurons in rats. Brain Res. 2009;1294: 38–44.

490. Cunningham ET Jr, Sawchenko PE. Anatomical specificity of noradrenergic inputs to the paraventricular and supraoptic nuclei of the rat hypothalamus. J Comp Neurol. 1988;274: 60–76.

491. Gullo D, Sinha AK, Woods R, Pervin K, Ekins RP. Triiodothyronine binding in adult rat brain: compartmentation of receptor populations in purified neuronal and glial nuclei. Endocrinology. 1987;120: 325–331.

492. Jones SA, Jolson DM, Cuta KK, Mariash CN, Anderson GW. Triiodothyronine is a survival factor for developing oligodendrocytes. Mol Cell Endocrinol. 2003;199: 49–60.

493. Walpita CN, Van der Geyten S, Rurangwa E, Darras VM. The effect of 3,5,3'-triiodothyronine supplementation on zebrafish (Danio rerio) embryonic development and expression of iodothyronine deiodinases and thyroid hormone receptors. Gen Comp Endocrinol. 2007;152: 206–214.

494. Richard S, Flamant F. Regulation of T3 Availability in the Developing Brain: The Mouse Genetics Contribution. Front Endocrinol . 2018;9: 265.

495. Bernal J. Thyroid Hormones and Brain Development. Vitamins & Hormones. Academic Press; 2005. pp. 95–122.

496. Walter IB. Triiodothyronine exerts a trophic action on rat sensory neuron survival and neurite outgrowth through different pathways. Eur J Neurosci. 1996;8: 455–466.

497. Talhada D, Feiteiro J, Costa AR, Talhada T, Cairrão E, Wieloch T, et al. Triiodothyronine modulates neuronal plasticity mechanisms to enhance functional outcome after stroke. Acta Neuropathol Commun. 2019;7: 216.

498. Davis PJ, Zhou M, Davis FB, Lansing L, Mousa SA, Lin H-Y. Mini-review: Cell surface receptor for thyroid hormone and nongenomic regulation of ion fluxes in excitable cells. Physiol Behav. 2010;99: 237–239.

499. Losi G, Garzon G, Puia G. Nongenomic regulation of glutamatergic neurotransmission in hippocampus by thyroid hormones. Neuroscience. 2008;151: 155–163.

500. Zendedel A, Kashani IR, Azimzadeh M, Pasbakhsh P, Omidi N, Golestani A, et al. Regulatory effect of

triiodothyronine on brain myelination and astrogliosis after cuprizone-induced demyelination in mice. Metab Brain Dis. 2016;31: 425–433.

501. Kapri D, Fanibunda SE, Vaidya VA. Thyroid hormone regulation of adult hippocampal neurogenesis: Putative molecular and cellular mechanisms. Vitam Horm. 2022;118: 1–33.

502. Vara H, Martínez B, Santos A, Colino A. Thyroid hormone regulates neurotransmitter release in neonatal rat hippocampus. Neuroscience. 2002;110: 19–28.

503. Bagamasbad PD, Espina JEC, Knoedler JR, Subramani A, Harden AJ, Denver RJ. Coordinated transcriptional regulation by thyroid hormone and glucocorticoid interaction in adult mouse hippocampus-derived neuronal cells. PLoS One. 2019;14: e0220378.

504. Calzà L, Aloe L, Giardino L. Thyroid hormone-induced plasticity in the adult rat brain. Brain Res Bull. 1997;44: 549–557.

505. McAninch EA, Bianco AC. Thyroid hormone signaling in energy homeostasis and energy metabolism. Ann N Y Acad Sci. 2014;1311: 77–87.

506. Grøntved L, Waterfall JJ, Kim DW, Baek S, Sung M-H, Zhao L, et al. Transcriptional activation by the thyroid hormone receptor through ligand-dependent receptor recruitment and chromatin remodelling. Nat Commun. 2015;6: 1–11.

507. Diez D, Grijota-Martinez C, Agretti P, De Marco G, Tonacchera M, Pinchera A, et al. Thyroid Hormone Action in the Adult Brain: Gene Expression Profiling of the Effects of Single and Multiple Doses of Triiodo-l-Thyronine in the Rat Striatum. Endocrinology. 2008;149: 3989–4000.

508. Gil-Ibañez P, García-García F, Dopazo J, Bernal J, Morte B. Global Transcriptome Analysis of Primary Cerebrocortical Cells: Identification of Genes Regulated by Triiodothyronine in Specific Cell Types. Cereb Cortex. 2015;27: 706–717.

509. Bauer M, Heinz A, Whybrow PC. Thyroid hormones, serotonin and mood: of synergy and significance in the adult brain. Mol Psychiatry. 2002;7: 140–156.

510. Bilezikian JP, Loeb JN. The influence of hyperthyroidism and hypothyroidism on alpha- and beta-adrenergic receptor systems and adrenergic responsiveness. Endocr Rev. 1983;4: 378–388.

511. Mason GA, Bondy SC, Nemeroff CB, Walker CH, Prange AJ Jr. The effects of thyroid state on beta-adrenergic and serotonergic receptors in rat brain. Psychoneuroendocrinology. 1987;12: 261–270.

512. Strömbom U, Svensson TH, Jackson DM, Engström G. Hyperthyroidism: specifically increased response to central NA-(alpha-)receptor stimulation and generally increased monoamine turnover in brain. J Neural Transm. 1977;41: 73–92.

513. Clur A. Reverse tri-iodothyronine as part of alpha 2 adrenergic receptors. Med Hypotheses. 1986;21: 281–292.

514. Tejani-Butt SM, Yang J. A time course of altered thyroid states on the noradrenergic system in rat brain by quantitative autoradiography. Neuroendocrinology. 1994;59: 235–244.

515. Williams LT, Lefkowitz RJ, Watanabe AM, Hathaway DR, Besch HR. Thyroid hormone regulation of beta-adrenergic receptor number. J Biol Chem. 1977;252. Available: https://pubmed.ncbi.nlm.nih.gov/15999/

516. Rubio A, Raasmaja A, Maia AL, Kim KR, Silva JE. Effects of thyroid hormone on norepinephrine signaling in brown adipose tissue. I. Beta 1- and beta 2-adrenergic receptors and cyclic adenosine 3',5'-monophosphate generation. Endocrinology. 1995;136. doi:10.1210/endo.136.8.7628360

517. Caria MA, Dratman MB, Kow L-M, Mameli O, Pavlides C. Thyroid hormone action: nongenomic modulation of neuronal excitability in the hippocampus. J Neuroendocrinol. 2009;21: 98–107.

518. Gharami K, Das S. Thyroid hormone-induced morphological differentiation and maturation of astrocytes are mediated through the beta-adrenergic receptor. J Neurochem. 2000;75. doi:10.1046/j.1471-4159.2000.0751962.x

519. Fuenmayor D, Gonzalez-Vegas JA. Effects of altered thyroid state on the inhibition produced by locus coeruleus in Purkinje cells in the rat. Experientia. 1980;36: 841–842.

520. Taşkın E, Artis AS, Bitiktas S, Dolu N, Liman N, Süer C. Experimentally induced hyperthyroidism disrupts hippocampal long-term potentiation in adult rats. Neuroendocrinology. 2011;94: 218–227.

521. Tang YP, Ma YL, Chen SK, Lee EH. mRNA differential display identification of thyroid hormone-responsive protein (THRP) gene in association with early phase of long-term potentiation. Hippocampus. 2001;11: 637–646.

522. Shabani S, Farbood Y, Sarkaki A, Mard SA, Ahangarpour A, Khorsandi L. The effect of triiodothyronine on the hippocampal long-term potentiation in an animal model of the Alzheimer's disease: The role of BDNF and reelin. Neurology, Psychiatry and Brain Research. 2019;33: 82–88.

523. Bitiktaş S, Tan B, Kavraal Ş, Yousef M, Bayar Y, Dursun N, et al. The effects of intra-hippocampal L-thyroxine infusion on long-term potentiation and long-term depression: A possible role for the αvβ3 integrin receptor. J Neurosci Res. 2017;95: 1621–1632.

524. Rivas M, Naranjo JR. Thyroid hormones, learning and memory. Genes Brain Behav. 2007;6 Suppl 1: 40–44.

525. Sui L, Wang F, Liu F, Wang J, Li BM. Dorsal hippocampal administration of triiodothyronine enhances long-term memory for trace cued and delay contextual fear conditioning in rats. J Neuroendocrinol. 2006;18: 811–819.

526. Yu D, Zhou H, Zou L, Jiang Y, Wu X, Jiang L, et al. Hippocampal Administration of Levothyroxine Impairs Contextual Fear Memory Consolidation in Rats. Front Cell Neurosci. 2017;11: 223.

527. Sabatino L, Vassalle C, Del Seppia C, Iervasi G. Deiodinases and the Three Types of Thyroid Hormone Deiodination Reactions. Endocrinol Metab (Seoul). 2021;36: 952–964.

528. Tu HM, Legradi G, Bartha T, Salvatore D, Lechan RM, Larsen PR. Regional expression of the type 3 iodothyronine deiodinase messenger ribonucleic acid in the rat central nervous system and its regulation by thyroid hormone. Endocrinology. 1999;140: 784–790.

529. Papaleonidopoulos V, Papatheodoropoulos C. β-adrenergic receptors reduce the threshold for induction and stabilization of LTP and enhance its magnitude via multiple mechanisms in the ventral but not the dorsal hippocampus. Neurobiol Learn Mem. 2018;151: 71–84.

530. Grigoryan G, Ardi Z, Albrecht A, Richter-Levin G, Segal M. Juvenile stress alters LTP in ventral hippocampal slices: involvement of noradrenergic mechanisms. Behav Brain Res. 2015;278: 559–562.

531. Quinlan P, Horvath A, Eckerström C, Wallin A, Svensson J. Altered thyroid hormone profile in patients with Alzheimer's disease. Psychoneuroendocrinology. 2020;121. doi:10.1016/j.psyneuen.2020.104844

532. Figueroa PBS, Ferreira AFF, Britto LR, Doussoulin AP, Torrão A da S. Association between thyroid function and Alzheimer's disease: A systematic review. Metab Brain Dis. 2021;36: 1523–1543.

533. Dolatshahi M, Salehipour A, Saghazadeh A, Sanjeari Moghaddam H, Aghamollaii V, Fotouhi A, et al. Thyroid hormone levels in Alzheimer disease: a systematic review and meta-analysis. Endocrine. 2022; 1–21.

534. Bavarsad K, Hosseini M, Hadjzadeh M-A-R, Sahebkar A. The effects of thyroid hormones on memory impairment and Alzheimer's disease. J Cell Physiol. 2019. doi:10.1002/jcp.28198

535. Accorroni A, Chiellini G, Origlia N. Effects of Thyroid Hormones and their Metabolites on Learning and Memory in Normal and Pathological Conditions. Curr Drug Metab. 2017;18: 225–236.

536. James T, Kula B, Choi S, Khan SS, Bekar LK, Smith NA. Locus coeruleus in memory formation and Alzheimer's disease. Eur J Neurosci. 2021;54. doi:10.1111/ejn.15045

537. Dahl MJ, Mather M, Werkle-Bergner M, Kennedy BL, Guzman S, Hurth K, et al. Locus coeruleus integrity is related to tau burden and memory loss in autosomal-dominant Alzheimer's disease. Neurobiol Aging. 2022;112. doi:10.1016/j.neurobiolaging.2021.11.006

538. Chen Y, Chen T, Hou R. Locus coeruleus in the pathogenesis of Alzheimer's disease: A systematic review. Alzheimer's & dementia (New York, N Y). 2022;8. doi:10.1002/trc2.12257

539. Chaalal A, Poirier R, Blum D, Laroche S, Enderlin V. Thyroid Hormone Supplementation Restores Spatial Memory, Hippocampal Markers of Neuroinflammation, Plasticity-Related Signaling Molecules, and β-Amyloid Peptide Load in Hypothyroid Rats. Mol Neurobiol. 2019;56: 722–735.

540. Belakavadi M, Dell J, Grover GJ, Fondell JD. Thyroid hormone suppression of β-amyloid precursor protein gene expression in the brain involves multiple epigenetic regulatory events. Mol Cell Endocrinol. 2011;339: 72–80.

541. Lee JS, Soh Y, Kim H-G, Lee KM, Kwon YN, Yoon SS, et al. Interactive Effects of Apolipoprotein E ε4 and Triiodothyronine on Memory Performance in Patients With Subjective Cognitive Decline. Front Med. 2020;7: 298.

542. Farbood Y, Shabani S, Sarkaki A, Mard SA, Ahangarpour A, Khorsandi L. Peripheral and central administration of T3 improved the histological changes, memory and the dentate gyrus electrophysiological activity in an animal model of Alzheimer's disease. Metab Brain Dis. 2017;32: 693–701.

543. Contreras-Jurado C, Pascual A. Thyroid hormone regulation of APP (β-amyloid precursor protein) gene expression in brain and brain cultured cells. Neurochem Int. 2012;60: 484–487.

544. Chaalal A, Poirier R, Blum D, Gillet B, Le Blanc P, Basquin M, et al. PTU-induced hypothyroidism in rats leads to several early neuropathological signs of Alzheimer's disease in the hippocampus and spatial memory impairments. Hippocampus. 2014;24: 1381–1393.

545. Tan ZS, Vasan RS. Thyroid function and Alzheimer's disease. J Alzheimers Dis. 2009;16: 503–507.

546. Hage MP, Azar ST. The Link between Thyroid Function and Depression. J Thyroid Res. 2012;2012: 590648.

547. Karlović D, Marusić S, Martinac M. Increase of serum triiodothyronine concentration in soldiers with combat-related chronic post-traumatic stress disorder with or without alcohol dependence. Wien Klin Wochenschr. 2004;116: 385–390.

548. Friedman MJ, Wang S, Jalowiec JE, McHugo GJ, McDonagh-Coyle A. Thyroid hormone alterations among women with posttraumatic stress disorder due to childhood sexual abuse. Biol Psychiatry. 2005;57: 1186–1192.

549. Buras A, Battle L, Landers E, Nguyen T, Vasudevan N. Thyroid hormones regulate anxiety in the male mouse. Horm Behav. 2014;65: 88–96.

550. Bárez-López S, Montero-Pedrazuela A, Bosch-García D, Venero C, Guadaño-Ferraz A. Increased anxiety and fear memory in adult mice lacking type 2 deiodinase. Psychoneuroendocrinology. 2017;84: 51–60.

551. Bocco BMLC, Werneck-de-Castro JP, Oliveira KC, Fernandes GW, Fonseca TL, Nascimento BPP, et al. Type 2 Deiodinase Disruption in Astrocytes Results in Anxiety-Depressive-Like Behavior in Male Mice. Endocrinology. 2016;157: 3682–3695.

552. Martinez-deMena R, Calvo R-M, Garcia L, Obregon MJ. Effect of glucocorticoids on the activity, expression and proximal promoter of type II deiodinase in rat brown adipocytes. Mol Cell Endocrinol. 2016;428: 58–67.

553. Joëls M, Fernandez G, Roozendaal B. Stress and emotional memory: a matter of timing. Trends Cogn Sci. 2011;15: 280–288.